1-1-2014

The Role of Caspase-6 in Amyotrophic Lateral Sclerosis

Mollie R. Mitchem
Royal College of Surgeons in Ireland, mollie.mitchem@yahoo.com

1-1-2014

The Role of Caspase-6 in Amyotrophic Lateral Sclerosis

Mollie R. Mitchem

— Use Licence —

Creative Commons Licence:

The Role of Caspase-6 in Amyotrophic Lateral Sclerosis

Mollie R. Mitchem

A Thesis Submitted to the Royal College of Surgeons in Ireland in Fulfilment of the Requirement for the Degree of Master of Science

Department of Physiology

August 2014

RCSI

Thesis supervisor: **Prof. Jochen H.M. Prehn**

Thesis Declaration

I declare that this thesis, which I submit to RCSI for examination in consideration of the award of degree of Master of Science, is my own personal effort. Where any of the content presented is the result of input or data from a related collaborative research programme this is duly acknowledged in the text such that it is possible to ascertain how much of the work is my own. I have not already obtained a degree in RCSI or elsewhere on the basis of this work. Furthermore, I took reasonable care to ensure that the work is original, and, to the best of my knowledge, does not breach copyright law, and has not been taken from other sources except where such work has been cited and acknowledged within the text.

Signed _____

Student Number _____

Date _____

Technical Support Declaration

Ms Ina Woods provided technical assistance with genotyping and cross breeding.

Dr. Hans-Georg Koenig and Ms Sinead Kinsella provided technical assistance with mRNA experiments (Figure 3.1).

Ms Woods, Dr. Hans-Georg Koenig, and Ms Kinsella's contribution is much appreciated.

Project Summary

Caspases are a major contributor to the apoptotic pathway. We intended to investigate the role of caspases, namely caspase-6, which has not been fully characterized in Amyotrophic Lateral Sclerosis (ALS). We utilized quantitative PCR (qPCR) to determine *caspase-6* mRNA expression in nervous tissue from neocortex as well as ntg SOD1^{G93A}; *caspase-6*$^{-/-}$ gastrocnemius muscle (pnd 35), ntg SOD1^{G93A}; *caspase-6*$^{+/+}$ gastrocnemius muscle (pnd 35), and compared this with purified primary motorneurons, microglia-enriched and astrocyte-enriched cultures from primary E12 spinal cord tissue. No significant differences in *caspase-6* mRNA expression were detected in the sample types examined compared to nervous tissue.

We decided to investigate if caspase-6 protein levels were altered in a transgenic mouse model of ALS. We measured pro caspase-6 levels in tg and ntg SOD1^{G93A} lumbar spinal cord at pnd 70, pnd 120, and pnd endstage (150-160 days). We found that pro caspase-6 showed a tendency towards an increase with the progression of ALS, yet this was is not at statistically significant levels. To further elucidate the role of caspase-6 during ALS disease progression, we developed a cross-breeding program to produce a SOD1^{G93A} mouse colony deficient for *caspase-6*. The loss of motor function is a phenotypic indicator of ALS disease onset and progression in transgenic SOD1^{G93A} mice. Motor function and behavioural analysis paradigms were used to assess the effect of *caspase-6* deletion on functional defects and the lifespan of SOD1^{G93A}; *caspase-6* colony. Surprisingly, we found that *caspase-6* deficiency does not protect limb function, endurance, and motility in SOD1^{G93A} mice and has no effect on body weight. We recorded the lifespan of SOD1^{G93A}; c*aspase-6*$^{-/-}$ mice to examine the effect of *caspase-6* deletion during disease progression. Non-parametric analysis revealed that genetic deletion of *caspase-6* did not increase survival in tg SOD1^{G93A}; *caspase-6*$^{-/-}$ mice compared to tg SOD1^{G93A}; *caspase-6*$^{+/+}$ littermates, in fact it significantly decreased survival.

It has been hypothesized that caspase-6 may have a role in the degeneration in skeletal muscle that occurs prior to the onset of motorneuron degeneration in the spinal cord (Graham *et al*. 2006). We wanted to determine if motor endplates from hindlimb skeletal muscle showed any morphological changes in *caspase-6* deficient mice compared to ntg SOD1^{G93A} mice. Our findings showed no obvious signs of variation. We also compared weight and morphology of gastrocnemius muscle in SOD1^{G93A} mice and showed that deletion of *caspase-6* does not affect muscular atrophy in this mouse model for ALS.

Our initial hypothesis was that deletion of *caspase-6* would protect neurons against cell death and therefore improve the phenotype in the $SOD1^{G93A}$ ALS mouse model. However we found the opposite were true and that deletion of *caspase-6* enhanced disease progression and decreased lifespan. We hypothesize that caspase-6 is protective during ALS pathogenesis as the degenerative phenotype is worse when *caspase-6* is removed, however further work is required to fully characterise the role of caspase-6.

Acknowledgements

I would like to sincerely thank my supervisor Professor Jochen Prehn for giving me this great opportunity. I truly appreciate your support, guidance, and patience during my time at RCSI. I have gained invaluable experience and am so grateful that I was able to spend three wonderful years here. I would like to thank all the Department of Physiology and Medical Physics for your friendship and scientific inspiration. I want to especially thank Hans-Georg, Caoimhin, Heiko, Karen, Katie, Sinead, Ina, Sarah C., and Mark.

I would like to thank my co-supervisor Dr. Marion Hogg for the excellent training, advice, and especially patience that I received during my time at RCSI. I sincerely appreciate your support and friendship. Through the ups and downs of my masters, you were a great leader and supervisor who challenged me to be a better scientist, so thank you!

I would like to thank my family, especially my parents. Thank for your support and encouragement during my degree. I really appreciate all the skype calls to make me laugh and feel "at home" at least for a little while. I also want to thank the Sommerville family for taking such good care of me in Dublin. I really appreciate that you took me into your home and your family over the past year.

I have to especially thank my dear friends Lorna, Naadiya, and Rachel for you friendship and support. I could not have done this without your help, encouragement, friendship and laughter! I will really miss all of you but I know we will remain very close friends. I would also like to thank Katie Nolan for endless chats over tea, and Gary Brennan for candy bar runs to keep us going, and just plain silly moments with Megan Masters at lunch. You all made my time at RCSI even more enjoyable.

A huge thank you to Gary Sommerville for his love and support before and during my master's degree. Thanks for listening to me troubleshoot experiments and for always seeing the positive in every situation. You are a great scientist and I am so lucky to have you as a guide as well as my best friend.

Finally, I would like to thank Science Foundation Ireland for funding this study. Thank you for enabling me to carry out such exciting and important research.

Abbreviations

α-BTX	α-bungarotoxin
AIF	Apoptosis-Inducing Factor
ALS	Amyotrophic Lateral Sclerosis
Apaf-1	Apoptotic protease activating factor-1
Bak	Bcl-s Antagonist or Killer Protein
Bax	Bcl-2 Associated X Protein
BCA	Bicinchoninic Acid
BRF	Biomedical Research Facility
bp	Base Pair
BSA	Bovine Serum Albumin
BV-2	Immortalized Microglia cell line
CC	Central Canal
CNS	Central Nervous System
CSF	Cerebrospinal Fluid
Cu	Copper
C57BL/6	C57 Black Six Mice
ºC	Degrees Celsius
DEPC	Diethylpyrocarbonate
DH	Dorsal Horn
DMEM	Dulbecco's Modified Eagle's Medium
DMSO	Dimethyl Sulfoxide
DNA	Deoxyribonucleic Acid
DRG	Dorsal Root Ganglia
ECL	Enhanced Chemiluminescence
EndoG	Endonuclease G
fALS	Familial Amyotrophic Lateral Sclerosis

FAS	Cell Surface Death Receptor
FDA	Food and Drug Administration
FTD	Frontotemporal Dementia
FUS	Fused in Sarcoma
G^{93A}	SOD1 mutation at codon 93 Alanine replaced with Glycine
GAPDH	glyceraldehyde 3-phosphate dehydrogenase
GL-261	Astrocytoma cell line
HD	Huntington's disease
HRP	Horseradish Peroxidase
IP	Intraperitoneal Injection
IHC	Immunohistochemistry
JAX	Jackson Laboratories
LMN	Lower Motorneurons
LMP	Lysosome Membrane Permeabilization
mL	Milli Litre
mm	Milli Meter
MND	Motor Neuron Disease
MOMP	Mitochondrial Outer Membrane Polarization
mRNA	Messenger Ribonucleic Acid
NaCl	Sodium Chloride
NMJ	Neuromuscular Junction
NSC-34	Motorneuron/neuroblastoma hybrid
NSP	Non-Specific Band
Ntg	Non-transgenic
PFA	Paraformaldehyde

PaGE	Paw Grip Endurance
PBS	Phosphate Buffered Saline
pH	Power of Hydrogen
PUMA	p53 Unregulated Modulator of Apoptosis
PCR	Polymerase Chain Reaction
PLS	Primary Lateral Sclerosis
PBP	Progressive Bulbar Palsy
PCD	Programmed Cell Death
PMA	Progressive Muscular Atrophy
PND	Postnatal Day
ROS	Reactive Oxygen Species
RPMI	Roswell Park Memorial Institute medium
RT-qPCR	Real Time quantitative Polymerase Chain Reaction
RNA	Ribonucleic Acid
REC	Research Ethics Committee
RIPA	Radioimmunoprecipitation Assay
RQ	Relative Quality
sALS	Sporadic Amyotrophic Lateral Sclerosis
SEM	Standard Error of the Mean
SDS	Sodium Dodecyl Sulfate Polyacrylamide
SMAC	Second Mitochondria-Derived Activator of Caspase
SOD1	Superoxide Dismutase One
STS	Staurosporine
TAE	Tris buffer containing acetic acid
TBS-T	Tris-Buffered Saline Tween-20

TDP-43	TAR DNA binding protein of 43 kDa
Tg	Transgenic
TNF-α	Tumour Necrosis Factor alpha
UMN	Upper Motorneuron
VH	Ventral Horn
µm	Micro Meter
µmol	Micro Molar
µL	Micro Litre
Wt	Wildtype
Zn	Zinc
zVAD-fmk	z-benzyloxycarbonyl, fmk-fluoromethylketone

Table of Contents

List of Figures and Tables

CHAPTER 1

Introduction

Chapter 1: Introduction

1.1 Motorneuron diseases

Motor neuron disease (MND) is a progressive neurodegenerative disease identified by the degeneration of motor neurons within the central nervous system (CNS). Upper motor neurons (UMN) and lower motor neurons (LMN) are attacked, which leads to progressive muscle weakness, atrophy, and paralysis. Motorneuron disease can be further characterized into four forms: Amyotrophic Lateral Sclerosis (ALS), Progressive Bulbar Palsy (PBP), Progressive Muscular Atrophy (PMA), and Primary Lateral Sclerosis (PLS) (mndassociation.org).

Neurodegenerative disorders are becoming increasingly prevalent and carry a significant economic burden due to the care-intensive nature of the disease. As a growing health problem, a more in depth understanding of MND etiology and pathogenesis is salient.

1.2 Amyotrophic Lateral Sclerosis

Amyotrophic Lateral Sclerosis, also referred to as Lou Gehrig's disease, is a fatal progressive motorneuron disease that has no cure. The disease was first described by French physician and neurobiologist, Jean-Martin Charcot and his colleagues when conducting studies of the spinal cord between 1865-1869 (Kumar *et al*. 2011). The term "amyotrophic lateral sclerosis" would not be given by Charcot until 1874, but his observations of the disease have virtually remained unaltered to present day (Kumar *et al*. 2011). In the United States, the disease is more commonly known as Lou Gehrig's disease in honour of a New York Yankees American baseball player who was diagnosed with the disease in 1936 and who later died of ALS in 1941 at the age of 37. Diagnosis of the disease can be difficult for physicians as the symptoms that are associated with ALS are also common in other types of diseases, for instance myasthenia gravis or Kennedy's disease in which patients also experience muscle weakness. Because there is no specific test for ALS, physicians are forced to rely on a formal set of criteria for diagnosis (Hardiman *et al*. 2011). Most manifestations of typical forms of the disease can be seen first in the limbs as muscle weakness and muscular atrophy, and sometimes slurred speech and dysphagia (Kiernan, 2009; Gordon, 2013). Other symptoms of the disease, although more rare, may include frontotemporal dementia (FTD) and loss of

bulbar function (Kiernan *et al*. 2011). In most cases, patients die as a result of respiratory failure. As ALS is restricted to motorneuron dysfunction the senses of sight, touch, smell, hearing, and tastes are unaffected. In most cases, bladder and eye muscles are not affected.

The median duration of survival for ALS patients after diagnosis are 1-5 years with the average age of onset between 50-60 years (Rowland and Schneider, 2001). As the most common motorneuron disease, ALS has a prevalence of 1-2 per 100,000 people/year and an incidence of 6-8 per 100,000 people/year in the United States (Pasinelli and Brown, 2006). In 1994, a consensus was held by the World Federation of Neurology to determine the diagnosis criteria known as the El Escorial criteria (Miller *et al*. 1999). These disease parameters were revised in 1998 for recognition of laboratory testing and re-named the Airlie House criteria (Miller *et al*. 1999). Based on the degree of certainty of diagnosis, the criteria stated that clinical evaluation must show degeneration of LMN and/or UMN in the same topographical anatomical region of the CNS (Hardiman *et al.* 2011). Patients that are described to have these criteria, discounting other similar diseases, are diagnosed with ALS.

Currently there is only one Food and Drug Administration (FDA)-approved treatment that is available to ALS patients called Riluzole. Unfortunately, Riluzole extends the life of ALS patients by just 3-6 months and is only beneficial for the alleviation of associated symptoms of the disease (Miller *et al*. 2007; Bellingham, 2011). Although the mechanism of action is not clearly understood, Riluzole has been shown to protect cultured neurons from anoxic damage, toxic effects of glutamic-acid-uptake inhibitors, and from the toxic factor in the CSF of patients with ALS (Doble, 1996). There are no drugs present on the market that reverse the disease.

1.3 Amyotrophic Lateral Sclerosis disease pathology

ALS is a multifaceted disease that involves many pathophysiological mechanisms. A complex interaction between genetic and molecular pathways has been widely studied for the treatment of ALS (Pasinelli and Brown, 2006; Vucic and Kiernan, 2009; Hardiman *et al*. 2011; Chen *et al*. 2013). Although, there have been many studies on the cause of ALS, there is little conclusive data on the cause, probable factors, and cure for ALS (Hardiman *et al.* 2011). It has been proposed that the degeneration of motorneurons is primarily caused by a cellular death process known as apoptosis, but other cellular dysfunctions have been studied to explain the progression and onset of ALS, for instance mitochondrial dysfunction (De Vos *et al*. 2008; Magrane and Manfredi, 2009; Shi *et al*. 2009). Mediators of motorneuron death

are known to include: oxidative stress, mitochondrial dysfunction and excitotoxicity, caspase-mediated death, intracellular aggregates, axonal transport dysfunction, and growth factor deficiency (Pasinelli and Brown, 2006).

As a complex disease with many factors, ALS occurs in two distinct forms, sporadic (sALS) and familial (fALS). The familial form of ALS accounts for approximately 10% of cases with patients showing a genetic-linkage (Pasinelli and Brown, 2006; Chen *et al*. 2013). This is far less than the sporadic (sALS) form which occurs in 90% of cases where patients have no family history of the disease (Pasinelli and Brown, 2006; Byrne, Bede *et al*. 2011; Hardiman, van den Berg *et al*. 2011) In fALS, two members of the family must be diagnosed with ALS for sporadic occurrence to be omitted (Byrne, Bede *et al*. 2011). Important breakthroughs in the understanding of the familial form (fALS) of ALS have been beneficial for the identification of genetic factors associated with the disease (Tan, W. *et al.* 2014). One of the most studied genes with many known mutations associated with ALS, *superoxide dismutase* 1 (SOD1) accounts for more than 20% of all fALS cases (Tan, W. *et al.* 2014).

1.3.1 Spinal Cord Structure

ALS involves dysfunction and degeneration of motorneurons of the brainstem and spinal cord. Spinal nerves transmit sensory information from the muscles and CNS, communicating motor commands necessary for voluntary movement. Death of both upper and lower motorneurons is implicated in ALS. The death of upper motorneurons, located in the motor cortex in the brain, leads to hyperexcitability of reflexes and appearance of pathological reflexes, as well as spasticity (Dadon-Nachum *et al*. 2011). Death of lower motorneurons in the brainstem and spinal cord, particularly in the ventral horn, present symptoms that include muscular weakness and atrophy, followed by progressive paralysis (Dadon-Nachum *et al*. 2011). Mouse models are commonly used to study ALS, which provides direct comparison to humans for clinical relevance. This is due to the similarity of human and mouse spinal cord structure. Humans and mice have 31 pairs of spinal nerves. Because the ventral horn of the lumbar spinal cord is rich in motorneurons, the study of this area is salient to understanding one of the first clinical symptoms of ALS, loss of fine motor control of the lower limbs. Motorneurons are abundant in the ventral and lateral horns of the spinal cord in mice. Differences between mouse and human spinal cord organization include a lack of grey matter surrounding white matter in the mouse spinal cord. Another major difference is that motor tracts within the spinal cord of humans are not restricted to the ventral horns. This provides a

significant level of variability in the positioning of the corticospinal tracts between humans and animal models. Lateral columns contain corticospinal bundles in primates and humans, while these bundles can be found in the dorsal columns of rodents (Brown, 1971). Although there are some differences in the structure of spinal cord between murine models and humans, the complexity of the nervous system is comparable for clinical purposes.

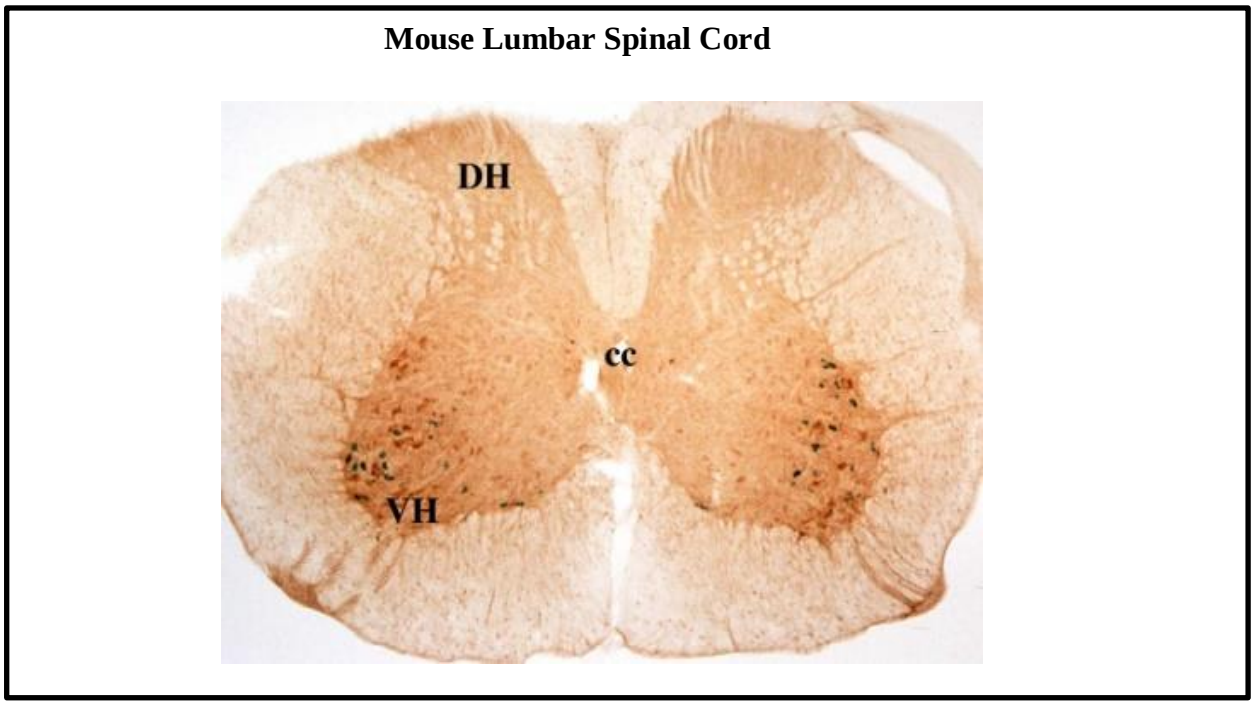

Figure 1.1 Mouse lumbar spinal cord structure

The mouse lumbar spinal cord includes the dorsal horn (DH) which is located posteriorly and the ventral horn (VH) which consist of motorneurons that innervate the lower limbs. Connected to the ventricular system is the central canal (cc) which contains cerebrospinal fluid (CSF). Image adapted from Tokyo Metropolitan Institute for Neuroscience website (http://tmin.igakuken.or.jp).

1.3.2 Genetic mutations implicated in ALS disease pathology

In recent years, accumulating data on genetic and non-genetic causes of ALS has emerged. Several genetic mutations that have been identified as causative of ALS, many of which have been discovered in the last 3-5 years (Al-Chalabi, Jones *et al*. 2012). Due to similar clinical

phenotypes of sALS and fALS cases, there is a need for an understanding of how genetic factors are involved. It is understood that the disease displays a Mendelian pattern of inheritance in fALS. The discovery of many of the genes with mutations in fALS cases occurred via linkage analysis. Genetic linkage studies look for the tendency for genetic markers to be inherited together as a consequence of physical proximity on a chromosome. The genetic basis of ALS was unknown until 1989 when the first locus (ALS1) associated with dominant familial adult-onset ALS was identified. The gene at this locus was identified as SOD1 (Rosen *et al*. 1993). Since this poignant discovery, linkage studies have given rise to 10 loci discovered in association with high-risk ALS (Leblond *et al*. 2014). The most commonly mutated in adult onset ALS are: SOD1, FUS, TARDBP (known as TDP-43), and C9ORF72 (Leblond *et al*. 2014). With this information, studies to investigate the role of fALS-genes in sALS have been on-going. In less than 2% of sALS cases, mutations in SOD1, FUS, and TARDBP have been discovered (Anderson and Al-Chalabi, 2011). In a more recent study, the most common mutation, in the C9ORF72 gene, was found in 6% of sALS cases worldwide and 15-20% cases in Sweden and Finland (Rademakers, R. *et al*. 2013). More information is needed to fully understand the implications of genetic mutations associated with the etiology of ALS. Further study of genetic mutations in ALS could be the key to disease prevention and treatment by inhibition of mutations in high-risk genes.

1.3.3 Superoxide Dismutase One

In ALS, mutations in the SOD1 gene account for over 2% of all cases (Rosen *et al*. 1993). In 1993, a gene encoding enzyme, SOD1, was discovered and has been linked to over 170 genetic defects that are responsible, in part, for facilitating the premature degeneration of motorneurons (Pasinelli and Brown, 2006; Al-Chalabi, Jones *et al.* 2012; Leblond *et al*. 2014). The gene is composed of five exons encoding a 153 amino acid metalloenzyme, which is referred to as Cu/Zn superoxide dismutase 1 (Saccon *et al*. 2013). Highly conserved across species, SOD1 is ubiquitously expressed and the deleterious effect of mutant SOD1 is considered to be due to a toxic gain of function (Fridovich, 1995). Gurney *et al*. have developed a reliable mouse model that overexpresses human mutant SOD1. This widely used mouse model has a point mutation that was originally identified in ALS patients at codon 93, replacing Glycine with Alanine, and is referred to as $SOD1^{G93A}$. With this mutation, mice and rats develop progressive motorneuron degeneration and closely mimic the phenotype seen in ALS patients (Gurney *et al*. 1994). SOD1 binds copper and zinc ions to form a homodimer which, as a dismutase, removes dangerous superoxide radicals by metabolizing

them to molecular oxygen and hydrogen peroxide (Saccon *et al*. 2013). This is necessary as a defence against reactive oxygen species (ROS), which is toxic. When mutant SOD1 protein is misfolded, motorneuron degeneration may be caused by impaired axonal transport, protein aggregate production, inhibited heat-shock proteins, and inhibition of anti-apoptotic proteins (Pasinelli and Brown, 2006).

1.3.4 "Dying-back" hypothesis

In ALS animal models, evidence points to neuronal dysfunction before clinical manifestation of the disease. Muscle weakness is generally one of the first symptoms of the disease in humans, prompting clinical evaluation and eventual diagnosis for ALS patients. Is has been hypothesized that motor unit loss and associated muscle function may precede motorneuron death. This phenomenon known as the "dying-back" hypothesis shows a distal to proximal axonal degeneration and is a common pattern seen in degenerative disorders in the peripheral and central nervous system (Fischer *et al*. 2004; Dadon-Nachum *et al*. 2011). In a study completed by Fischer *et al*., the axon, cell body, and neuromuscular junction (NMJ) was examined at multiple timepoints to show the spatiotemporal progression of motorneuron pathology in the $SOD1^{G93A}$ mouse (Fisher *et al*. 2004). The results showed an earlier denervation of axons at the NMJ at post natal day (pnd) 47, motor axons in the ventral root decreasing between pnd 47 and 80, and loss of α-motor neuron cell bodies in the lumbar spinal cord after pnd 80. The findings from this study may represent an example of a "dying-back" motor neuropathy, where the distal axon degenerates before the onset of symptoms, before neuronal degeneration (Fischer *et al*. 2004). Several mechanisms have been suggested for the "dying-back" pattern leading to progressive loss of motorneurons in ALS. One theory suggests an aggregation of insoluble complexes, possibly mutant SOD1, which causes an insufficient maintenance of the distal axon. As a result, axonal abnormalities that inhibit retrograde transport allow for selective damage to motor neurons which may prevent the cell body from receiving target-derived neurotropic factors (Dadon-Nacum *et al*. 2011). According to the "dying-back" hypothesis, if cell body degradation occurs later in the disease compared to axonal degeneration, a new focus should be set on motor neuron terminals to prevent or delay the progression of ALS.

1.4 Apoptosis

For many diseases, including ALS, apoptosis has been investigated as a possible contributor to disease onset and progression. Apoptosis is a process that is often referred to as programed

cell death (PCD) (Fusch and Stellar, 2011). It is a cell regulation process that occurs in developing and adult tissue and is necessary for homeostasis. The process of apoptosis is regulated by caspases which are cysteine aspartic proteases that cleave at specific sites to generate active fragments, leading to cell death (Graham *et al*. 2011). Apoptosis can be described by its morphology which includes membrane blebbing, cell rounding, cytoskeletal collapse, fragmentation, cytoplasmic condensation, nuclear pyknosis, chromatin condensation/fragmentation, and formation of membrane-enveloped apoptotic bodies (Ghavami *et al*. 2014). Multiple stress stimuli known as activators of apoptosis include: Deoxyribonucleic acid (DNA) damage, circulating cytotoxins, and inflammation (Youle and Strasser, 2008; Yeretssian, Correa *et al*. 2011).

1.4.1 Intrinsic Apoptotic Pathway

The intrinsic apoptotic pathway plays a pivotal role in normal development and homeostatic control of adult tissue. As a result, the role of this apoptotic pathway is important in the study of diseases where excessive or insufficient cell death may play a part in disease pathogenesis. The intrinsic apoptotic pathway has been proposed as a mechanism of motorneuron death in ALS due to mitochondrial dysfunction (Cozzolino and Carri, 2012; Vehviläinen *et al*. 2014). An event is referred to as mitochondrial outer membrane permeabilization (MOMP) is the central key to the intrinsic apoptosis pathway because it allows for the release of cytochrome *c* from the cytosol (Marino *et al*. 2014). Cytochrome c binds to the adaptor protein, apoptotic protease activating factor-1 (Apaf-1) and recruits caspase-9 to form the apoptosome which initiates apoptosis (Fuchs and Stellar, 2011). Activation of MOMP can be triggered by several factors. One such factor includes the upregulation of transcriptional factors like p53 and ogliomerization of BH3-only proteins (BAX or BAK) in the outer mitochondrial membrane (Cory and Adams, 2011). This can stimulate MOMP to form supramolecular channels that allow for the flow of soluble proteins from the intermembrane space of the mitochondria (Cory and Adams, 2011). When MOMP is activated, other pro-apoptotic factors are also co-released with cytochrome-c. These include: 1. Apoptosis-inducing factor (AIF) 2. Endonuclease G (EndoG) and 3. Second mitochondria-derived activator of caspase (SMAC) (Marino *et al*. 2014). Because MOMP activates multiple cell death pathways through the release of these factors, it is considered the “point-of-no-return” in the intrinsic apoptosis pathway. For example, both AIF and EndoG can promote caspase-independent nuclear fragmentation (Kroemer and Martin, 2005).

1.4.2 Cysteine-dependent, Aspartate-Specific Proteases

Caspases are key regulators of the cell death process in apoptosis and also play a part in non-apoptotic processes such as synaptic plasticity, axon guidance, cell differentiation, inflammatory processes, and proliferation (Martinon and Tschopp, 2004; Block and Hong, 2005; Uribe *et al*. 2012). Caspases are proteolytic enzymes, with an affinity to the aspartate and cysteine in their active center, that propagate the apoptotic process through a proteolytic cascade. Caspases are present in the cytoplasm as zymogens, which are inactive enzyme precursors. These latent zymogens contain an N-terminal prodomain. The prodomain is surrounded by the region that forms two subunits containing the catalytic domain. Caspases are heterotetrameric complexes, and include two small and two large subunits with the initial proteolytic activation at specific aspartate sites (Marino *et al*. 2014). Cleavage at the C-terminal, separating the small subunit from the rest of the molecule, culminates an active caspase which autocatalyticlly cleaves off the prodomain (Los *et al*. 1999). Caspases can be classified into two different groups, initiator and effector caspases. Initiator caspases exist as monomers in cells and are self-activated through proximity-induced dimerization, whereas effector caspases are activated by proteolytic processing by and initiator caspase (Shi, 2004). Initiator caspases (caspases-8 and caspases-9) are activated first by upstream signals (Los *et al*. 1995). Effector caspases (caspase-3, caspase-6, caspase-7) are then activated (Fuchs and Stellar, 2011; Ghavami *et al*. 2009). Initiator caspases have long prodomains that bind to large adaptors to promote caspase activation, whereas effector caspases have a short prodomain and execute apoptosis after initiator caspases have been activated (Fuchs and Stellar, 2011). Initiator caspases are activated by external cell death triggering molecules. Caspase-8 is activated by molecules such as Tumour Necrosis Factor alpha (TNF-α), TNF-related apoptosis-inducing ligand (TRAIL), and Fas whereas caspase-9 is generally activated due to internal stress (starvation and cellular dysfunction) which triggers a release of cytochrome *c* from the mitochondria (Fuchs and Steller, 2011). After the addition of the adaptor protein, Apaf-1, this facilitates the formation of the apoptosome complex. Activation of the apoptosome propagates the activation of other caspases which initiates a proteolytic caspase cascade and eventual death of the cell (Friedlander, 2003).

Caspase-6 is activated through proteolytic cleavage, as are the effector caspases caspase-3 and caspase-7. Caspase-6 has a catalytic cysteine located at position 163 of the p20 subunit

and is comprised of a short pro-domain, large subunit (p20), short linker region, and a small subunit (p10) (Klaiman et al 2009). Generated from the zymogen by cleavage at the D23 residue, the active form of caspase-6 is a heterotetramer which consists of two p20 and two p10 subunits and is cleaved between the pro-domain and the p-20 subunit and at the D179 and D193 residues subunits (Srinivasula, S.M. *et al*. 1996).

There is very little information on the mechanisms of caspase-6 activation, but it is often considered downstream of caspase-3 activity (Cohen, G.M., 1997; Slee, E.A. *et al*. 2001; Adrain, C. *et al*. 2005; Guerrero *et al*. 2008). In addition, it has been reported that inhibitor of apoptosis protein (IAP) that inhibit active caspase-3, caspase-7, and caspase-9 do not inhibit caspase-6 (Deveraux and Roy *et al*. 1998). Cowling *et al*. showed that in cytochrome c-induced apoptosis *in vivo*, caspase-6 demonstrates upstream activity and is a major activator of caspase-8 (Cowling and Downward, 2002).

Although the mechanism remains unclear, subsequent work has provided support for the idea that caspase-6 can self-activate *in vivo,* despite being an effector caspase (Wang *et al*. 2010). It has been shown that caspase-6 has the ability to self-activate, but does not induce cell death in HEK293T cells (Klaiman *et al*. 2009). In a study completed by Edgington *et al*. an activity-based probe that labels executioner caspases-3,-6,-7 *in vivo* was utilized to demonstrated that caspase-6 can bind substrates even in the absence of cleavage of the proenzyme and does not require active caspase-3 or caspase-7 in certain conditions (Edgington L.E. *et al*. 2012).

It has also been shown that active caspase-6 has the ability to cleave initiator caspase-2 and caspase-8, but it is not clear how this process is engaged (Slee *et al*. 1999; Inoue *et al*. 2009). The effector caspases are considered phylogenetically similar, but caspase-6 does not share the same substrate recognition sequence as caspase-3 and caspase-7 (Thornberry, N.A *et al*. 1997). Furthermore, caspase-6 is exceptional in that the inhibitor of the apoptosis family of proteins that inhibit caspase-3 and caspase-7 do not inhibit caspase-6 (Deveraux, Q.L. *et al*. 1997). In addition, studies have shown that caspase-6 can be activated in the absence of caspase-3 or caspase-7 activity and can significantly precede the activation of caspase-3 (LeBlanc *et al*. 1999; Doostzadeh-Cizeron *et al*. 2000; Allsopp *et al.* 2000).

1.4.3 Caspase-6, alternative and potential roles

The potential therapeutic role of caspase-6 in neurodegenerative disease has become a research focus due to novel findings implicating caspase-6 in Alzheimer's disease (AD) (LeBlanc, 2013) and Huntington disease (HD) (Waldron-Roby *et al*. 2012). It has been suggested that caspase-6 may have an upstream role in the pathogenesis of neurodegenerative diseases (Graham *et al*. 2011) and may be a possible therapeutic target in neurodegenerative disease, although this remains controversial due to recent studies (Harris et al., 2010) that have published conflicting data. The evidence of caspase-6 activation as an early event in AD has become a focus in recent research due to its association with pathologies that define AD (LeBlanc, 2013). It has been proposed that inhibition of caspase-6 as a novel target for the disease may be beneficial for preventing AD progression (LeBlanc, 2013) and demonstrates a high level of relevancy since caspase-6 is activated in both sporadic and familial forms of AD (Guo *et al*. 2004; Albrecht *et al*. 2007, 2009).

In vivo studies are important to understanding the clinical manifestations and phenotypical effects of *caspase-6* deficiency for neurodegenerative disease. In one study, *caspase-6* deficient mice (Casp6-/-) showed age-dependent behavioral and region-specific neuroanatomical changes, indicating that *caspase-6* deficiency may have an effect in brain regions that are involved in neurodegenerative diseases, for instance the cortex in AD and the striatum in HD (Uribe *et al*. 2012). Active caspase-6 was discovered to be present in brains of patients that did not have apoptotic morphology in patients with AD, which suggests an alternative earlier function for caspase-6 other than an effector caspase (Albrecht *et al*. 2007, Graham *et al*. 2010). Caspase-6 activation has also been shown to correlate with lower cognitive performance in AD (Albrecht *et al*. 2007; Ramcharitar *et al*. 2013; LeBlanc, 2014). Other alternative roles include caspase-6 involvement in B-lymphocyte activation. Watanabe *et al*. demonstrated the regulatory role of caspase-6 in B-lymphocyte activation and differentiation into plasma cells via modification of cell cycle entry *in vivo*, which gives new insight to how to eliminate dysregulated B cells in autoimmune disorders and cancers (Wantanabe *et al*. 2008). In addition, caspase-6 may have a role in regulating inflammatory processes *in vivo* (Berta et al. 2014).

Axon degeneration has been implicated in neurodegeneration and has been linked to the pathogenesis of AD (Kanaan *et al*. 2013) and ALS (Fischer *et al*. 2004). In naturally occurring cell death, axons are removed along with their cell bodies, often as a result of

competition for limiting amounts of trophic factors like NGF (Raff et al., 2002). It has been suggested axon degeneration occurs due to the distinct activation of caspase-6 (Nikolaev *et al*. 2009; Vohra *et al*. 2010), although conflicting data demonstrates that active caspase-3 is required before the activation of caspase-6 to initiate axon degeneration (Slee *et al*. 1999; Walsh *et al*. 2008; Simon et al 2012.) To investigate the potential role of caspase-6 in axons Uribe *et al*., discovered that neuronal growth factor (NGF) withdrawal-induced axonal degeneration could be prevented in caspase-6 null sympathetic cervical ganglion neurons *in vitro* (Uribe *et al*. 2012). Other studies using sympathetic cervical ganglion neurons and dorsal root ganglion (DRG) have shown that withdrawal of trophic support and dynactin I dysfunction result in caspase-6 dependent axonal degeneration (Vohra *et al*. 2010). Other insults to neurons including DNA damage with etoposide, ER stress with tunicamycin, and microtubule destabilization with vinblastine

In contradiction, a study completed by Simon *et al*. demonstrated that NGF withdraw utilizing DRG explants showed that small amounts of active caspase-3 are required to stimulate caspase-6 activation and subsequent axon degeneration *in vitro* (Simon *et al*. 2012). It is possible that this may provide and explanation for previous studies which may have misinterpreted caspase-6 and its direct involvement in axonal degeneration due to failed detection of small amounts of active caspase-3. Additional experiments involving genetic deletion of *caspase-3* in vivo demonstrated more complete axon protection than deletion of c*aspase-6* in *in vitro* sensory neuron cultures (Simon *et al*. 2012). These results and conflicting data from previous studies highlight the need to identify and characterize the potential alternative functions of caspase-6 in neurodegenerative diseases like AD and ALS.

Evidence of caspase activation has been previously identified and evaluated in the ALS mouse model, SOD1 (Pasinelli *et al*. 2000; Li *et al*. 2000). Several experimental observations indicate that mutant SOD1 toxicity involves sequential activation of caspase-1 and caspase-3 in transgenic mice and in cellular models of ALS (Pasinelli *et al*. 2000; Li *et al*. 2000; Geugan *et al*. 2003). It has been hypothesized that caspase-1 activity contributes to an inflammatory pathway causing early astrocytosis in mutant SOD1 mice (Pasinelli *et al*. 2000). Caspase-3 has also been implicated as a mediator of ALS in $SOD1^{G93A}$ mice due to prominent activation in astrocytes which may be direct targets for SOD1-mediated toxicity and subsequent increased disease progression (Pasinelli *et al*. 2000). Until recently much of the research has yet to focus on the understanding of caspase-6, due to the hypothesis that upstream caspases promote a cascade to downstream caspases. The lack of understanding for

caspase-6 mechanisms and biology in neuronal death has propagated novel research in transgenic mouse models for ALS (Graham *et al*. 2006). We expect caspase-6 to be upstream of other caspases and to demonstrate an alternative role from its previously named effector title in the SOD1^{G93A} mouse model.

1.5 Aims of this study

The aim of this project was to assess the role of caspase-6 in amyotrophic lateral sclerosis-mediated neurodegeneration in an animal model of ALS, the SOD1^{G93A} mouse. A growing need exists for a therapeutic treatment paradigm that can be used to treat patients with ALS. Caspases are a major contributor to the apoptotic pathway and have been implicated in neurodegenerative disease pathology (Pasinelli *et al*. 1998, 2000; Uribe *et al*. 2012). Due to a lack of understanding of the role of caspases in ALS disease progression, an investigation of the implications of *caspase-6* deficiency on survival, motor function, and axon viability may identify possible targets for therapeutic intervention. We intend to investigate the role of caspases, namely caspase-6, which has not been fully characterized in motorneurons. We hypothesize that the ablation of caspase-6 in an ALS mouse model, the SOD1^{G93A} mouse, may be protective against axonal degeneration and delay disease onset and progression.

To investigate the role of apoptosis and caspase-6 in ALS, our aims were:

- To characterize pro caspase-6 mRNA expression in skeletal muscle and motorneurons
- To investigate caspase-6 expression levels during disease progression in the ALS mouse model, SOD1^{G93A}
- To generate a tg SOD1^{G93A} mouse deficient in *caspase-6* (tg SOD1^{G93A}; *caspase-6*$^{-/-}$)
- To determine the effect of caspase-6 deficiency on disease onset and symptom progression in the SOD1 mouse model. Rotarod®, grip strength, PaGE, stride length, and body weight will be used to determine disease progression.
- To investigate if *caspase-6* deficiency alters the lifespan of SOD1^{G93A} mice
- To elucidate the effect of genetic deletion of *caspase-6* on axonal/motor endplates at pnd endstage in tg and ntg SOD1^{G93A}; *caspase-6*$^{-/-}$ mice.

CHAPTER 2

Materials and Methods

2.1 Chemical List

Table 2.1 List of Chemicals

Chemical Name	Catalogue No.	Manufacturer	Molarity
Protease inhibitor	P2850	Sigma-Aldrich	
Sodium-Pentobarbitone	267543	Vetoquinol	
Phosphate buffered saline	17-516Q	Lonza	
Jung Tissue Freezing Medium (OTC)	14020108926	Leica Microsystems	
Paraformaldehyde	p6148-500g	Sigma-Aldrich	
Staurosporine	ALX-380-014-M001	ENZO Life Sciences	
DMSO	D8418	Sigma-Aldrich	
OptiPrep Density Gradient Medium	D1556-250ml	Sigma-Aldrich	

2.2 Equipment

Table 2.2 List of Equipment

Equipment	Manufacturer	Model	Application
Rotarod (R)	Steolting	Ugo Basile	Motor Function
Grip Strength Meter	Steolting	Ugo Basile	Motor Function
Cryostat	Leica	3050 S	Cryo sectioning
NanoDrop	Thermo Scientific	NanoDrop 2000c	RNA measurement
Thermal Cycler	MJ Research	PTC-200	PCR
Light Cycler	Roche	Lightcycler 2.0	PCR
Fluorescent microscope	Nikon	TE 200-S	IHC
Semi-dry transfer cell	BioRad	TransBlot SD	Western blotting

Chemiluminescent imager	Fujifilm	LAS 4000	Western blotting
Plate reader	Tecan	GENios	Western blotting

Table 2.3: Dissection equipment

Tools	**Manufacturer**	**Application**
Vannas Sisscors	VWR	Micro dissection
Scissors	VWR	Micro dissection
Forcepts	VWR	Micro dissection
Dissection microscope	Olympus (SZ51)	Micro dissection

2.3 Ethical Approval

Ethical approval was received for this project from the RCSI Research Ethics Committee (Ref: REC447bbb). A licence was obtained from the Irish Government, so that procedures could be legally carried out. This was granted under the Cruelty to Animals Act, 1976 (Ref: B100/4415). A record of sacrificed animals was kept and annual reports were submitted to the Department of Health and Children.

2.4 Animals

Table 2.4: Mouse strains used for this project

Animals	Genotypes	Source	Application
SOD1 ^{G93A}	Transgenic (Tg/ ^{G93A}) Non-Transgenic (ntg)	The Jackson Laboratories, Bar Harbor, Maine, USA	Motor function Primary neuronal cultures Cross breeding
Caspase-6	knockout (*Caspase-6* -/-) heterozygous (*Caspase-6* +/-) wild type (*Caspase-6* +/+)	The Jackson Laboratories, Bar Harbor, Maine, USA	Motor function Cross breeding

2.4.1 SOD1^{G93A} mouse model

SOD1^{G93A} mice C57B6.Cg-Tg (SOD1G93A) 1Gur/J mice were purchased from The Jackson Laboratory (Bar Harbor, Maine) and maintained in house. SOD1^{G93A} breeding pairs were generated on a congenic C57BL/6 background and were inbred for eight generations in the Biomedical Research Facility at RCSI. SOD1^{G93A} mice were housed and bred during this study in accordance with the "working with ALS mice, preclinical testing and colony management", guidelines provided by The Jackson Laboratories (Leitner, 2009). No more than 5 mice were housed per experimental cage. No more than 3 females were housed per breeding cage and were separated to individual cages after evidence of pregnancy was identified. Multiple litters were acquired from several breeding cages to acquire the animals numbers needed for each genotype. Litter size ranged from 4-10 mice per litter and female breeders were replaced after 6 months of age for optimum breeding. Mice were housed at constant temperature (22 °C) on a 12 h light/dark cycle (07:00 h on, 19:00 h off), with *ad libitum* food and water available. Transgenic and ntg SOD1^{G93A} genotypes were confirmed by tail snip DNA extraction and PCR.

2.4.2 *Caspase-6*$^{-/-}$ gene deficient mice

Caspase-6 deficient mice were purchased from The Jackson Laboratory (Bar Harbor, Maine) and maintained in house. Heterozygous mice were backcrossed to a C57 BL/6 background for 10 generations before purchase. After weaning on postnatal day (pnd) 28, pups from litters of the same generation were housed in groups of three to five per cage and maintained at 21±1 °C on a 12-h light/dark cycle (07:00 h on; 19:00 h off), with *ad libitum* access to food and water. No more than 5 mice were housed per experimental cage. No more than 3 females were housed per breeding cage and were separated to individual cages after evidence of pregnancy was identified. Multiple litters were acquired from several breeding cages to acquire the animals numbers needed for each genotype. Litter size ranged from 4-10 mice per litter and female breeders were replaced after 6 months of age for optimum breeding. Transgenic and ntg SOD1^{G93A} genotypes were confirmed by tail snip DNA.

2.4.3 SOD1 ^{G93A} *Caspase-6* $^{-/-}$ cross breeding

The SOD1 ^{G93A}*; caspase-6*$^{-/-}$ colony was generated by cross-breeding male tg SOD1 ^{G93A} mice with *caspase-6*$^{-/-}$ females generating the F1 generation of SOD1 ^{G93A};*caspase-6*$^{+/-}$ mice. From the F1 generation, ntg SOD1^{G93A}*; caspase-6*$^{+/-}$ females were crossed with tg SOD1 ^{G93A}*;caspase-6*$^{+/-}$ males. The F2 colony generated 6 genotypes, ntg SOD1 ^{G93A}*;caspase-6*$^{+/+}$, ntg SOD1 ^{G93A}*;caspase-6*$^{+/-}$, ntg SOD1 ^{G93A}*;caspase-6*$^{-/-}$, tg SOD1 ^{G93A}*;caspase-6*$^{+/+}$, tg *SOD1* ^{G93A}*;caspase-6*$^{+/-}$ and tg SOD1 ^{G93A}*;caspase-6*$^{-/-}$, with all genotypes generated equal in incidence and in a ratio consistent with Mendelian inheritance. The SOD1 ^{G93A}*; caspase-6*$^{-/-}$ colony cross-breeding was confirmed by using tail snip DNA for SOD1^{G93A} and *caspase-6* genes. All six genotypes did not differ in development, fertility, or size to SOD1 ^{G93A} mice. Multiple litters were acquired from several breeding cages to acquire the animals numbers needed for each genotype since heterozygous mice were not utilized.

2.5 Genotyping- DNA extraction

In order to confirm the genotypes of the SOD1 ^{G93A} and SOD1 ^{G93A}; *Caspase-6* cross-breeding colony, a tail snip DNA polymerase chain reaction (PCR) was utilized for analysis. A 2 millimetre section of tail was removed from the mice of interest and placed into an Eppendorf tube and stored at -20 ºC until further processing. DNA was extracted with the use

of a High Pure PCR Template Kit (Roche) according to the manufacturer's instructions. The PCR was performed on the eluted DNA and the samples were run on a 2% agarose gel alongside a 100 bp ladder. Bands were visualized via SYBR Safe DNA gel stain (7%) (Life Technologies). Transgenic SOD1 samples were identified by the presence of a 236 bp band and the wild type allele determined by the presence of a 324 bp band. The presence of a single 620 bp fragment denotes *Caspase*$^{+/+}$ and a single 340 bp fragment denotes the deleted allele in *Caspase*$^{-/-}$ mice. A fragment at both 620 bp and 340 bp denotes *Caspase*$^{+/-}$ genotype.

2.5.1 Polymerase Chain Reaction

Polymerase chain reaction (PCR) refers to the *in vitro* amplification of DNA. Oligonucleotide primers were commercially synthesized to be complementary to the 5 prime (5') and 3 prime (3') ends of the DNA sequence of interest. Samples were run in the thermal cycler with a annealing program that was preset. Each primer sequence required a variation of the standard cycles. Target DNA is denatured at 95 ºC for 10 minutes prior to primer annealing, which occurs between 50-60 ºC according to the individual primer properties. This facilitates the annealing of specific complementary primers to corresponding DNA sequences. Raising the temperature to 72 ºC allows Taq Polymerase to produce a complementary second strand of DNA by exponential elongation of the annealed primers. This process results in the production of double stranded copies of the specific DNA sequence of interest.

2.5.2 Agarose Gel Electrophoresis

After the PCR was performed with the extracted DNA, the samples were run on a 2% agarose gel alongside a 100 bp ladder. Transgenic SOD1 samples were identified by the presence of a 236 bp band and the wild type allele determined by the presence of a 324 bp band. The presence of a single 620 bp fragment denotes *Caspase*$^{+/+}$ and a single 340 bp fragment denotes the deleted allele in *Caspase*$^{-/-}$ mice. A fragment at both 620 bp and 340 bp denotes *Caspase*$^{+/-}$ genotype.

Table 2.5: SOD1^{G93A} primers

SOD1 forward primer 0042 (SOD1 transgenic)	5' CTAGGCCACAGAATTGAAAGATCT 3'
SOD1 reverse primer 0043 (SOD1 transgenic)	5' GTAGGTGGAAATTCTAGCATCATC 3'
SOD1 forward primer 0113 (wildtype allele-specific)	5' CATCAGCCCTAATCCATCTGA 3'
SOD1 reverse primer 0114 (wildtype allele-specific)	5' CGCGACTAACAATCAAAGTGA 3'

Table 2.6: SOD1^{G93A} Reagents/Components

Reaction Component	**Volume (µl)**	**Final Concentration**
ddH_2O	3.52	-
10x AB PCR Buffer	0.84	0.70 X
25 mM MgCl2	0.48	1.00 mM
2.5 mM dNTP	0.96	0.20 mM
20 µm SOD1 primer 0042	0.45	0.75 mM
20 µm SOD1 primer 0043	0.45	0.75 mM
20 µm SOD1 primer 0113	0.80	1.33 mM
20 µm SOD1 primer 0114	0.80	1.33 mM
Taq DNA Polymerase (Invitrogen)	0.04	0.02 U/ul
DNA Loading Dye	1.66	0.69 mM
DNA	2.00	-

Table 2.7: SOD1^{G93A} Cycling Conditions

Step	Temp ºC	Time	Note
1	95	3 min	-
2	95	30 sec	-
3	60	30 sec	-
4	72	45 sec	Repeat steps 2-4 for 35 cycles
5	72	2 min	
6	4	-	hold

Table 2.8: Caspase-6 primers

Caspase-6 (common)	5’ CTCCACGGCCTAATGCAGTTCCTGG 3’
Caspase-6 (wildtype allele-specific)	5’ CTGAGGGGCGGAGCACCTTTGCTG 3’
Caspase-6 (mutant allele-specific)	5’ GCCTTCTTGACGAGTTCTTCTGAGG 3’

Table 2.9: Caspase-6 Reagents/Components

Reaction Component	Volume (µl)	Final Concentration
ddH_2O	4.32	-
10x Kappa Rxn Buffer (B)	1.20	1.00 X
2.5 mM dNTP	0.96	0.20 mM
20 µm *Caspase-6* primer (common)	0.60	1.00 µM
20 µm *Caspase-6* primer (wildtype)	0.60	1.00 µM
20 µm *Caspase-6* primer (mutant)	0.60	1.00 µM
KAPATaq DNA Polymerase	0.06	5 U/ul
DNA Loading Dye	1.66	0.69 mM
DNA	2.00	-

Table 2.10: *Caspase-6* Cycling Conditions

Step	Temp ºC	Time	Note
1	94	3 min	-
2	94	30 sec	-
3	58	30 sec	-
4	72	45 sec	Repeat steps 2-4 for 35 cycles
5	72	2 min	
6	4	-	hold

2.6 Motor Function Analysis

Motor Function performance included Rotarod (Steogling, Italy), grip strength (Ugo Basile), PaGE (Paw Grip Endurance), stride length, and weight measurement. Analysis was performed in the Behavioural Testing Room located in the Biomedical Research Facility (BRF) in RCSI. Tests were recorded in the same sequence twice weekly and the average was used for data analysis. All of the mice used were trained to use the motor function equipment from pnd 70. Prior to performance analysis, each strain of mice was age, sex, and litter matched, with the exception of ntg SOD1^{G93A}; *caspase-6* $^{+/+}$ and tg SOD1^{G93A}; *caspase-6* $^{+/+}$ control groups (Ludolph, 2010). A five minute rest period was given between each test to ensure maximum ability per recording.

2.6.1 Rotarod

The Rotarod test provides a measurement of forelimb strength. Parameters for the Rotarod test were set to accelerating rotations per minute (RPM) from 5-42 RPM over a 180 second time frame. Mice were placed on a rotating bar with separation panels and were required to remain on the accelerating bar until they dropped to a magnetic plate below that would record the endpoint of the measurement. The mice were trained to remain on the bar for 10 days prior to experimental data recording.

2.6.2 Grip Strength

Grip strength meter is a sensitive and accurate method to detect the onset and progression of symptoms in $SOD1^{G93A}$ mice (Weydt *et al*. 2003; Brooks and Dunnett, 2009). The grip strength meter (Ugo Basile, Italy) measures forelimb strength and the force applied (g) to resist the involuntary backward movement when a mouse is pulled by its tail. The mice instinctively grasp a trapeze shaped bar when they are dragged across it, recording the force. Grip strength meter analysis was followed Rotarod$^{(R)}$ analysis with a resting period of at least 5 minutes between both. The mice were given 3-4 attempts to gain the maximum grip strength recording. Mice were trained to grasp the bar for 10 days prior to experimental data recording.

2.6.3 PaGE

The PaGE test is used to measure the strength of the forelimbs and hindlimbs. Loss of function in the limbs is an indication of disease onset and progression. The PaGE test requires the mouse to use both fore and hindlimbs to hang upside down on a mesh metal grate for as long as possible or a maximum of 60 seconds.

2.6.4 Stride Length

The stride length test analyses motor function integrity in the hindlimbs by measuring changes in gait. The hind feet are painted with a non-toxic paint and mice are trained to walk on a strip of paper. Three consecutive paw prints on the left and right foot are measured and averaged for analysis. This test is completed once a week from pnd 63 to endstage.

2.6.5 Body Weight

Weight analysis is used as an indication of disease onset and progression. Weight for each mouse was measured on a standard weighing scale and recorded in the afternoon for consistency. The weight for each mouse was taken twice weekly and averaged. One factor in defining endstage status is determined with a 20% reduction in body weight (Kieran, Kalmar *et al*. 2004; Kieran, Hafezparast *et al*. 2005; Knippenberg, Thau *et al*. 2010).

2.6.6 Righting Reflex

ALS disease end stage can be determined by the loss of righting reflex. This occurs when a mouse has reached the point where when it is placed on its side it fails to right itself after 30 seconds (Ludolph, Bendotti *et al*. 2010). This method of characterizing the end stage timepoint (which occurs around pnd 150-160) is the most consistent determination of end stage ALS in $SOD1^{G93A}$ mice (Leitner, 2009).

2.7 Time-mating procedure

C57/BL/6 female mice were time mated at 8 weeks old to produce E12 embryos. The time mating procedures were adapted to alter the female's oestrous cycles using the Whitten Effect (Green 1976). Male mice were housed individually for 3 days prior to breeding. Females were housed at 4-5 animals per cage, for 2 days, which brings the females into their oestrous cycles simultaneously upon exposure to male androgens or bedding from male cages. The female mouse oestrous cycle occurs over 4-5 days, with ovulation on day 3, therefore yielding the maximum number of pregnancies within a short time. Females were added to the male cages on Monday morning and removed on Wednesday afternoon, to facilitate nocturnal breeding. The females were checked at 7 am for the presence of a copulatory plug and records were taken to estimate E0. Female mice were also weighed prior to time mating and at the E7 and E12 stages of pregnancy.

2.8 Transcardial Perfusion

Transcardial perfusion in mice was carried out with Phosphate Buffered Saline (PBS) to remove blood from tissues of interest. Mice were given i.p. injection of sodium pentobarbitone (Dolethal®; Vetoquinol, Buckingham, United Kingdom) (40 mg/kg) and placed in a separate cage from littermates until anaesthetic took effect. When animal was unconscious the pinch reflex was used to ensure complete anaesthesia. The ribs and diaphragm were cut away to expose the heart. A 26 gauge needle and syringe filled with 1x PBS was placed into the left ventricle of the heart and the right atrium was cut at the same time as the intracardial perfusion commenced. To ensure that each animal was completely perfused, 10-20ml of 1x PBS was used. After the perfusion was complete, the spinal cord was dissected and microdissected into thoracic and lumbar sections by cutting at the

theracolumbar junction. This area can be noted by a bulge in the spinal cord. Muscle tissue was post-fixed in 4% paraformaldehyde-PBS (7.4 pH) for 20 minutes at room temperature, washed with PBS for 5 minutes, then transferred into 30% sucrose overnight (until the tissue sank to bottom of cryotube). Tissue was air dried and mounted in Jung (OTC) tissue freezing medium (Leica Microsystems, Nussloch, Germany). Dissected spinal cord and skeletal muscle were snap frozen using liquid nitrogen in cryotubes and stored at -80^{o}C.

2.9 Immunohistochemistry

Muscle sections were stained with alpha-bungarotoxin (Molecular Probes, 1:10,000), which binds with high affinity to the α-subunit of the nicotinic acetylcholine receptor (AChR) of neuromuscular junctions, for 20 minutes at room temperature. After rinsing, muscle sections were post-fixed in 4% paraformaldehyde (PFA) for 10 minutes. Sections were rinsed thoroughly and cover slipped for analysis under a fluorescent microscope.

Table 2.11: Molecular Probes Used for Immunoblotting

Antibody Name	Catalogue number	Antibody type	Manufacturer	Dilution
α-Bungarotoxin	B-13422	Alexa Fluor 488	Life Technologies	1:10,000

2.10 Microscopy

Sections were analysed with a Nikon TE200-S fluorescence microscope. Images were captured using the Wasabi and Spot imaging software and saved as TIFF files.

2.11 Cell Culture

NSC-34 (motorneuron/neuroblastoma hybrid) cell line was provided by the Cashman laboratory (Cashman *et al*. 1992), and GL-261(astrocytoma) and BV-2 (immortalized microglia) cell lines were purchased from the American Type Culture Collection (ATCC). The ATCC contains a large collection of microbial stocks, including microbes containing mammalian DNA segments. NSC-34 cells were maintained in Dulbecco's Modified Eagle's Medium (DMEM) supplemented with 10% Fetal Bovine Serum, 2mM L-glutamine, 100

units/ml Penicillin and 0.1% Streptomycin. GL-261 and BV-2 cell lines were maintained in Roswell Park Memorial Institute medium (RPMI) supplemented with (10% Fetal Bovine Serum, 2mM L-glutamine, 100 units/ml Penicillina and 0.1 mg/ml Streptomycin).

2.12 Western Blotting

2.12.1 Sample Preparation for tissue

Spinal cord was dissected from SOD1^{G93A} and SOD1^{G93A}; *caspase-6* mice at pnd 70, pnd 90, pnd 120, and pnd endstage (150-160 days) and snap frozen until homogenate processing. Samples were homogenized in Radioimmunoprecipitation assay (RIPA) lysis buffer (Tris-Cl pH7.4, NaCl, Sodium Dodecyl Sulfate Polyacrylamide (SDS), (Sodium Deoxycholate, Triton x100) with an IKA T-25 Basic Ultra-Turrax homogenizer and incubated on ice for 20 minutes. The samples were then centrifuged at 13,000 g for 20 minutes at 4 ºC to remove any debris resulting in a clear supernatant which was stored at -80 until protein quantification.

2.12.2 Sample Preparation for cell lines

NSC-34, GL-261, and BV-2 cell lines were trypsinized and washed once in PBS. The PBS was removed and the pellet was re-suspended in RIPA lysis buffer, volume dependent on cell pellet size. Samples were then triturated approximately 20 times each with a p200 pipette to resuspend the pellet. The tubes were left on ice to lyse for 20 minutes. Following this, the samples were centrifuged at 13,000 g for 20 minutes at 4 ^{o}C. The supernatant was removed for protein quantification. Samples were stored at -80 ^{o}C.

2.12.3 Protein Quantification

To measure the total protein concentration of brain and spinal cord homogenates a bicinchoninic acid (BCA) protein quantification kit was used (Uptima). To determine protein concentrations a BSA standard was used to generate a standard curve. In this protein assay, sterile flat bottomed 96 well plates were used and the BSA standard was loaded firstly in triplicate (0 µg, 2 µg, 4 µg, 6 µg, 8 µg, 10 µg). Each well was loaded with 2 µl of sample for measurement in triplicate. Sodium Chloride (0.9% NaCl) (150 µl) was added to each well.

In addition, three reagents included in the protein quantification kit (A, B, and C) were mixed at a ratio of 25:25:1 and 150 µl added to each well. The BCA assay was incubated at 37ºC in

the dark for 30 minutes. Protein concentration were determined by measuring the absorbance at 560 nm. The blank background absorbance reading for the 0 µg of BSA was subtracted from each sample. Protein samples for western blot were made up to 40 µg of protein in laemmli buffer (0.5M Tris-Cl, pH 6.8, 10% SDS, 30% glycerol, 5% β-mercaptoethanol, 0.012% bromophenol blue) (6x made up to 1x with sample). The samples were boiled at 95 °C for 5-10 min before being loaded onto an SDS-Page gel.

Table 2.12: Stacking gel composition

Stacking gel (3 mL)		
Gel percentage	**5%**	**Units**
H_2O	2.1	mL
30% Acrylamide	500	µL
1.0 M Tris-HCl (pH 6.8)	380	µL
10% SDS	30	µL
10% APS	30	µL
TEMED	7	µL

Table 2.13: Resolving Gel Composition

Resolving gel (5 mL)				
Gel percentage	10%	12%	15%	Units
H_2O	1.9	1.6	1.1	mL
30% *bis*-/acrylamide mix	1.7	2.0	2.5	mL
1.5 M Tris-HCl (pH 8.8)	1.3	1.3	1.3	mL
10% SDS	50	50	50	µL
10% APS	50	50	50	µL
TEMED	5	5	5	µL

The Mini-PROTEAN Tetra Electrophoresis System from BioRAD was used to prepare the gels. The assembly was arranged to cast a gel that was 1.5 mm in width, 8 cm x 8 cm in length and breadth. The resolving gel was left for approximately 20 minutes to allow for polymerization. Stacking gel was added and a 10 well-comb was inserted. The gel was then left to set for 20 minutes.

2.12.4 Electrophoresis

Gels were loaded into the BioRAD electrophoresis system which includes a mounting hold unit and two electrodes at each end. Negatively-charged proteins migrate downwards, toward the anode. Samples were normalized to equal volume with laemmli buffer and in equal concentration (40 µg). Samples were then heated for 10 minutes at 95^{o}C to denature proteins. Electrophoresis buffer (25 mM Tris-Cl, pH 8.3, 250 mM glycine and 0.1% SDS) was added to up to the brim of the inner chamber of the BioRad mounting system. Four microliters of protein marker (PageRuler, Fermentas, Germany) is added to the last well to determine migration and molecular weight. Samples (40 µg) were loaded into the wells and the gels were set to run at 80 V to drive the samples through the stacking gel. After clearance of the stacking gel (aprox 20 minutes), the voltage was increased to 120 V through the resolving gel. Samples were run until the blue bromophenol dye-front reached the bottom of the gel. Following gel electrophoresis, the proteins were blotted onto a nitrocellulose membrane using the semi-dry transfer method.

2.12.5 Semi-dry transfer

Whatman Filter paper was cut to measure 9cmx6cm and 8cmx5cm and nitrocellulose membranes (Protran™) were cut to measure 9.5cmx6.5cm. The nitrocellulose membranes were activated for 5 minutes in deionised water and then placed in transfer buffer (25 mM Tris, 192 mM Glycine, 20% methanol (v/v) and adjusted to pH 8.3). Filter paper was soaked in transfer buffer prior to application on the BioRad transfer system. Filter paper was placed directly on the anode connected plate and an activated membrane was placed on top of the filter paper. The gel was removed from the electrophoresis system and the stacking gel was discarded before placing the resolving gel on top of the nitrocellulose membrane. Caution was taken to avoid air bubbles between the gel and the membrane. This was followed by two more pieces of filter paper on top of the gel. The transfer was run at a constant voltage of 18

V for ~60 minutes. Following completion of the transfer, membranes were rinsed in TBS-T (15 mM Tris-HCl, 200 mM NaCl, pH 6.8 and 0.1% Tween-20). Immersion in Ponceau Red (1% Ponceau S in 5% acetic acid) was used to check the success of the transfer and even protein loading across the lanes. The membranes were washed in TBS-T to remove all traces of Ponceau Red and blocked for 1-2 hours in 5% low fat milk in TBS-T.

Table 2.14: Primary Antibodies for Western Blot

Primary Antibody	**Species**	**Manufacturer**	**Dilution**	**Incubation**
Anti-Human SOD1	Human	Sigma-Aldrich	1:1,000	2 hours RT
Anti-caspase-6	Rabbit	Cell Signalling (#9762)	1:1,000	Overnight
cleaved-caspase-6	Goat	Santa Cruz (sc-22177)	1:1,000	Overnight
Cleaved- caspase-3	Rabbit	Cell Signalling (#9661)	1:1,000	Overnight
Anti-beta-actin	Mouse	Sigma-Aldrich (A5441)	1:5,000	2 hours RT
Anti-Tubulin	Rabbit	Sigma-Aldrich (T9026)	1:5,000	2 hours RT

Table 2.15: Secondary Antibodies for Western Blot

Secondary Antibody	Manufacturer	Dilution	Incubation
Peroxidase conjugated goat anti-mouse	Jackson ImmunoResearch Laboratories Inc., USA	1:5,000	2 hours RT
Peroxidase conjugated goat anti-rabbit	Jackson ImmunoResearch Laboratories Inc., USA	1:5,000	2 hours RT
Peroxidase conjugated rabbit anti-goat	Jackson ImmunoResearch Laboratories Inc., USA	1:5,000	2 hours RT

2.12.6 Immunoblotting

Proteins of interest were detected on the membrane by specific primary antibodies which bind to target antigens with high affinity. To minimize non-specific antibody binding, membranes were first incubated in blocking buffer for 1 hour at 4 ºC. Primary and secondary antibodies were incubated in blocking buffer (5% non-fat dry milk in 0.1% TBS-T). Membranes were incubated overnight at 4°C with the primary antibodies listed in Table 2.14. Following primary antibody incubation, membranes were washed three times in TBS-T and incubated with horseradish peroxidase-conjugated (HRP) secondary antibodies (Table 2.15) (1:5000, Jackson ImmunoResearch) at room temperature for 2 hrs. Membranes were subjected to an additional three washes in TBS-T before HRP signal detection using enhanced chemiluminescence (ECL) detection reagent (Amersham Biosciences, Buckinghamshire, UK). Several exposure times were used to accurately detect signal by using a Fujifilm LAS 4000 digital imaging system. An image of the protein marker was also captured with the white light. Following the identification of the desired band, membranes were incubated with loading control β-Actin or α-Tubulin (pending the success of β-Actin) for 2 hrs at room tempature (1:5000, Jackson ImmunoResearch). Membranes were washed three times in TBS-T and incubated with HRP secondary antibodies (Table 2.15). Membranes received an additional three washes in TBS-T before HRP signal detection using ECL detection reagent and multiple exposures were implemented to accurately detect signal using the Fujifilm LAS 4000 digital imaging system.

2.13 Densitometry

Densitometry is used to measure protein levels on a western blot. A Fuji LAS 4000 CCD system generated the resulting images after the membrane was exposed to chemiluminescence. The images were analysed using Image J and Adobe Photoshop software. Loading controls included β-Actin or α-Tubulin. Loading control values are subtracted for each band to give the loading intensity of individual well. Differences in intensity are represented as protein expression relative to control, untreated levels. Each sample was run a total of three times (n=3) to control for variance. Due to limited starting material and minimizing animal numbers, repeats of this experiment were not performed, therefore data analysis was completed using one Western blot for each timepoint.

2.14 OptiPrep

Time mated C57BL/6 mice were sacrificed at E12 and hysterectomies were performed to remove embryos. Motorneuron rich ventral horns of embryonic mouse spinal cords spinal cords were removed under sterile conditions and mixed neuronal cultures were prepared using an adapted version of previously described protocols (Gingras, Gagnon et al. 2007). Ventral horns are micro-dissected following neurogenesis at E10-12. All operations were carried out at room temperature. After dissection, the samples were incubated in Solution D for 20 mins (Optiprep kit, Sigma-Aldrich) to begin the isolation of total cellular fraction. The samples were dissociated by repeated passage through a syringe needle (21 gauge). The subsequent suspension was layered over Solution C and centrifuged at 12,000 x g for 10 minutes to remove all cell debris. The supernatant was discarded and the pellet suspended in OptiPrep solution diluted with Solution B to give a 1.06 g/ml solution, equivalent to 5.2 g/50 ml iodixanol. The re-suspended pellet was layered over the 1.06 g/ml solution and centrifuged at 8,000 x g for 15 minutes. The banded cells were collected in the upper layer. To pellet the motorneuron fraction, the samples were centrifuged at 7,000 x g for 10 minutes for collection.

2.15 Quantitative reverse transcriptase polymerase chain reaction

Gastrocnemius muscle was dissected from ntg SOD1^{G93A}; *caspase-6*$^{-/-}$ and ntg SOD1^{G93A}; *caspase-6*$^{+/+}$ mice at pnd 35 and homogenized for mRNA extraction. Additionally, primary mixed neuronal cultures were prepared from the motorneuron rich ventral horns of embryonic

mouse spinal cords via OptiPrep to generate pure motorneurons from C57/BL/6 mice. Total RNA was extracted from astrocytoma, microglia, and pure motoneurons and cortical neurons extracted from embryonic mouse spinal cord. Real-time quantitative PCR (qPCR) was used to determine pro caspase-6 levels.

2.15.1 Total RNA preparation from tissue

Gastrocnemius muscle samples were placed in a glass mortar and pestle which was previously cooled to -80ºC. Each muscle sample was homogenized individually and the mortar and pestle was cleaned between each sample with 100% ethanol to prevent cross-contamination. Each muscle was weighed and trimmed to a standard weight of 140 mg. To prevent the muscle tissue from thawing, the mortar and pestle was placed on ice and liquid nitrogen was poured onto the muscle just before grinding the fibrous tissue into into a fine powder. The resulting powder was collected into an Eppendorf tube containing RIPA buffer and placed on ice until further processing.

Samples were thawed on ice and homogenized in 800 µL of trizol under the fume hood using a needle and syringe or a homogenizer in a glass round bottomed tube. Homogenized samples were transferred to an Eppendorf tube and centrifuged at 12,000 x g for 10 minutes at 4 ºC. Samples were incubated for 15 minutes at room temperature before adding 200 µL of chloroform. The Eppendorf tubes containing Trizol and chloroform were shaken by hand and incubated for 3 minutes at room temperature. Samples were centrifuged at 13,000 x g for 15 minutes at 4 ºC separating the aqueous chloroform, protein and trizol phases. The aqueous phase was transferred to a new Eppendorf tube containing 450 µL of isopropanol for RNA precipitation. Samples were incubated for a further 10 minutes at room temperature and centrifuged again at 16, 000 x g for 15 minutes at 4 ºC. The supernatant was removed leaving a pellet of RNA which was washed with 1 mL of 75% ethanol by vortexing the sample and centrifugation at 12,000 x g for 5 minutes at 4 ºC. Residual ethanol was allowed to evaporate off before re-dissolving the RNA in 30 µL of Diethylpyrocarbonate (DEPC) water (Ambion) which is an efficient deactivator of RNase. The RNA product was then incubated at 58 ºC for 10 minutes at 800 x g, and then stored at -80 ºC until cDNA synthesis.

2.15.2 Total RNA extraction from tissue

RNA was extracted using Qiazol extraction and/or RLT-buffer lysis and RNeasy processing according to the manufacturer's guidelines (Qiagen, Sussex, UK). cDNA synthesis was

performed based on equal amounts of RNA using the Superscript™ II Reverse Transcriptase (Invitrogen, California, USA). qPCR analysis was performed using the LightCycler (Roche Diagnostics, Basel, Switzerland) and the QuantiTech SYBR Green PCR kit (Qiagen) following the manufacturer's recommendations and standard cycles and melting temperatures. The sense and antisense primers for glyceraldehyde-3-phosphate dehydrogenase (*gapdh*) were sense 5′-AAC TTT GGC ATT GTG GAA GG-3′, antisense 5′-ACA CAT TGG GGG TAG GAA CA-3′; for*SOD1* 5′-TCC CCA GAG ACA TGG AGA AC-3′ and 5′-GTC GTG TGG AAG ACA TCA CG-3′. RNA levels were normalized to *gapdh* mRNA expression and expressed as n-fold expression over control.

2.15.3 RNA quantification

RNA from tissue samples and cells were assessed for concentration and quality using the NanoDrop® ND-1000 spectrophotometer. The NanoDrop® ND-1000 is a full-spectrum (220-750nm) spectrophotometer that measures 1µl samples with high accuracy and reproducibility. For each sample the following results were recorded:

- Concentration (ng/µl): sample concentration in ng/µl
- 260/280**:** ratio of sample absorbance at 260 and 280nm. The ratio of absorbance at 260 and 280nm is used to assess the purity of DNA and RNA. A ratio of ~1.8 is generally accepted as "pure" for DNA; a ratio of ~2.0 is generally accepted as "pure" for RNA. Values above 2.2 would indicate the presence of protein whereas values below 1.8 would indicate an element of sample degradation.

2.15.4 cDNA synthesis for mRNA

Total RNA was reverse transcribed to produce cDNA from total RNA and cDNA synthesis was carried out in a thermal cycler. A standardized run template was established and used to facilitate cDNA synthesis from tissue samples. DNase treatment was carried out to prevent carryover of genomic DNA. 2 µg of total RNA from each sample was added to an Eppendorf tube containing 1 µL 10 X DNase Buffer, 1 µL DNase I H_2O to give a final volume of 10 µL. Samples were incubated at room temperature for 15 minutes before adding 1 µL EDTA. Samples were then heated to 65º C for 8 minutes before the addition of 1 µL random hexamers (DN6) and incubated at 65º C for 2 minutes and transferred immediately to ice. A mix containing 2 µL H_2O, 4 µL 5 X Buffer, 1 µL 0.1 M DTT and 1 µL 10 mM dNTPs was added to each tube and samples were heated at 42º C for 2 minutes. 1 µL Superscript II^{TM}

Reverse Transcriptase was added to each sample and heated at to 42º C for 50 minutes followed by 75º C for 10 minutes. Samples were held at 4 ºC when the run was complete and were stored at -20 ºC until quantified. Two controls were included in each cDNA synthesis run wherein one RNA sample was substituted with H_2O and a second sample was run without reverse transcriptase (No RT).

2.15.5 Real time quantitative analysis

Quantitative reverse transcriptase PCR (RT-qPCR) measures the relative number of mRNA transcripts of a gene in comparison to a control (beta-actin) transcript. A Lightcycler 2.0 from Roche Diagnostic using glass capillaries was used to measure mRNA expression by fluorescence. A master mix solution containing 10 µL of SYBR Green, 1 µL of forward and reverse primer mix (25 µM) and 7 µL of dH_2O was added to each cDNA sample (2 µL) at 4 ºC. Primers were reconstituted and stored at a concentration of 100 µM. RNA free water (2 µL) was added to the glass capillary tubes followed by 18 µL of the RNA samples. RT-qPCR experiments included two controls, the first control contained control cDNA and the second contained DNA/RNA free water as a substitute for cDNA. Control samples were treated under the same conditions. Lightcycler capillary tubes were centrifuged at 600 x g for 10 seconds prior to loading into the Lightcycler. A programme was determined for each mRNA in which the melting temperature and cycle number were optimized for each primer set according to the template (Table 2.16).

Table 2.16: Lightcycler program template

Function	Temperature	Time	Cycles
Denaturation	95 ºC	10 minutes	1
Amplification	95 ºC	30 seconds	40
Amplification	60 ºC	30 seconds	40
Amplification	72 ºC	30 seconds	40
Melting Curve	95 ºC	1 second	1
Melting Curve	65 ºC	15 seconds	1
Melting Curve	95 ºC	1 second	1
Melting Curve	40 ºC	1 second	1
Cooling/ storage	4 ºC	6 hours	1

Table 2.17: List of primer sequences

Target Gene	Sense primer (5')	Antisense primer (3')
Caspase-6	TGAAATGCTTTAACGACCTCAG	GTGGCTTGAAGTCGACACCT
Beta-actin	AGGTGTGATGGTGGGAATG G	GGTTGGCCTTAGGGTTCAGG
GAPDH	AAC TTT GGC ATT GTG GAA GG	ACA CAT TGG GGG TAG GAA CA

2.16 Statistical analysis

Motor function was assessed by ANOVA and *post-hoc* analysis by Tukey's multiple comparison test. A statistically significant difference between recordings was considered when $p \leq 0.05$. All data are expressed as mean ± SEM. All behavioral studies were age, gender and litter matched and included 12 mice per treatment group or genotype in accordance with ALS guidelines for pre-clinical studies (Ludolph, Bendotti *et al*. 2007; Ludolph, Bendotti *et al*. 2010). Kaplan-Meier survival plots were used to analyse survival between colonies. For Western blot analysis, two-tailed Mann-Whitney U-tests for non-parametric data or two-tailed student t-tests for normally distributed data sets were used. Statistical analysis was performed by PASW statistics version 20 Software (IBM, Dublin, Ireland).

For gene expression analysis via qPCR, fold changes were generated using the Comparative CT method which uses the following arithmetic formula to achieve results for relative quantification: **$2^{-\Delta\Delta CT}$**

Relative quantification established the change in expression of *caspase-6* relative to the nervous tissue reference sample. In the comparative CT method, relative quantity (RQ) of other sample types was expressed relative to the reference sample that was used as the basis for comparative results. Therefore, the reference was the 1X sample and all other quantities were expressed as an n-fold difference relative to the reference. ΔCT was achieved by subtracting the endogenous control CT from samples' CT, therefore ΔCT = CT (sample) – CT (endogenous control). The ΔΔCT was worked out by comparing expression levels relative to the reference sample, thus ΔΔCT = ΔCT (sample) - ΔCT (calibrator). Using the $2^{-\Delta\Delta CT}$ method, the data presented is the fold change in *caspase-6* gene expression normalised to the endogenous reference gene β-actin and relative to the nervous tissue sample.

Biological and technical replicates were carried out for each sample type, and statistical significance was determined using a paired 2-tailed student t-test. Statistical significance was set at p-value <0.05.

CHAPTER 3

Caspase-6 expression in motorneurons and during motorneuron degeneration in SOD1^{G93A} mice

Chapter 3: Caspase-6 expression in motorneurons and during motorneuron degeneration in SOD1^{G93A} mice

3.1 Introduction

Caspase-dependent apoptosis is a major subject of interest in neurodegenerative research. Studies have shown that evidence for apoptotic cell death is present in the form of chromatin condensation and reduction in cell size at the onset of symptoms in SOD1^{G93A} mice, as compared to wild type littermates (Pasinelli and Houseweart, 2000). Li *et al*. demonstrated that inhibition of caspase-1 and caspase-3 via apoptosis inhibitor zVAD-fmk (z-benzyloxycarbonyl, fmk-fluoromethylketone) delays disease onset in SOD1^{G93A} mice but has no effect on survival, the most clinically relevant aim (Li *et al*. 2000). Caspase-1 is activated before the onset of symptoms whereas caspase-3 is activated at later stages of the disease which elucidates motorneuron death at an increased rate (Pasinelli and Houseweart, 2000). Additionally, caspase-6 activation has been observed before caspase-3 in excitotoxic models *in vivo* (Ferrer, I. *et al*. 2000; Henshall *et al*. 2002). It has also been shown that unlike other effector caspases, caspase-6 has the ability to self-activate, but does not induce cell death in HEK293T cells (Klaiman *et al*. 2009). A study completed by Edgington *et al*. confirmed this finding by utilizing an activity-based probe that labels executioner caspases-3,-6,-7 *in vivo*. The results demonstrated that caspase-6 can bind substrates even in the absence of cleavage of the proenzyme and does not require active caspase-3 or caspase-7 in certain conditions (Edgington L.E. *et al*. 2012).

Caspase-6 is widely expressed in the brain (Guo *et al*. 2004, Albrecht *et al*. 2007, Graham *et al*. 2010) and peripheral tissues (Singh *et al*. 2002). Pro caspase-6 is ubiquitously expressed as evidenced by study completed by Raina *et al*. which showed that caspase-6 was found in association with senile plaques in almost all cases of AD and was present at low levels in neurons in both AD and control cases (Raina *et al*. 2001). Increased expression of pro caspase-6 seen in human fetal tissue and brains of AD subjects (Raina *et al*. 2001; Godefroy *et al*. 2013) may contribute to mediator of apoptotic cell death in neurodegenerative disease; it is salient to understand what occurs when caspase-6, an effector caspase that is typically considered to be downstream of caspase-3, is inhibited *in vivo*, therefore we decided to investigate the role of caspase-6 in the SOD1^{G93A} animal model.

3.2 Results

3.2.1 Caspase-6 mRNA is expressed in motorneurons

We aimed to explore whether *caspase-6* was expressed in motorneurons. We utilized quantitative PCR (qPCR) to determine caspase-6 mRNA levels in nervous tissue (neocortex) as well as ntg SOD1^{G93A}; *caspase-6*$^{-/-}$ gastrocnemius muscle (pnd 35), ntg SOD1^{G93A}; *caspase-6*$^{+/+}$ gastrocnemius muscle (pnd 35), and compared this with purified primary motorneurons, microglia-enriched and astrocyte-enriched cultures from primary E12 spinal cord tissue. We were interested in expression of *caspase-6* mRNA levels in astrocytes and microglia due to the hypothesis that the unregulated activation of these cell types is a response to neuronal death in ALS and propagates neuronal injury which may lead to the progression of the disease (Hall *et al*, 1998, Clement *et al*, 2003, Block and Hong, 2005). It has also been shown that caspase-6 is involved in regulation of astrocyte survival in HIV neurodegeneration (Noorbakhsh *et al*. 2010). We were also interested in *caspase-6* mRNA expression levels in gastrocnemius muscle from ntg SOD1^{G93A}; *caspase-6* mice due to the hypothesis that caspase-6 is implicated in the "dying-back" phenomenon which shows a distal to proximal axonal degeneration in the SOD1^{G93A} mouse model (Fischer *et al*. 2004) and may be involved in degeneration of skeletal muscle. Primary mixed neuronal cultures were prepared from the motorneuron rich ventral horns of embryonic mouse spinal cords. Ventral horns were micro-dissected following neurogenesis at E10-12. Optiprep was used to generate purified motorneuron cultures. Total RNA was extracted from neocortex nervous tissue, microglia and astrocytes from primary tissue as well as ntg SOD1^{G93A}; *caspase-6*$^{-/-}$ gastrocnemius muscle, ntg SOD1^{G93A}; *caspase-6*$^{+/+}$ gastrocnemius muscle, and purified primary motorneurons. Real-time quantitative PCR (RT-qPCR) was used to determine *caspase-6* levels in different sample types and expression was normalized to β-Actin. No significant differences in *caspase-6* mRNA expression were detected in the sample types examined compared to nervous tissue. This experiment is based on a single run; therefore a repeat of this experiment is necessary due to the lack of sample numbers for these sample types/conditions.

A)

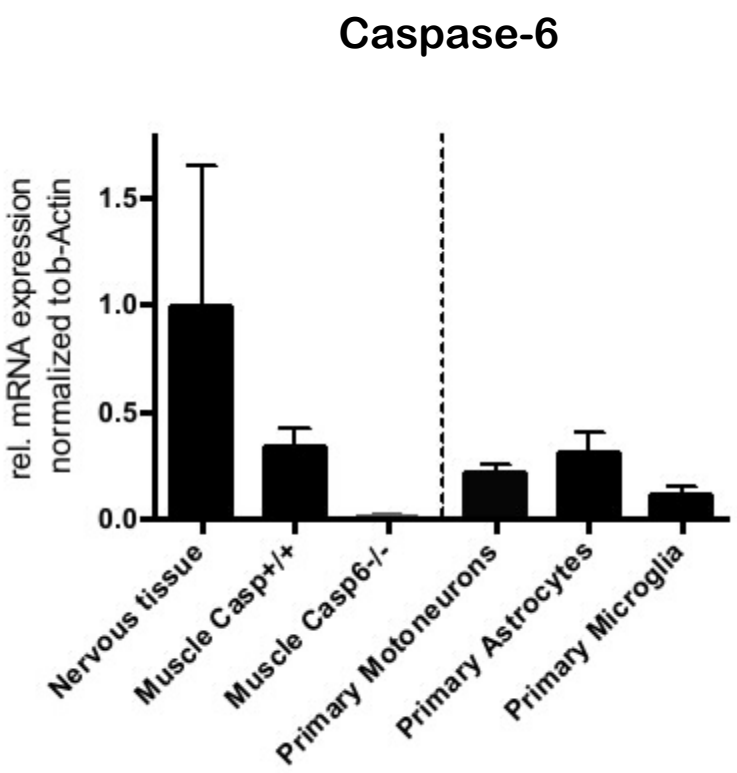

Figure 3.1: Quantitative PCR analysis of *caspase-6* mRNA expression levels

A) Total RNA was extracted from nervous tissue (neocortex) and their *caspase-6* mRNA expression levels compared to ntg SOD1^{G93A}*; caspase-6*$^{+/+}$ and ntg SOD1^{G93A}*; caspase-6*$^{-/-}$ gastrocnemius muscle (pnd 35) expression levels by real-time quantitative PCR (qPCR). Additionally, primary neuronal cultures were prepared from the (motorneuron) rich ventral horns of embryonic mouse spinal cords. An optiprep gradient centrifugation step was used for the generation of purified motorneurons. Ventral horns were micro-dissected following neurogenesis at E10-12 and primary motorneuron, astrocyte and microglia cultures were derived from *caspase-6*$^{+/+}$ neural tissue. The cell culture lysates were processed to qPCR in order to compare *caspase-6* expression levels in motorneurons to glial expression. Following determination of cell or tissue-specific *caspase-6* mRNA expression levels, their values were normalized to the individual *β*-actin expression level. No significant differences in *caspase-6* mRNA expression were detected in each sample type examined compared to nervous tissue. A two-tailed t-test (paired) was used to assess statistical significance. Error bars represent the standard error of the mean (SEM).

3.2.2 Pro-caspase-6 protein levels can be detected by Western blot

Western blot analysis was carried out to identify the protein levels of pro caspase-6 (36 kDa) in non-transgenic (ntg) SOD1^{G93A} lumbar spinal cord homogenate (Figure 3.2). A pro caspase-6 antibody (Cell Signalling) was utilized for identification of pro caspase-6. Following several attempts, blocking of non-specific binding could not be achieved; however the pro caspase-6 band can be identified by the absence of a band in the caspase-6$^{-/-}$ sample lane. The antibody reportedly detects both pro caspase-6 (36 kDa) and cleaved caspase-6 (15 kDa) by Western blotting, however no cleaved caspase-6 could be detected in SOD1^{G93A} mice.

A)

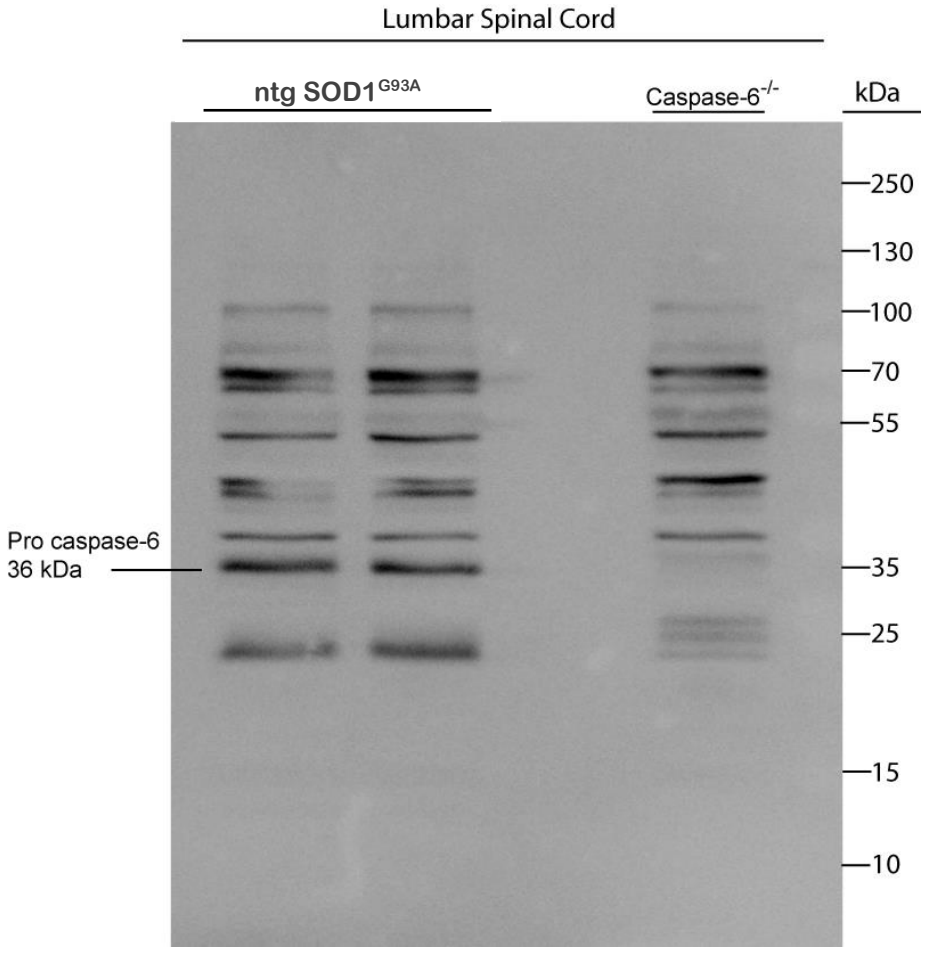

Figure 3.2: Pro caspase-6 protein levels can be detected by western blot

A) Western blot analysis was carried out to identify the expression of pro caspase-6 (36 kDa) in non-transgenic ntg SOD1^{G93A} lumbar spinal cord homogenate. Pro caspase-6 is detected as a band at 36 kDa which is absent in the caspase-6$^{-/-}$ sample.

To further characterize the caspase-6 antibody we performed Western blot analysis of NSC-34 cells treated with 0.1% Staurosporine (STS) dissolved in dimethlsulfoxide (DMSO) to induce apoptosis and DMSO as a control (Figure 3.3). STS is insoluble in water therefore DMSO is used as a control. This was carried out to identify if we could detect the active form. Pro caspase-6 was again detected in ntg SOD1^{G93A} lumbar spinal cord and NSC-34 cell lysates of both treatment groups. As expected, pro caspase-6 was not observed in c*aspase-6* $^{-/-}$ lumbar spinal cord. Cleaved caspase-6 could not be detected in the STS-treated samples. We conclude that cleaved caspase-6 is not detected by this antibody. Cleaved caspase-3 was clearly detected as a band of 19kDa in STS-treated NSC-34 lysates indicating apoptosis was induced by STS treatment but not by DMSO in the NSC-34 cells.

A)

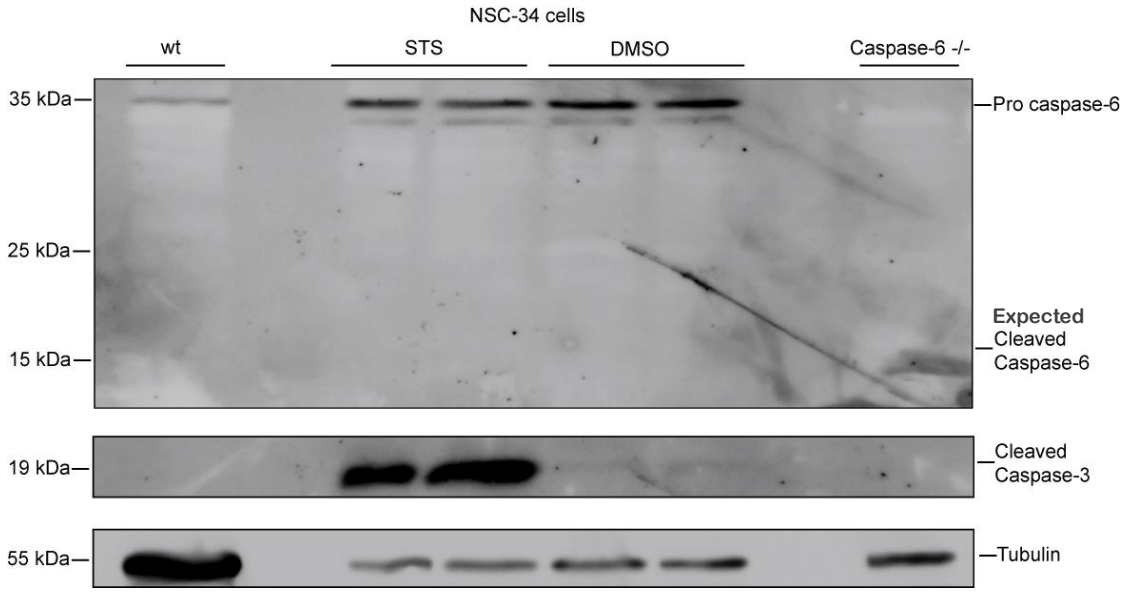

Figure 3.3: Detection of caspase-6 in Staurosporine treated NSC-34 cells

A) Western blot analysis of NSC-34 cells treated with 0.1% Staurosporine (STS) to induce apoptosis and dimethlsulfoxide (DMSO) control for 4 hours. NSC-34 cell lysates, ntg SOD1^{G93A} and c*aspase-6* $^{-/-}$ lumbar spinal cord homogenates (controls) were probed with antibodies that recognize pro caspase-6 (36 kDa), cleaved caspase-6 (15 kDa), cleaved caspase-3 (19 kDa), and α-tubulin loading control (55 kDa). Pro caspase-6 was detected in all samples except *caspase-6*$^{-/-}$. Cleaved caspase-6 could not be detected in any samples.

Cleaved caspase-3 was detected in STS-treated NSC-34 lysates indicating apoptosis was induced by STS treatment.

3.2.3 Pro caspase-6 protein levels during disease progression in the SOD1^{G93A} mouse model of ALS

ALS is a progressive degenerative disease, and is usually identified firstly in the lower limbs as a loss of muscular function. Molecular mechanisms of apoptosis may be involved in motorneuron death produced by mutations in the SOD1 gene (Guegan *et al*. 2001). Activation of other caspases have been located in the spinal cord of tg SOD1^{G93A} mice, including caspase-9 and caspase-3 (Guegan *et al*. 2001). It has been observed via Western blot that activation of caspase-3 and caspase-7 occur during later stages of disease progression in SOD1^{G93A} mice (Pasinelli *et al*. 2000; Vuckosavc *et al*. 2000), therefore we hypothesized that caspase-6 expression levels or activation may be altered in SOD1^{G93A} mice.

To identify the role of caspase-6 in an ALS mouse model we measured pro caspase-6 levels in tg and ntg SOD1^{G93A} lumbar spinal cord homogenates throughout disease progression. Western blots were probed with an antibody that recognizes pro caspase-6 (36 kDa) and either β-actin or α-tubulin was used as a loading control (55 kDa). The caspase-6 specific band in SOD1^{G93A} lumbar spinal cord samples was identified by the absence of a band in the caspase-6$^{-/-}$ lane. Non-specific bands were also present (indicated by nsp) and cleaved caspase-6 could not be detected. Due to limited starting material and minimizing animal numbers, repeats of this experiment were not performed.

Although pro caspase-6 was detected as a band of 36 kDa in all samples, there were no significant changes in expression in SOD1^{G93A} spinal cord at pnd 70 (Figure 3.4), pnd 120 (Figure 3.5), or pnd endstage (Figure 3.6). Cleaved caspase-6 could not be detected at any of these timepoints, which is similar to the findings in the STS-treated NSC-34 cells.

It should be noted that at endstage, densitometric analysis of the pro caspase-6 signal normalised to the α-tubulin loading control, revealed that there were increased levels of pro caspase-6 in the tg lumbar spinal cord samples (n=4) compared to non-tg (n=4) littermates, however this was not statistically significant (Figure 3.6). Due to limited starting material and minimizing animal numbers, repeats of this experiment were not performed, therefore data analysis was completed using one Western blot for each timepoint.

A)

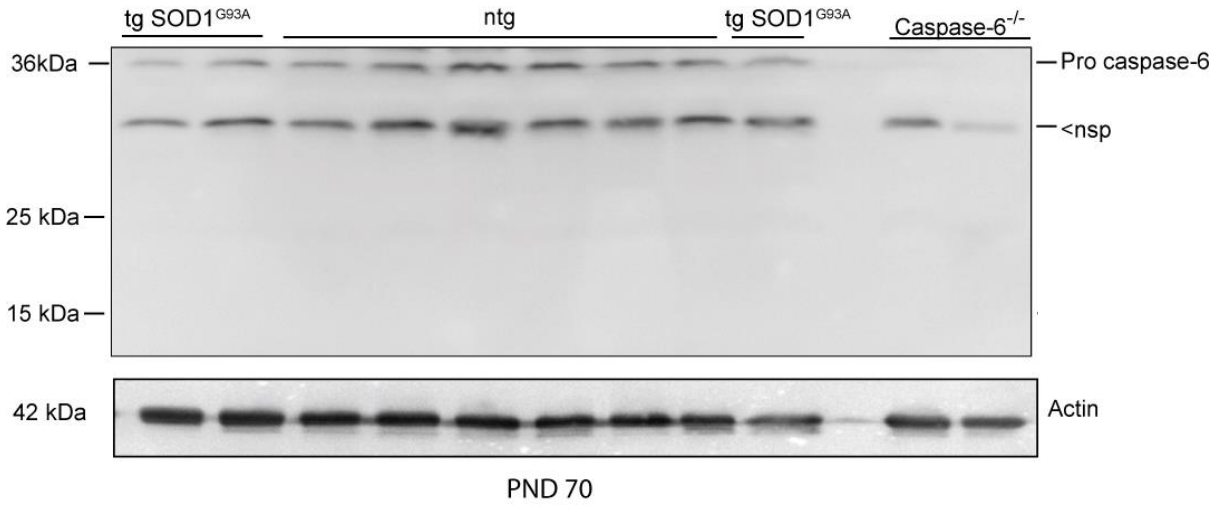

B)

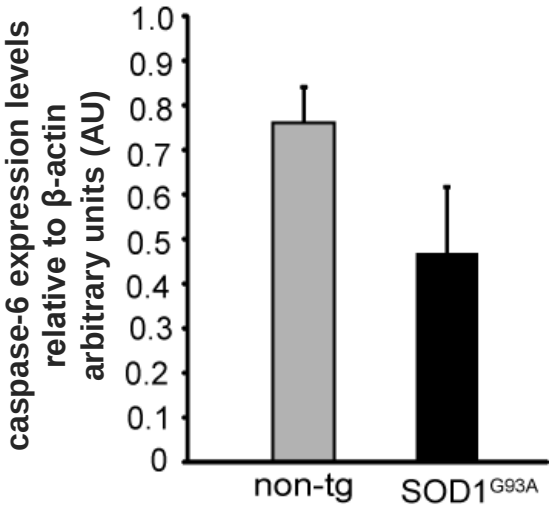

Figure 3.4: Caspase-6 protein expression in PND 70 lumbar spinal cord

A) Representative western blot of ntg and transgenic (tg) SOD1^{G93A} lumbar spinal cords homogenized in RIPA buffer at pnd 70. Samples were probed with antibodies that recognize pro caspase-6 (36 kDa), cleaved caspase-6 (15 kDa), and α-tubulin loading control (55 kDa). <nsp= non-specific band (B) Densitometry quantification of pro caspase-6 expression level at pnd 70 in the SOD1^{G93A} colony relative to β-actin showed no significant differences in expression. Cleaved caspase-6 could not be detected in any samples. Analysis was performed on n=3 tg samples and n=6 ntg samples. Limited starting material and keeping animal numbers to a minimum prevented repeats of this experiment (n=1). Error bars represent the SEM.

A)

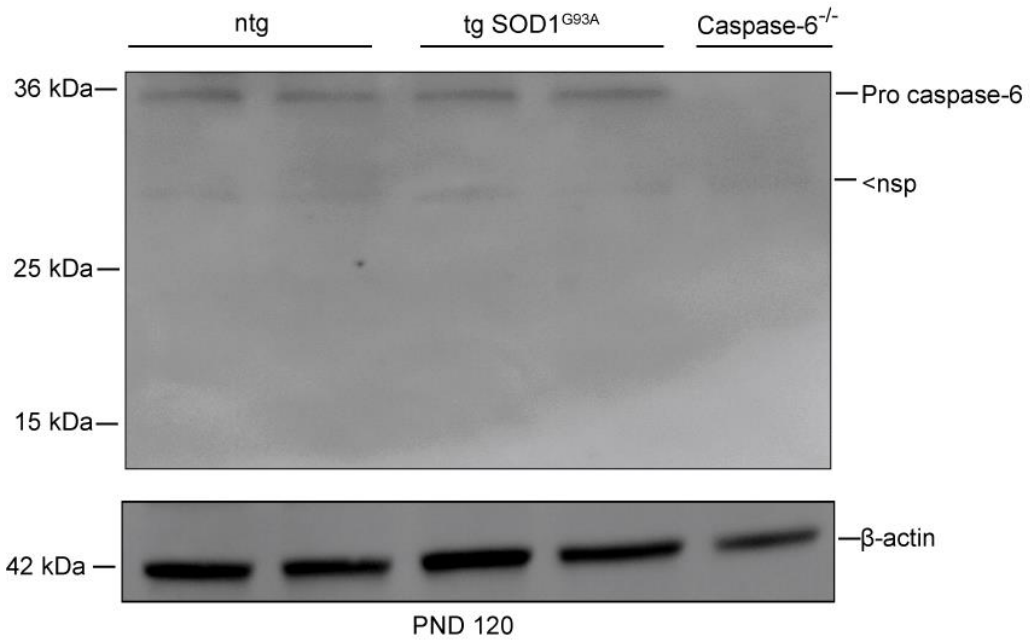

B)

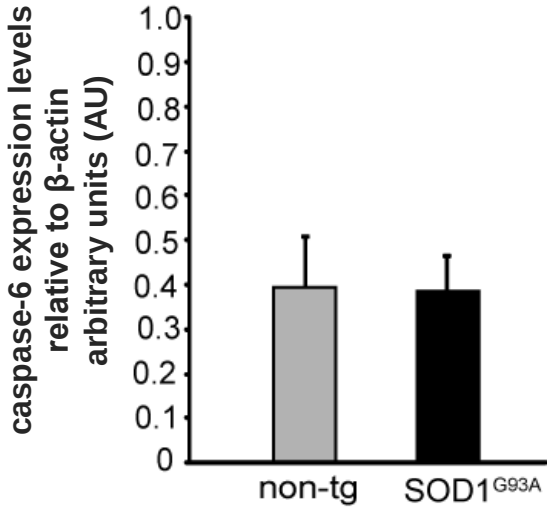

Figure 3.5: Caspase-6 protein expression in PND 120 lumbar spinal cord

A) Representative western blot of ntg and tg SOD1^{G93A} lumbar spinal cords homogenized in RIPA buffer at PND 120. Samples were probed with antibodies that recognize pro caspase-6 (36 kDa), cleaved caspase-6 (15 kDa), and α-tubulin loading control (55 kDa). <nsp= non-specific band. (B) Densitometric quantification of caspase-6 expression levels at pnd 120 in the SOD1^{G93A} colony relative to β-actin showed there was no significant difference in expression between tg and ntg animals. Cleaved caspase-6 could not be detected in any

samples. Analysis was performed on n=4 tg samples and n=4 ntg samples. Limited starting material and keeping animal numbers to a minimum prevented repeats of this experiment (n=1). Error bars represent the SEM.

A)

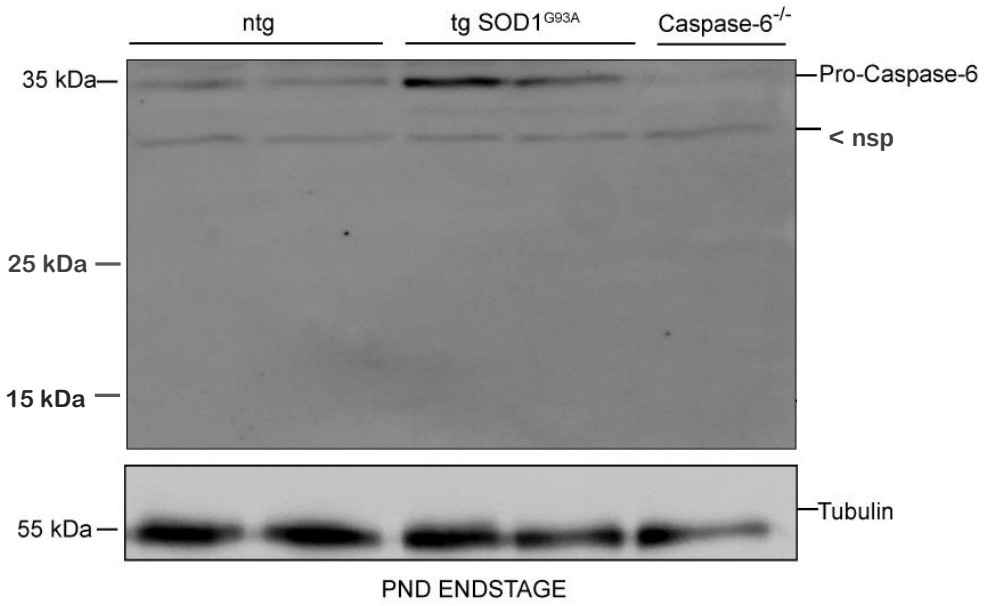

B)

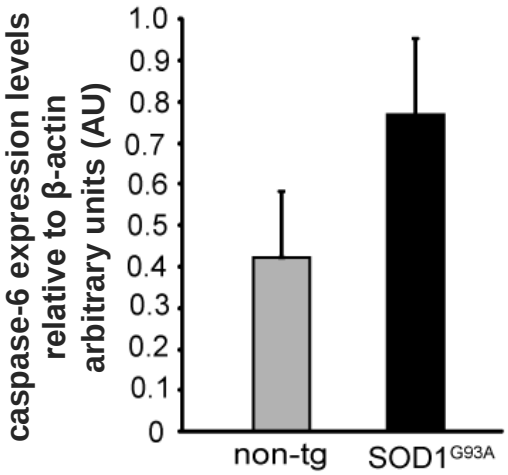

Figure 3.6: Caspase-6 protein expression in PND endstage lumbar spinal cord

(A) Representative western blot of ntg and tg SOD1^{G93A} lumbar spinal cords homogenized in RIPA buffer at pnd endstage (which occurs around pnd 150-160). Samples were probed with antibodies that recognize pro caspase-6 (36 kDa), cleaved caspase-6 (15 kDa), and α-tubulin loading control (55 kDa). <nsp= non-specific band. (B) Densitometric quantification of caspase-6 expression levels at pnd endstage in the SOD1^{G93A} colony relative to β-actin showed that there was increased expression in tg samples but this was not significantly

different. Cleaved caspase-6 could not be detected in any samples. Blot represents experiments performed on n=4 ntg samples and n=4 tg samples. Limited starting material and keeping animal numbers to a minimum prevented repeats of this experiment (n=1). <nsp= non-specific band Error bars represent the SEM.

3.3 Summary

We utilized quantitative PCR (qPCR) to determine pro caspase-6 mRNA in nervous tissue from neocortex as well as ntg SOD1^{G93A}; *caspase-6*$^{-/-}$ gastrocnemius muscle (pnd 35), ntg SOD1^{G93A}; *caspase-6*$^{+/+}$ gastrocnemius muscle (pnd 35), and compared this with purified primary motorneurons, microglia-enriched and astrocyte-enriched cultures from primary E12 spinal cord tissue. No significant differences in *caspase-6* mRNA expression were detected in the sample types examined compared to nervous tissue.

We decided to investigate if caspase-6 protein levels were altered in a transgenic mouse model of ALS. We identified pro caspase-6 in the lumbar spinal cord of both tg and ntg SOD1^{G93A} mice. Having observed the presence of pro caspase-6 in our mouse model, we wanted to determine if caspase-6 has a role in disease pathology. We found that pro caspase-6 showed a tendency towards an increase with the progression of ALS, yet this was is not at statistically significant levels. Successful detection of cleaved caspase-6 expression via Western blot in SOD1^{G93A} lumbar spinal cord was not achievable due to poor primary antibodies; therefore we cannot exclude the possibility of active caspase-6 across disease progression. While pro caspase-6 is not significantly upregulated in the lumbar spinal cord, it still may play a role in apoptosis mediated degeneration at earlier stages of the disease in another region. It has been hypothesized that caspase-6 may have a role in the degeneration in skeletal muscle occurs prior to the onset of motorneuron degeneration in the spinal cord (Graham *et al*. 2006). Although there is increasing information regarding ALS disease pathology every year, many efforts are focused on understanding motorneuron degeneration in the spinal cord. We were interested in discovering if caspase-6 played a larger pre-symptomatic role in an area that is only beginning to gain attention, in skeletal muscle (Chapter 4).

CHAPTER 4

The role of caspase-6 during motorneuron degeneration

Chapter 4: The role of caspase-6 during motorneuron degeneration

4 .1 Introduction

Due to beneficial evidence involving targeted deletion of *caspase-6* in HD and AD (Graham *et al*. 2010; Milnerwood *et al*. 2010; Galvan, V. *et al*. 2006; Nguyen, T.V. *et al*. 2008), we were interested in determining any implications of a *caspase-6* deficiency on ALS disease progression and survival by utilizing the SOD1^{G93A} mouse.

In this chapter, we determined whether *caspase-6* deficient mice display any change in body weight or motor function when compared to ntg SOD1^{G93A} mice. We also examined any differences in motor endplate morphology of *caspase-6*$^{-/-}$ mice compared to wildtype SOD1^{G93A} mice. To define the role of *caspase-6* deletion in the SOD1^{G93A} mouse model of ALS, we cross-bred *caspase-6*$^{-/-}$ mice with tg SOD1^{G93A} mice to generate a new mouse strain. Motor function tests and lifespan analysis were carried out in all of the genotypes generated. Finally, we determined if any differences were present in skeletal muscle weight and morphology in the SOD1^{G93A}*; caspase-6* mice.

4.2 Results

4.2.1 Characterisation of *caspase-6* deficient mice

To gain a better understanding of *caspase-6* deficiency *in vivo*, motor performance, body weight, and motor endplate morphology were characterized. Non-transgenic SOD1; *caspase-6* $^{-/-}$ mice were assessed by Rotarod test and the body weights were recorded and compared to ntg SOD1^{G93A} mice. The Rotarod test was chosen due its sensitivity for indicating disease onset and progression in the SOD1^{G93A} mouse model (Knippenberg, Thau *et al*. 2010). Rotarod analysis showed no significant difference in performance between *caspase-6* deficient and ntg SOD1^{G93A} mice (Figure 4.1B). Body weight was recorded prior to Rotarod testing using a standard weighing scale. There were no significant changes in body weight between ntg SOD1; *caspase-6* $^{-/-}$ and ntg SOD1^{G93A} mice (Figure 4.1A). Non-transgenic littermates are culled at the same time as the tg mice for direct comparison, even though they would survive much longer. Because ntg mice are culled at the same time as tg mice and the same pattern is seen (Figure 4.10) where tg SOD1^{G93A}; *caspase-6*$^{-/-}$ mice die earlier than tg SOD1^{G93A}; *caspase-6* $^{+/+}$mice. It should also be noted that all ntg SOD1^{G93A}; *caspase-6*$^{-/-}$ male mice were culled at pnd 165, the same time as tg SOD1^{G93A}; *caspase-6*$^{-/-}$, (data shown in Figure 4.10) and therefore female weight averages, which are naturally less, demonstrate a

decrease at this time point (Figure 4.1A). In addition, separate analysis of male and female data did not show any differences in body weight (data not shown). Initial characterization of *caspase-6* deficient mice was necessary for the continuation of additional motor function tests (chapter 4.2.3) in the SOD1^{G93A}; *caspase-6*$^{-/-}$ cross breeding.

A)

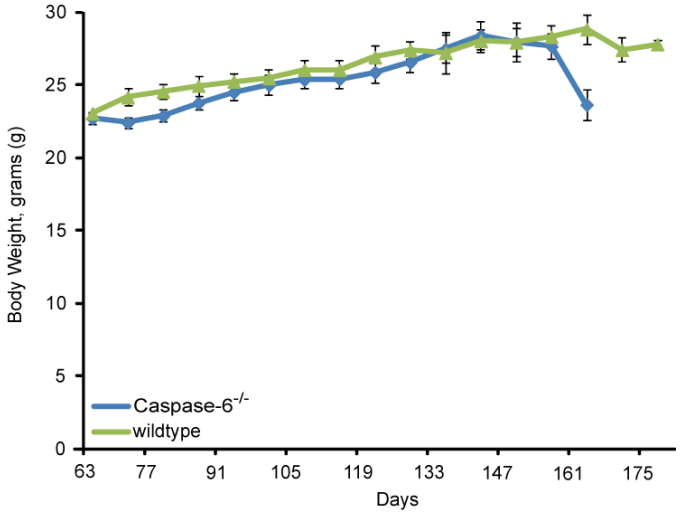

B)

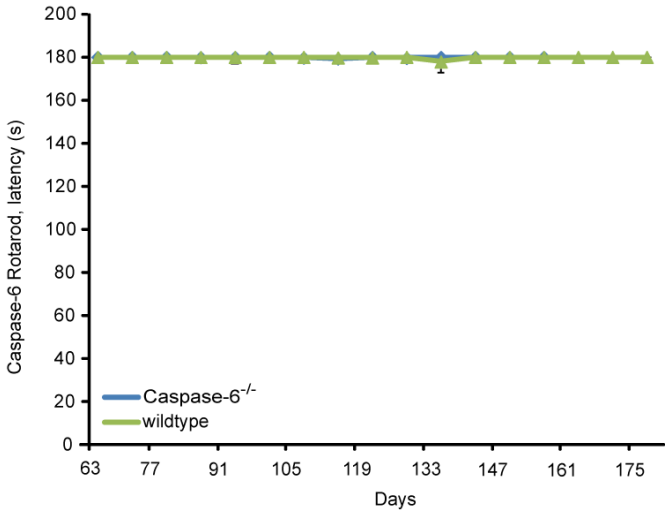

Figure 4.1: Motor function and body weight are not affected in non-transgenic SOD1^{G93A} mice deficient for caspase-6

A) Weight analysis is used as an indication of disease onset and progression. Male and female body weight measurement commenced at pnd 63 until the loss of righting reflex which occurs at approximately pnd 160 in tg SOD1^{G93A} mice. There was no significant

difference between ntg SOD1^{G93A}; *caspase-6* $^{+/+}$ and ntg SOD1^{G93A}; *caspase-6* $^{-/-}$ mice. Transgenic mice are culled at the same time and therefore show the same pattern (Figure 4.10) where tg SOD1^{G93A}; *caspase-6*$^{-/-}$ mice die earlier than tg SOD1^{G93A}; *caspase-6* $^{+/+}$mice. Analysis of male and female data separately showed no significant differences between male and female mice (data not shown). B) The Rotarod test provides an analysis of limb strength and loss of function is used as a measurement of disease onset and progression. The Rotarod test commenced at pnd 63 until the loss of righting reflex at approximately pnd 160. Data analysis showed no significant difference between ntg SOD1^{G93A}; *caspase-6* $^{+/+}$ and ntg SOD1^{G93A}; *caspase-6* $^{-/-}$. There were no significant differences seen when males and females were analysed separately (data not shown). Data analysis was completed with n= ≥5 per sex-matched group. Statistical tests used were-ANOVA followed by a *post hoc* Tukey test. Error bars represent the SEM.

Next, we wanted to determine if motor endplates from hindlimb skeletal muscle showed any morphological changes in *caspase-6* deficient mice compared to ntg SOD1^{G93A} mice. Gastrocnemius muscle was dissected from pnd 90 mice and sectioned at 30µm. Muscle sections from ntg SOD1^{G93A} mice and *caspase-6*$^{-/-}$ mice were stained with α-bungarotoxin (a-BTX) which binds with high affinity to the α-subunit of the nicotinic acetylcholine receptor (AChR) of neuromuscular junctions to identify motor endplates (Figure 4.2A). Analysis of motor endplates from *caspase-6*$^{-/-}$ gastrocnemius muscle showed no difference in morphology compared to ntg SOD1^{G93A}.

A)

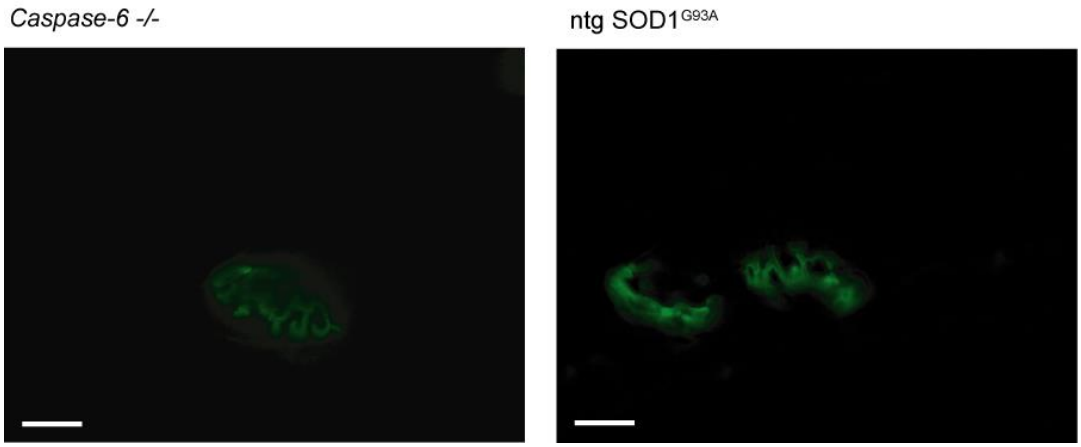

Figure 4.2: Neuromuscular endplates show no difference in morphology in ntg SOD1^{G93A} mice compared to *caspase-6*$^{-/-}$ mice

A) Gastrocnemius muscle was dissected from pnd 90 mice and sectioned at 30µm. Muscle sections from ntg SOD1^{G93A} mice and *caspase-6*$^{-/-}$ mice were stained with α-bungarotoxin (a-BTX) to identify motor endplates. Analysis of motor endplates from ntg SOD1^{G93A} mice compared to *caspase-6*$^{-/-}$ mice showed no differences in morphology. Preliminary data images are of n=1 per group. Scale bar=10µm

4.2.2 Generation of the SOD1^{G93A}; *caspase-6* $^{-/-}$ colony

To further elucidate the role of caspase-6 during ALS disease progression, we developed a cross-breeding program to produce a SOD1^{G93A} mouse colony deficient for *caspase-6* (Figure 4.3). SOD1^{G93A} are commercially available from the Jackson Laboratories, strain name B6.Cg-Tg (SOD1*G93A) 1Gur/J. *Caspase-6* deficient mice are also available from the Jackson Laboratories, strain name B6.129S6-*Casp6*^{tmlFlv}/J. Mice were weaned at 4 weeks and genotype was confirmed by tail snip PCR for SOD1^{G93A} (Figure 4.4A) and caspase-6 (Figure 4.4B) mice. Breeding commenced at 6 weeks when the mice reached sexual maturity (Leitner *et al*. 2009). Breeding paradigms were adapted to produce the genotypes of interest (Figure 4.3). Transgenic SOD1^{G93A} females are inefficient breeders (Leitner *et al*. 2009), therefore tg SOD1^{G93A} males were crossed with *caspase-6*$^{-/-}$ females to generate tg and ntg SOD1^{G93A}; *caspase-6*$^{+/-}$ mice. The resulting tg SOD1^{G93A}; *caspase-6*$^{+/-}$ males were crossed with *caspase-6*$^{-/-}$ females to generate male and female tg SOD1^{G93A}; *caspase-6*$^{-/-}$ and ntg SOD1^{G93A} *caspase-6*$^{-/-}$ mice necessary for this study. Due to low ntg SOD1^{G93A}; *caspase-6*$^{+/+}$ numbers, ntg SOD1^{G93A} mice from the SOD1^{G93A} colony were age, and sex matched and utilized as a

control. SOD1^{G93A} mice with a *caspase-6* deficiency were produced at expected Mendelian frequencies and do not display any obvious alteration in phenotype prior to onset of ALS symptoms. In addition deletion of *caspase-6* does not alter the expression of human SOD1 levels (Figure 4.5A).

A)

SOD1^{G93A} mice:

♂ **tg X** ♀ **ntg yields both tg and ntg males and females**

***SOD1^{G93A}** ♀ **tg = infertile**

SOD1^{G93A}/CASP6 mice:

♂ **tg SOD1^{G93A} / CASP6 +/+ X** ♀ **ntg SOD1^{G93A} / CASP6 -/-**

Resulting genotypes: tg SOD1^{G93A} / CASP6 +/-

ntg SOD1^{G93A} / CASP6 +/-

♂ **tg SOD1^{G93A} / CASP6 +/- X** ♀ **ntg SOD1^{G93A} / CASP6 -/-**

Resulting genotypes: tg SOD1^{G93A} / CASP6 +/-

ntg SOD1^{G93A} / CASP6 +/-

tg SOD1^{G93A} / CASP6 -/-

ntg SOD1^{G93A} / CASP6 -/-

Figure 4.3: Generation of the SOD1^{G93A} Caspase-6 -/- colony

A) SOD1^{G93A} and *caspase-6* $^{-/-}$ mice were cross bred to generate a SOD1^{G93A}; *caspase-6* $^{-/-}$ colony. Transgenic SOD1^{G93A} males were crossed with *caspase-6*$^{-/-}$ females to generate tg SOD1^{G93A}; *caspase-6*$^{-/-}$ mice for motor function and lifespan analysis.

A)

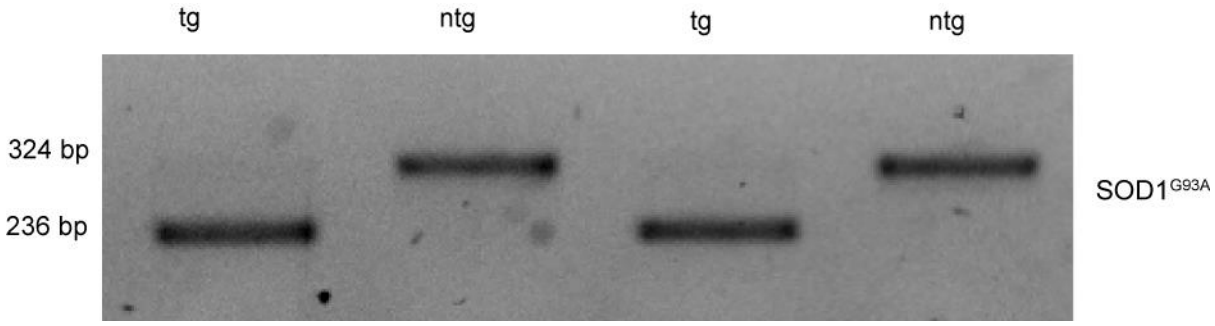

B)

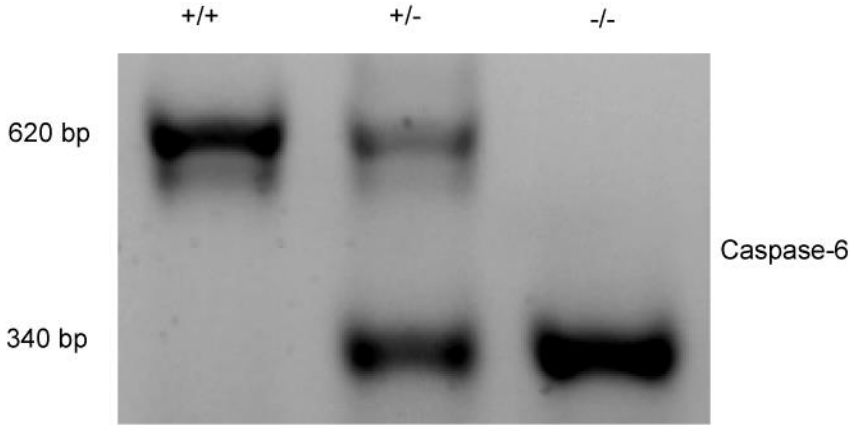

Figure 4.4: SOD1^{G93A} and caspase-6 genotypes were determined by polymerase chain reaction (PCR)

A) Tail snip DNA genotyping was carried out to identify genes of interest. A 2 millimetre (mm) section of tail was taken from each mouse and DNA was extracted from tail snips using a High Pure PCR Template Preparation Kit. Samples were run in the thermal cycler with an annealing program that was pre-set with primers specific to the gene of interest. Samples were then run on a 2% agarose gel and analysed. Non-transgenic SOD1 ^{G93A} was identified as a band at 324 bp and tg SOD1 ^{G93A} was identified by the presence of a band at 236 bp. B) SOD1^{G93A} and c*aspase-6* $^{-/-}$ mice were cross bred to generate a SOD1^{G93A};*caspase-6*$^{-/-}$ colony. *Caspase-6* (+/+, +/-, -/-) and SOD1 (tg and ntg) expression were identified in each litter produced. *Caspase-6* $^{+/+}$ was identified by a band at a 620 bp band, and *caspase-6* $^{-/-}$ was identified at 340 bp whereas heterozygouse *caspase-6* $^{+/-}$ had both bands 620 bp and 340 bp.

A)

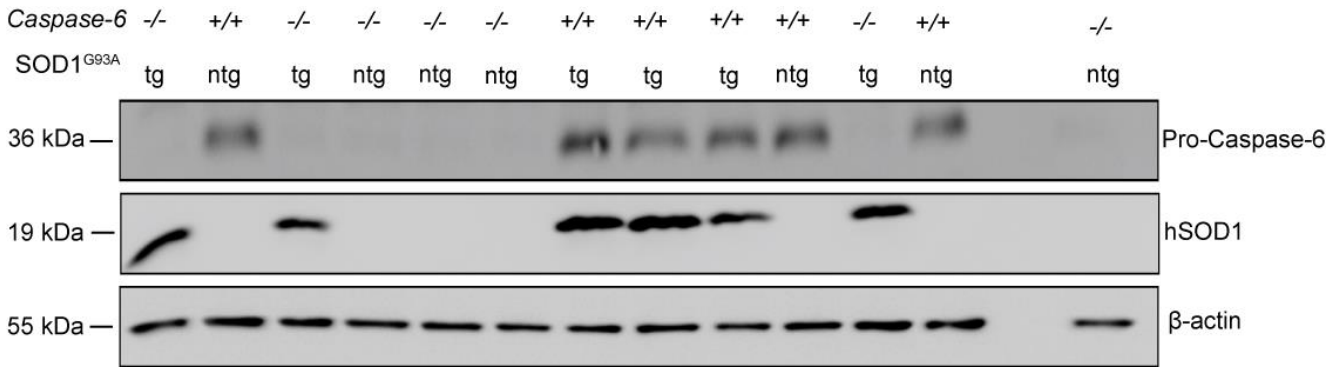

B)

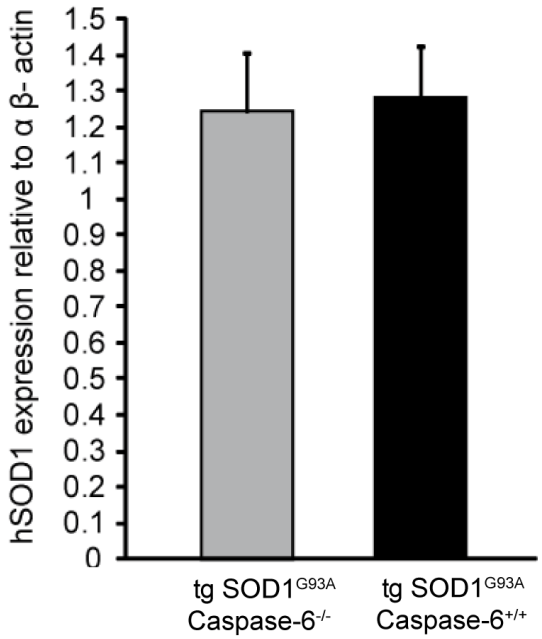

Figure 4.5: *Caspase-6* deficiency in SOD1^{G93A} mice did not alter the expression of human SOD1^{G93A} expression levels

A) Transgenic and ntg SOD1^{G93A}; *caspase-6* $^{-/-}$, tg and ntg SOD1^{G93A}; caspase-*6*$^{+/+}$ and *caspase-6* $^{-/-}$ (control) lumbar spinal cord homogenates were probed with antibodies that recognize pro caspase-6 (36 kDa), hSOD1 (19 kDa), and β-actin (55 kDa) loading control. *Caspase-6* deficiency did not alter the expression of human SOD1 in tg SOD1^{G93A} mice. B) Densitometric quantification of hSOD1 expression in tg SOD1^{G93A}; caspase-*6* $^{-/-}$ and tg SOD1^{G93A}; c*aspase-6*$^{+/+}$ showed no significant differences in hSOD1 expression levels relative to β-actin. Blot experiment was performed with n=3 mice per genotype. Error bars represented as SEM. Statistical analysis was performed using an Independent T-test.

4.2.3 Effect of *caspase-6*$^{-/-}$ deletion on disease progression and motor function in SOD1^{G93A} mice

The loss of motor function is a common phenotypic indicator of ALS disease onset and progression in transgenic SOD1^{G93A} mice. The onset of symptoms can be seen at pnd 90 with a progressive reduction in function until pnd endstage, usually 70 days after symptom onset. Endstage is determined when the ability for the mouse to right itself can no longer be achieved after 30 seconds on either side (Ludolph *et al*. 2010). The first physical symptoms of the SOD1^{G93A} mouse model were identified by Gurney and Pu *et al*, by observing hind leg extension, grooming habits, and weight loss (Gurney, Pu *et al*. 1994). Several methods of analysing motor function performance have been developed including Rotarod test, grip strength meter, PaGE test (Weydt *et al*. 2003), and stride length measurements (Gurney, Pu *et al*. 1994). These relevant methods for testing motor function are non-invasive and widely accepted for analysing the SOD1^{G93A} mouse model (Brooks and Dunnett, 2009). These tests have been used in several studies associated with evaluating pre-clinical therapies in SOD1^{G93A} mice (Ludolph, Bendotti *et al*. 2007; Scott, Kranz *et al*. 2008; Brooks and Dunnett 2009; Ludolph, Bendotti *et al*. 2010). Each group, ranging from 4-8 mice per group, was sex, age, and litter matched prior to motor function analysis based on the accepted guidelines for ALS animal studies (Ludolph, *et al*., 2010). The tg and ntg SOD1^{G93A}; c*aspase-6*$^{+/+}$ control mice were sex, age, and litter matched separately. Motor function analysis commenced at pnd 63 following a training period of 10 days. All motor function testing was recorded with tests completed in the same order, twice weekly.

The Rotarod test provides an analysis of limb strength and coordination, and loss of function is used as a measurement of disease onset and progression. Rotarod analysis shows a significant decrease in performance in tg SOD1^{G93A}; c*aspase*$^{-/-}$ mice from pnd 137 ($p \leq 0.05$) to pnd 159 ($p \leq 0.001$) compared to tg SOD1^{G93A}; c*aspase*$^{+/+}$ mice (Figure 4.6A). Male and female Rotarod performance was also analysed separately. Male Rotarod performance showed a significant decrease in performance in tg SOD1^{G93A}; c*aspase*$^{-/-}$ mice at pnd 145 ($p \leq 0.01$) compared to tg SOD1^{G93A}; c*aspase*$^{+/+}$ mice but no significance was seen during later timepoints (4.6B). Females demonstrated a decrease in performance in tg SOD1^{G93A}; c*aspase*$^{-/-}$ mice from pnd 135 ($p \leq 0.001$) to pnd 159 ($p \leq 0.050$) compared to tg SOD1^{G93A}; c*aspase*$^{+/+}$ mice (Figure 4.6C).

The PaGE test is used to measure the strength of the forelimbs and hindlimbs. Loss of function in the limbs is an indication of disease onset and progression. The PaGE test requires the mouse to use both fore and hindlimbs to hang upside down on a mesh metal grate for as long as possible or a maximum of 60 seconds. PaGE ability was reduced during early disease progression at pnd 95 in tg SOD1^{G93A}; *caspase-6*$^{-/-}$ in contrast to the onset of forelimb symptoms in tg SOD1^{G93A}; c*aspase*$^{+/+}$ at pnd 112 (Figure 4.7). Transgenic SOD1^{G93A}; c*aspase*$^{+/+}$ mice performed better in the PaGE test compared to their *caspase*$^{-/-}$ littermates from pnd 95 ($p \leq 0.010$) to pnd 112 ($p \leq 0.001$), but showed no significant differences from pnd 112 to endstage. Following the PaGE test, the grip strength test was used to measure forelimb strength and the force applied (g) to resist the involuntary backward movement when a mouse was pulled by its tail. Grip strength was performed twice weekly and the average of each reading was analysed across disease progression. Transgenic SOD1^{G93A}; *caspase-6*$^{-/-}$ mice showed a significant decrease in PaGE performance when compared to tg SOD1^{G93A} mice during disease onset (pnd 90) ($p \leq 0.010$) to late-stage of the disease (pnd 120) ($p \leq 0.010$) but no other significant differences were recorded (Figure 4.8A). Male and female grip strength analysis did not yield a significant difference between tg SOD1^{G93A}; *caspase-6*$^{-/-}$ and tg SOD1^{G93A}; c*aspase*$^{+/+}$ mice (Figure 4.8B/Figure 4.8C).

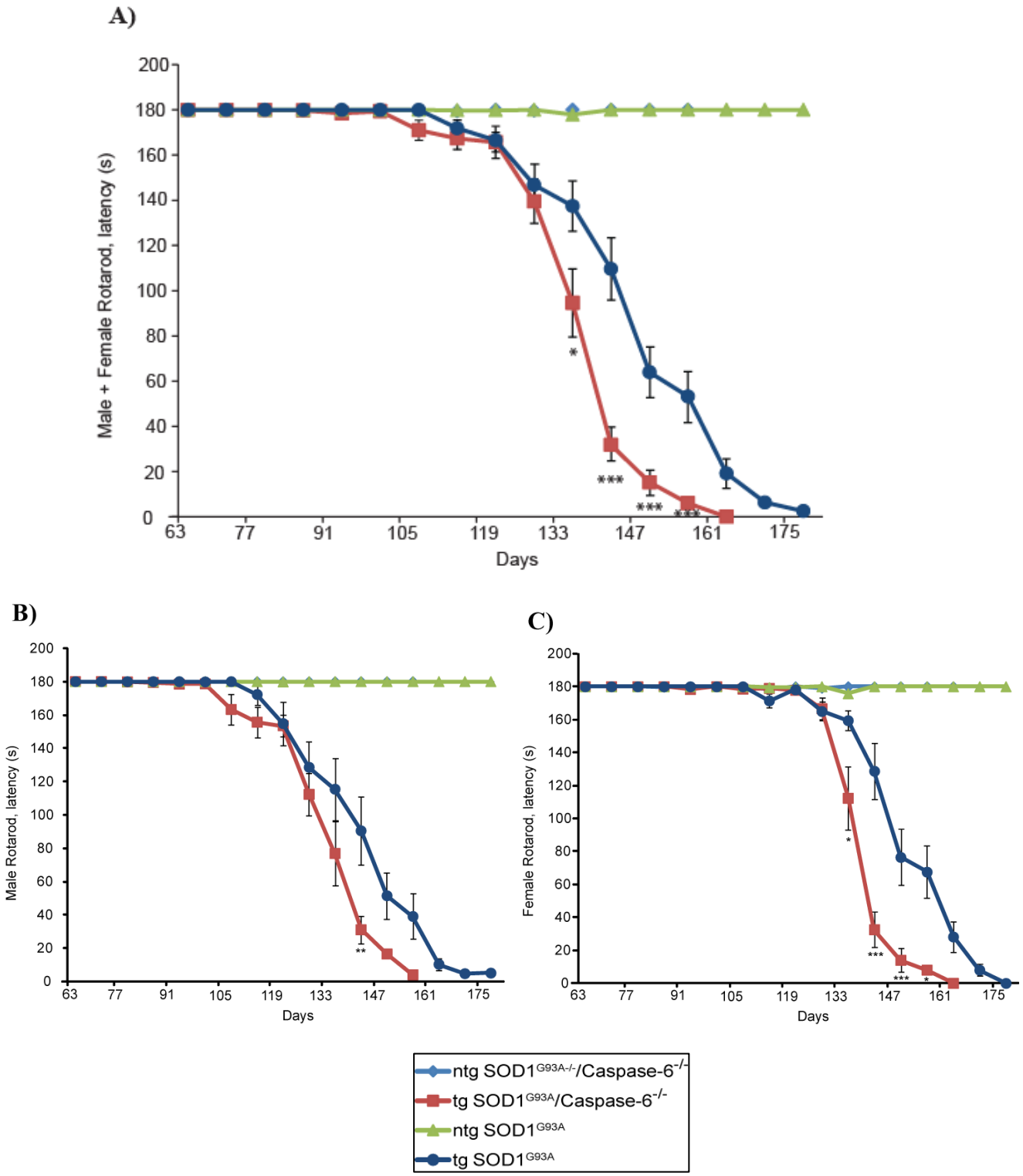

Figure 4.6: *Caspase-6* deficiency does not protect limb function across disease progression in SOD1^{G93A} mice

A) Rotarod performance measures both forelimb and hind limb function. Rotarod testing commenced at pnd 63 following a training period until the loss or right reflex at approximately pnd 160. Rotarod analysis depicts a significant decrease in performance in tg SOD1^{G93A}; *caspase*$^{-/-}$ mice compared to tg SOD1^{G93A}; *caspase*$^{+/+}$ mice from pnd 137

($p \leq 0.050$) to pnd 159 ($p \leq 0.001$) B) Male tg $SOD1^{G93A}$; c*aspase-6* $^{-/-}$ mice Rotarod$^{(R)}$ performance showed no overtly significant results but demonstrated a decrease in performance at pnd 145 when compared to male tg $SOD1^{G93A}$ mice. C) Female performance showed a decrease from tg $SOD1^{G93A}$; c*aspase*$^{-/-}$ mice compared to tg $SOD1^{G93A}$; c*aspase*$^{+/+}$ mice from pnd 135 ($p \leq 0.05$) to pnd 159 ($p \leq 0.05$). ANOVA (*post-hoc*, Tukey) was used to assess statistical significance. Data are mean ± SEM, n= 4-6 mice per sex-matched treatment group (* $p \leq 0.05$, ** $p \leq 0.01$, *** $p \leq 0.001$)

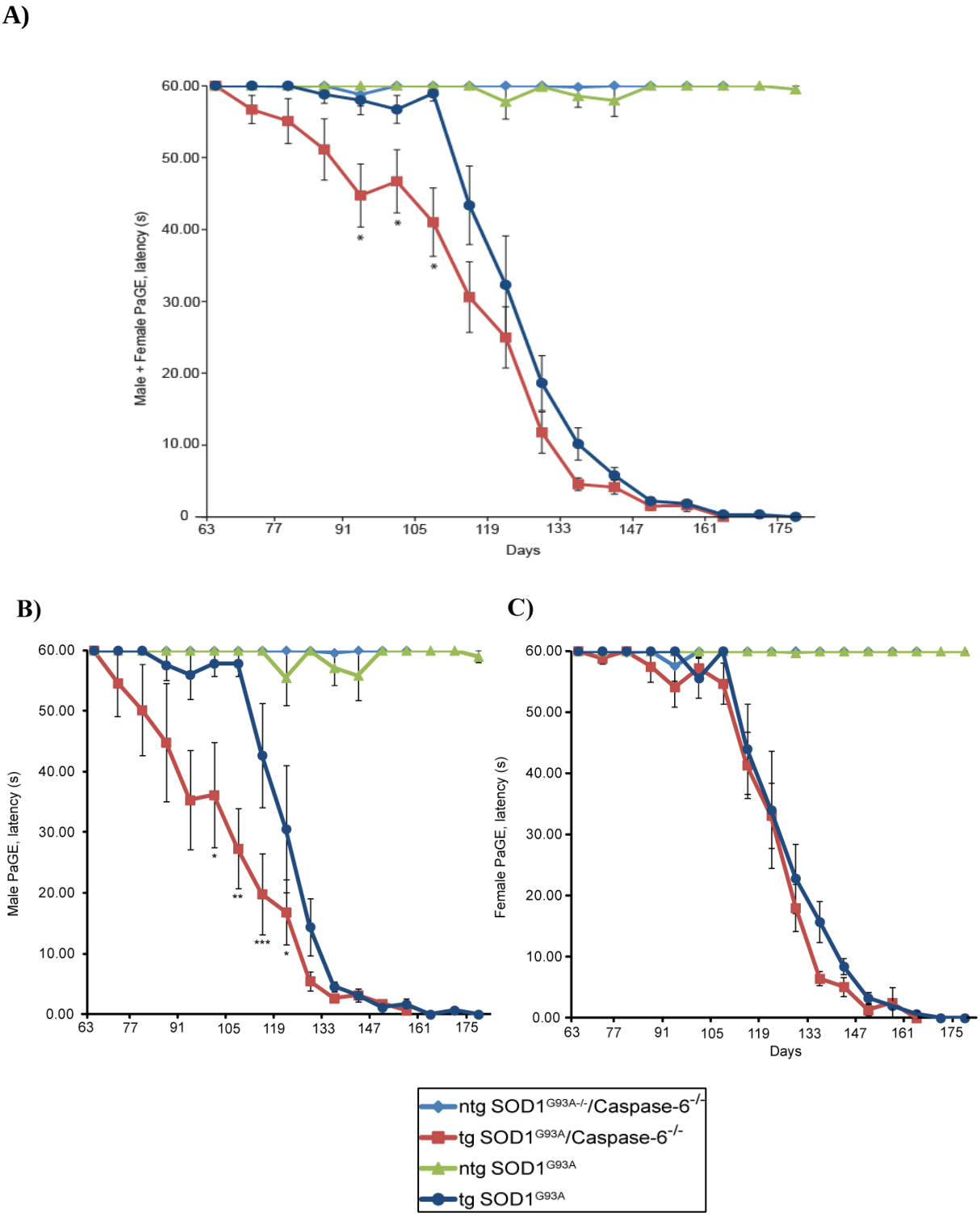

Figure 4.7 *Caspase-6* deficiency does not protect muscle endurance across ALS disease progression in SOD1^{G93A} mice

A) Mice were suspended on a mesh cage for up to a 60 second latency to fall. Mice were assessed twice a week and the two latency scores were averaged at the end of each week. Motor function testing commenced at pnd 63 following a training period until the loss or

righting reflex at approximately pnd 160. Transgenic SOD1^{G93A}; *caspase-6*$^{-/-}$ mice showed a decrease in PaGE performance when compared to tg SOD1^{G93A} mice during disease onset at pnd 90 until pnd 120 ($p \leq 0.05$) but no other significant differences were recorded. B) Male tg SOD1^{G93A}; *caspase-6*$^{-/-}$ mice demonstrated an earlier onset of loss of function than females and demonstrated a decrease in performance at disease onset (pnd 90) until late stage (pnd 120) compared to tg SOD1^{G93A}; *caspase-6*$^{+/+}$ mice. C) Female PaGE analysis showed no significance. ANOVA (*post-hoc*, Tukey) was used to assess statistical significance. Data are mean ± SEM, n= 4-6 mice per sex-matched treatment group (* $p \leq 0.05$, ** $p \leq 0.01$, *** $p \leq 0.001$)

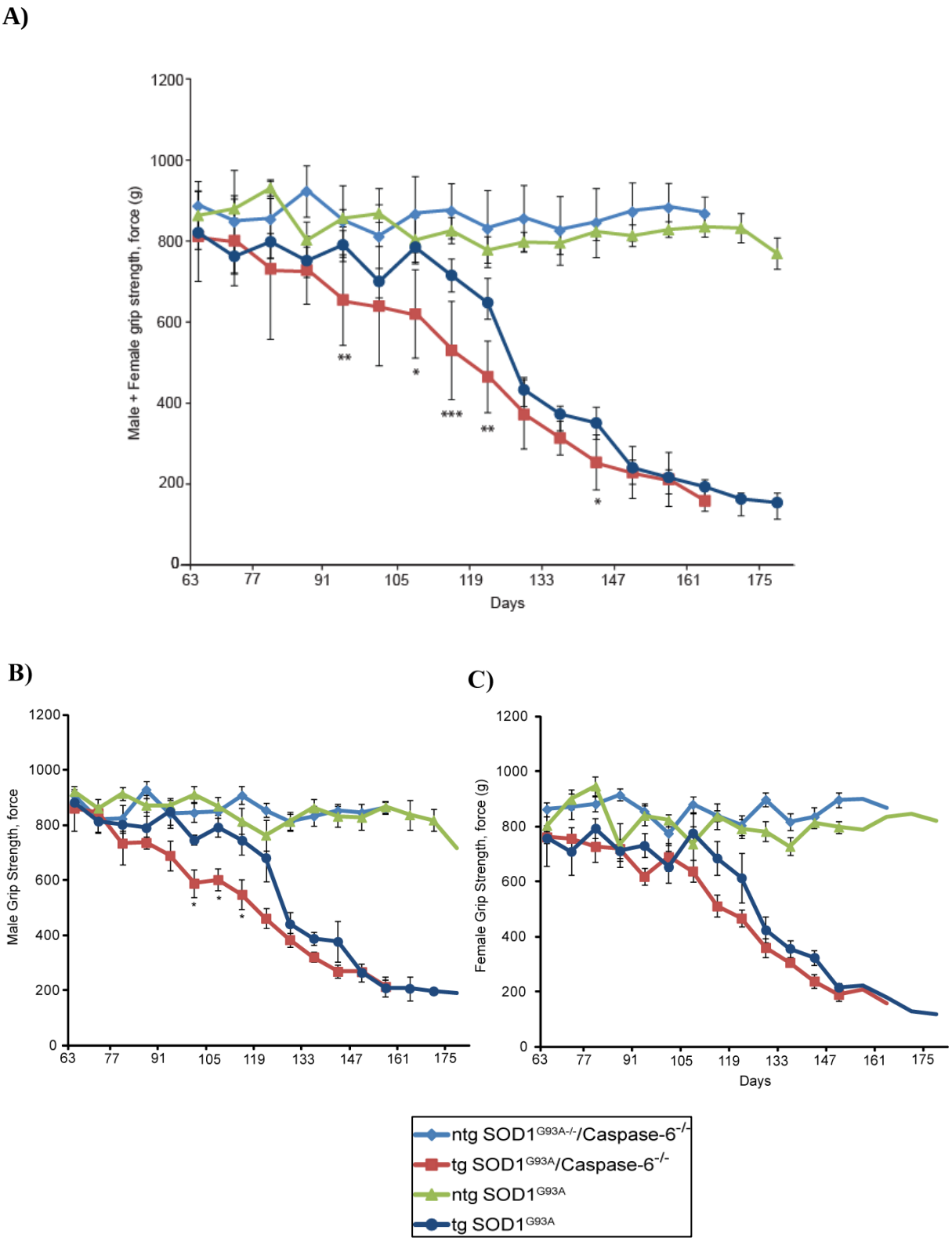

Figure 4.8: *Caspase-6* deficiency decreases grip strength endurance in SOD1^{G93A} mice

A) Grip strength meter assessment was used to determine forelimb strength. Mice were dragged across a trapeze which they instinctively grasped. The mice were pulled back and the

force of the resistance was recorded. Grip strength was performed twice weekly and the average of each reading was analysed across disease progression. Motor function testing commenced at pnd 63 following a training period until the loss or right reflex at approximately pnd 160. Transgenic SOD1^{G93A}; *caspase-6*$^{-/-}$ mice showed a decrease in PaGE performance when compared to tg SOD1^{G93A}; *caspase-6*$^{+/+}$ mice during disease onset (pnd 90) to late-stage of the disease (pnd 120) but no other significant differences were recorded. B) Male grip strength analysis showed significance at pnd 97 ($p=0.05$) to pnd 112 ($p=0.05$) for tg SOD1^{G93A}; *caspase-6*$^{-/-}$ compared to tg SOD1^{G93A}; *caspase-6*$^{+/+}$ mice. C) Female grip strength analysis showed no significance for tg SOD1^{G93A}; *caspase-6*$^{-/-}$ compared to tg SOD1^{G93A}; *caspase-6*$^{+/+}$ mice. ANOVA (*post-hoc*, Tukey) was used to assess statistical significance. Data are mean ± SEM, n= 4-6 mice per sex-matched treatment group (* $p\leq0.05$, ** $p\leq0.01$, *** $p\leq0.001$)

As previously described, stride lengths were measured on two consecutive left-to-left and right-to-right footprints and recorded twice a week. Transgenic SOD1^{G93A}; c*aspase-6* $^{-/-}$ mice showed a significant decrease in stride length during late-stage of the disease at pnd 140 ($p\leq0.001$) to endstage of the disease ($p\leq0.05$) when compared to tg SOD1^{G93A}; *caspase-6*$^{+/+}$ (Figure 4.9A). Male stride length was analysed with one significant result demonstrated by a decrease in stride length performance at pnd 160 for tg SOD1^{G93A}; c*aspase-6* $^{-/-}$ mice compared to tg SOD1^{G93A}; c*aspase-6* $^{+/+}$ mice (Figure 4.9B). Female stride length showed significance from pnd 140 ($p\leq0.01$) to pnd 147 ($p\leq0.001$) and at endstage of the disease (pnd 160) ($p\leq0.01$) when compared to tg SOD1^{G93A}; c*aspase-6* $^{+/+}$ (Figure 4.9C). Weight was also measured twice weekly and recorded for all genotypes. A decrease in body weight along with decreasing motor performance is an indication of disease progression in SOD1^{G93A} mice. Transgenic SOD1^{G93A}; c*aspase*$^{-/-}$ mice maintained their weight compared to tg SOD1^{G93A}; c*aspase*$^{+/+}$ controls from pnd 63 to end stage (Figure 4.10A). Male and female analysis also showed no significant results for body weight (4.10B/4.10C). These *in vivo* results suggest that *caspase-6* deficiency does not protect limb function, endurance, and motility across disease progression in SOD1^{G93A} mice and has no effect on body weight.

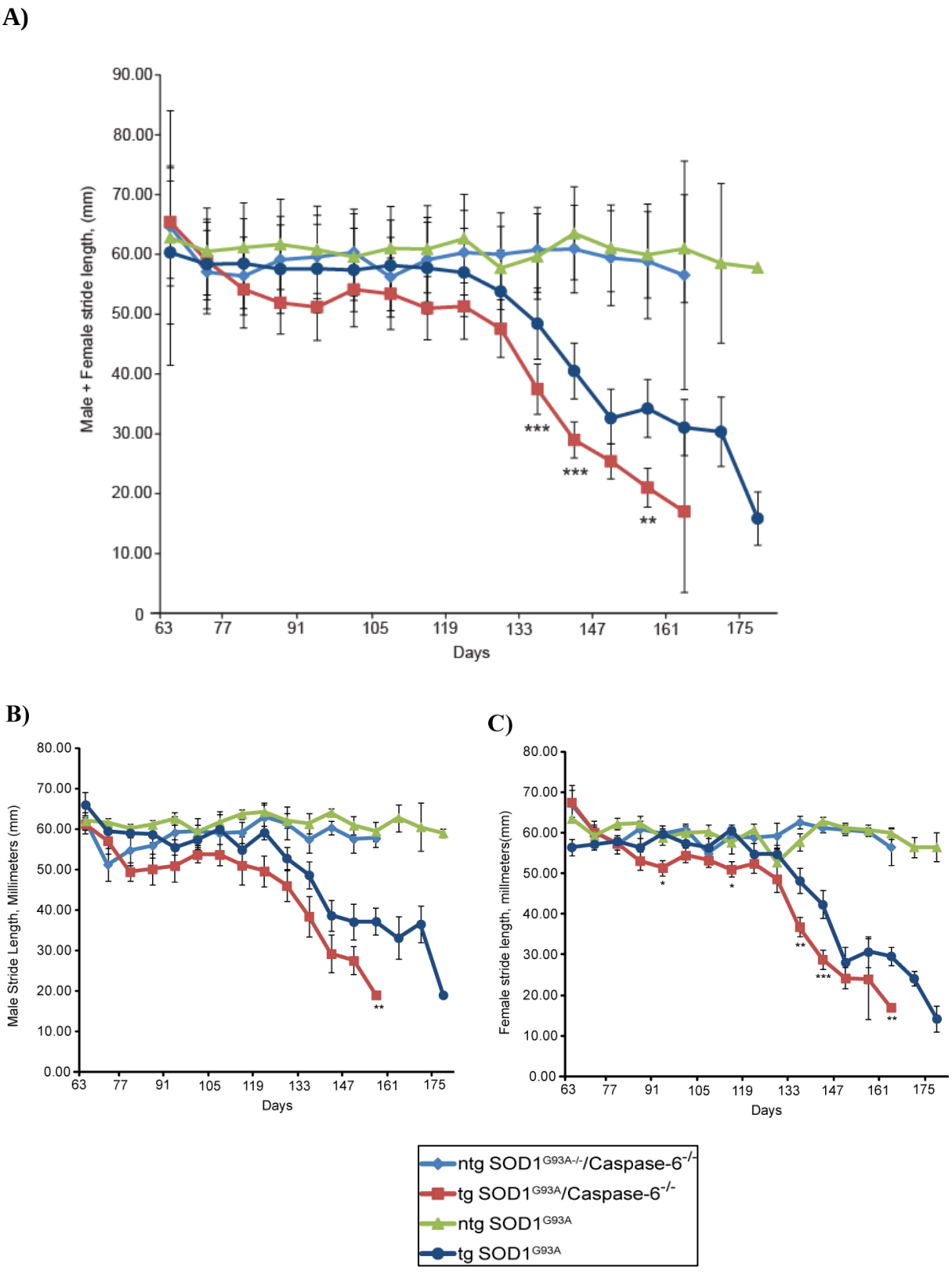

Figure 4.9: *Caspase-6* deficiency decreases hind limb motility in SOD1^{G93A} mice

A) The hind limbs of each mouse were painted with non-toxic paint and the mouse was trained to walk in a straight line along a sheet of paper. Two consecutive paw prints on the left and right foot were measured in millimetres (mm) and averaged for analysis. Stride

length measurement was performed weekly and recorded. Motor function testing commenced at pnd 90 following a training period until the loss or right reflex at approximately pnd 160. Transgenic SOD1^{G93A}; c*aspase-6* $^{-/-}$ mice showed a significant decrease in stride length when compared to tg SOD1^{G93A}; c*aspase-6* $^{+/+}$ mice during late stages of the disease (pnd 140) to endstage of the disease (pnd 160). B) Male stride length was analysed but no overtly significant results were found. C). Female stride length showed significance from pnd 140 ($p \leq 0.01$) to late-stage of the disease (pnd 160) when compared to tg SOD1^{G93A}; c*aspase-6* $^{+/+}$. ANOVA (*post-hoc*, Tukey) was used to assess statistical significance. n= 4-6 mice per sex-matched treatment group (* $p \leq 0.05$, ** $p \leq 0.01$, *** $p \leq 0.001$) Data are mean ± SEM.

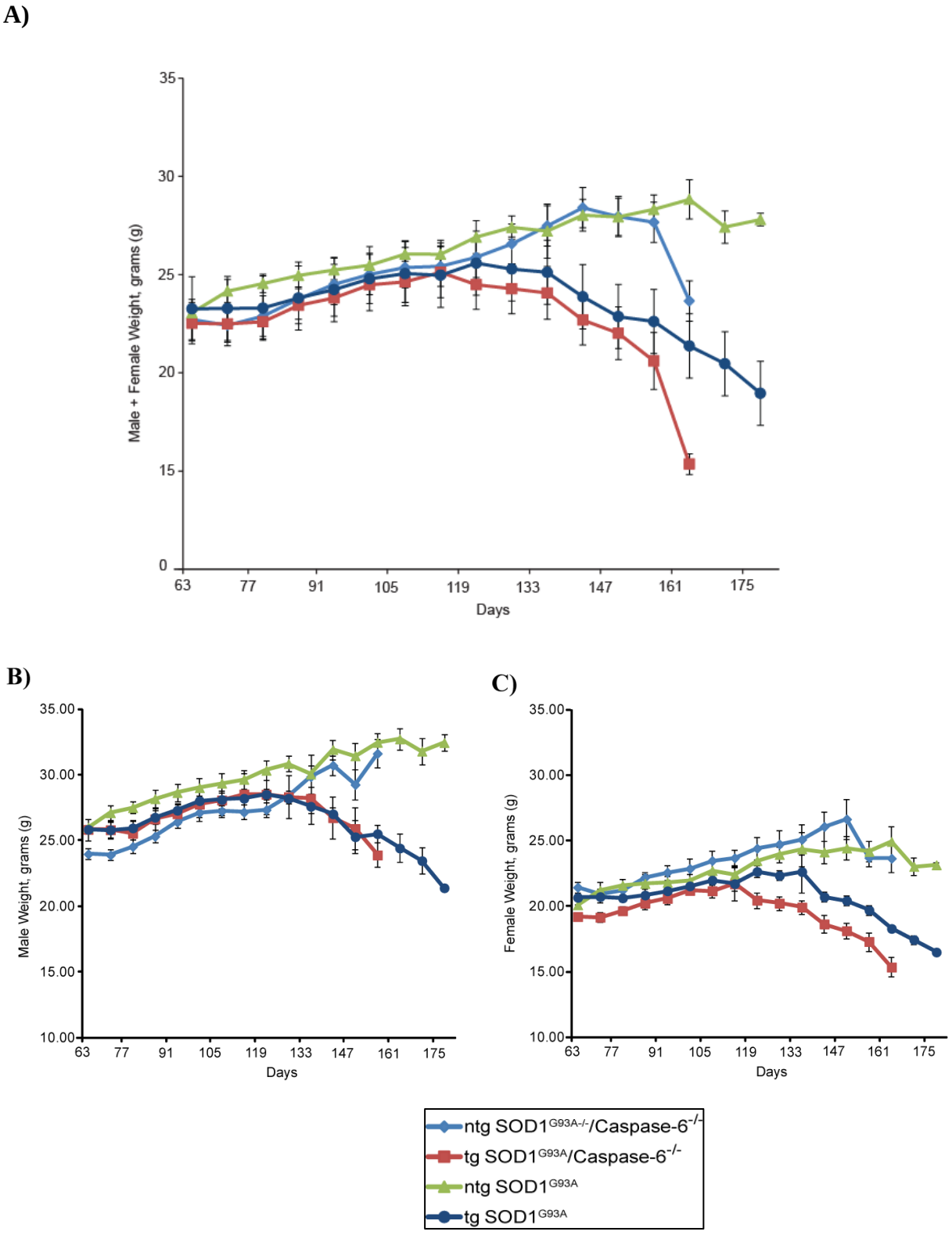

Figure 4.10: *Caspase-6* deficiency does not affect body weight across disease progression in SOD1^{G93A} mice

A) Body weight was measured for each mouse, twice weekly with the average weekly bodyweight recorded. Weight was measured on a laboratory scale and recorded in grams (g). Body weight measurement commenced at pnd 63 until the loss or right reflex at

approximately pnd 160. No significant difference was detected between tg SOD1^{G93A}; *caspase-6* $^{-/-}$ and tg SOD1^{G93A}; *caspase-6*$^{+/+}$ mice, however the *caspase-6* $^{-/-}$ mice consistently showed lower body weight throughout disease progression. B) Neither male nor female body weight analysis showed significant difference. ANOVA (*post-hoc*, Tukey) was used to assess statistical significance. n= 4-6 mice per sex-matched treatment group. Data are mean ± SEM

4.2.4 Effect of *Caspase-6* $^{-/-}$ deletion on lifespan and survival in SOD1^{G93A} mice

To further elucidate the role of caspase-6, we recorded the lifespan of SOD1^{G93A}; c*aspase-6* $^{-/-}$ mice to examine the effect of *caspase-6* deletion during disease progression. As previously described, mice were age, sex, and litter matched according to guidelines for pre-clinical ALS animal research (Ludolph, Bendotti *et al*., 2010). Survival was plotted on a Kaplan Meier curve. Non-parametric analysis revealed that genetic deletion of *caspase-6* did not increase survival in tg SOD1^{G93A}; *caspase-6*$^{-/-}$ mice compared to tg SOD1^{G93A} ; *caspase-6*$^{+/+}$ littermates, in fact it significantly decreased survival. Kaplan-Meier analysis of SOD1^{G93A}; *caspase-6*$^{-/-}$ colony showed a significant decrease in lifespan between tg SOD1^{G93A}; *caspase-6*$^{+/+}$ (167 ± 2 day) and tg SOD1^{G93A}; c*aspase-6*$^{-/-}$ (161 ± 1) mice (p=0.009) (Figure 4.11).

A)

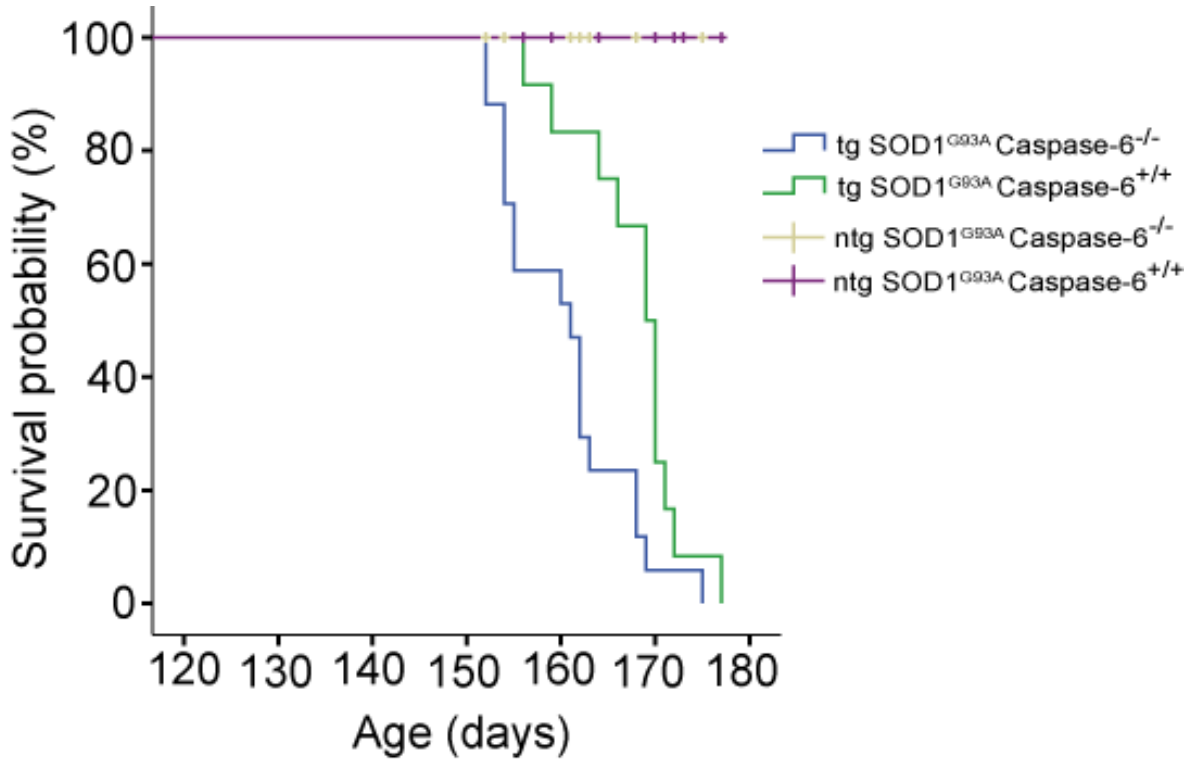

Figure 4.11: Decreased lifespan in the SOD1^{G93A}; caspase-6$^{-/-}$ colony

(A) Kaplan Meier analysis representing percentage of survival between SOD1^{G93A}*; caspase-6*$^{-/-}$ and SOD1^{G93A}; *caspase-6* $^{+/+}$ littermates. Endstage was assessed through an inability for any one mouse to right itself within 30 sec when placed on either side. Endstage mice were culled by intra-cardial perfusion. Lifespan was calculated for each mouse from date of birth up to/and including the day they were culled. Transgenic SOD1^{G93A}; *caspase-6* $^{+/+}$ (167 ± 1 day) mice survived longer than tg SOD1^{G93A}; *caspase-6*$^{-/-}$ (161 ± 1). Data represent n= 17 SOD1^{G93A}*; caspase-6* $^{-/-}$ (n=7 males and n=10 females) and n=14 wildtype mice (n=5 males and n=9 females). No significant differences were found when male versus female lifespan was analysed. Kaplan-Meier analysis was assessed using SPSS statistical analysis software.

A)

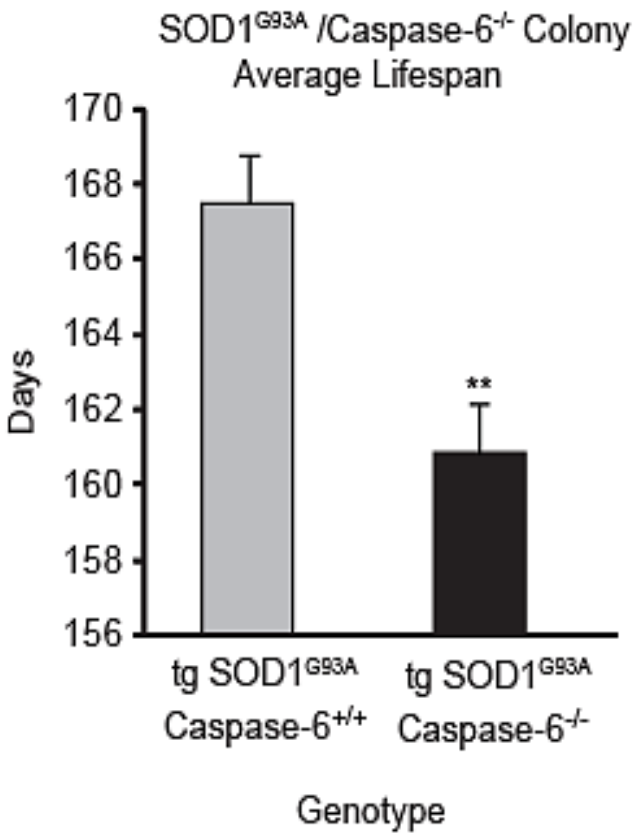

Figure 4.12: Average lifespan for tg mice from the SOD1^{G93A} Caspase-6 $^{-/-}$ colony

A) Lifespan was calculated for each mouse from date of birth up to/and including the day they were culled. Average lifespan was compared and statistical analysis showed that tg SOD1^{G93A}; *caspase-6* $^{+/+}$ (167 ± 2 day) mice survived longer than tg SOD1^{G93A}; *caspase-6*$^{-/-}$ (161 ± 1 day) (p=0.009) n= 4-6 mice per sex-matched treatment group (* p≤0.05, ** p≤0.01, *** p≤0.001) Data are mean ± SEM

These *in vivo* results described here suggest that *caspase-6* deficiency does not protect limb function, endurance, and motility across disease progression in SOD1^{G93A} mice and has no effect on body weight. In contrast to what we expected, *caspase-6* deletion appears to make ALS disease progression in the SOD1^{G93A} mouse model significantly worse.

4.2.5 Characterization of skeletal muscle in the SOD1^{G93A}; *caspase-6* $^{-/-}$ colony

In ALS, it has been proposed that abnormalities within skeletal muscle participate in triggering motor neuron degeneration and that alterations in different cell types may work together to exacerbate the disease (Pansarasa *et al*. 2014). A recent study completed by Wong and Martin (2010) showed that tg SOD1^{G93A} mice with site specific expression of SOD1 in skeletal muscle developed severe pathology involving oxidative damage, protein nitration, myofiber cell death and NMJ abnormalities (Wong and Martin, 2010). Another study utilized overexpressed mitochondria-targeted photoactivatable fluorescent proteins to identify abnormal mitochondrial dynamics in skeletal muscle of SOD1^{G93A} mice which occurred before disease onset (Luo *et al*. 2013). The primary location for motor dysfunction, either within motor neurons, within the motor axon, or at the level of the NMJ, is a question that is still unanswered. It has been hypothesized that the "dying-back" phenomena may be implicated in ALS disease pathology, where the distal axon degenerates before neuronal degeneration (Fischer *et al*. 2004). It has been suggested that this phenomena occurs in skeletal muscle (Fischer *et al*. 2004) and has become an area of interest in ALS disease research. Our group decided to look for evidence of muscular atrophy by investigating changes in weight and width of skeletal muscle in SOD1^{G93A};c*aspase-6*$^{-/-}$ colony compared to SOD1^{G93A} mice.

Gastrocnemius muscles from ntg SOD1^{G93A}; c*aspase-6*$^{+/+}$, tg SOD1^{G93A}; *caspase-6*$^{+/+}$, ntg SOD1^{G93A}; c*aspase-6*$^{-/-}$, and tg SOD1^{G93A}; c*aspase-6*$^{-/-}$ were dissected and photographed to compare the degree of muscular atrophy. The width of each muscle was measured and compared. A significant difference was observed for tg SOD1^{G93A}; c*aspase-6*$^{-/-}$ ($p \leq 0.001$) muscle width compared to ntg SOD1^{G93A}; c*aspase-6*$^{-/-}$ samples (Figure 4.13Ad). Muscle width in tg SOD1^{G93A}; c*aspase-6*$^{+/+}$ ($p \leq 0.001$) compared to ntg SOD1^{G93A}; c*aspase-6*$^{+/+}$ samples also showed significant difference. No significance was found between tg SOD1^{G93A}; *caspase-6*$^{+/+}$ and tg SOD1^{G93A}; c*aspase-6*$^{-/-}$ groups, suggesting that *caspase-6* deficiency does not affect muscle degeneration when measured at pnd endstage.

Gastrocnemius muscles were also weighed. Although tg SOD1^{G93A}; c*aspase-6*$^{-/-}$ muscle showed a decreased weight ($p \leq 0.001$) in comparison to ntg SOD1^{G93A}; c*aspase-6*$^{-/-}$ muscle, tg SOD1^{G93A}; c*aspase-6*$^{-/-}$ muscle weight did not yield significance when compared to tg SOD1^{G93A}; c*aspase-6*$^{+/+}$ muscle (Figure 4.13B). This data suggests that deletion of *caspase-6* does not affect directly affect muscular atrophy in SOD1^{G93A} mice.

A)

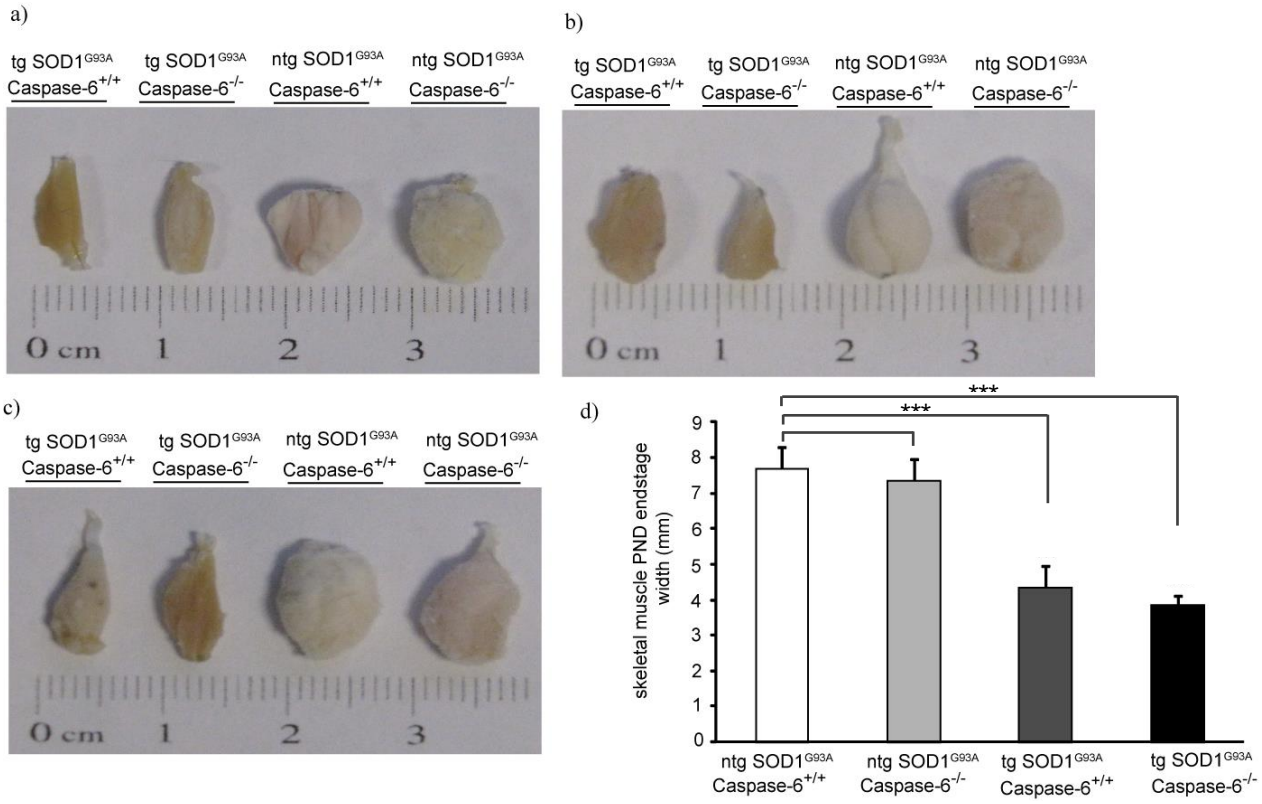

B)

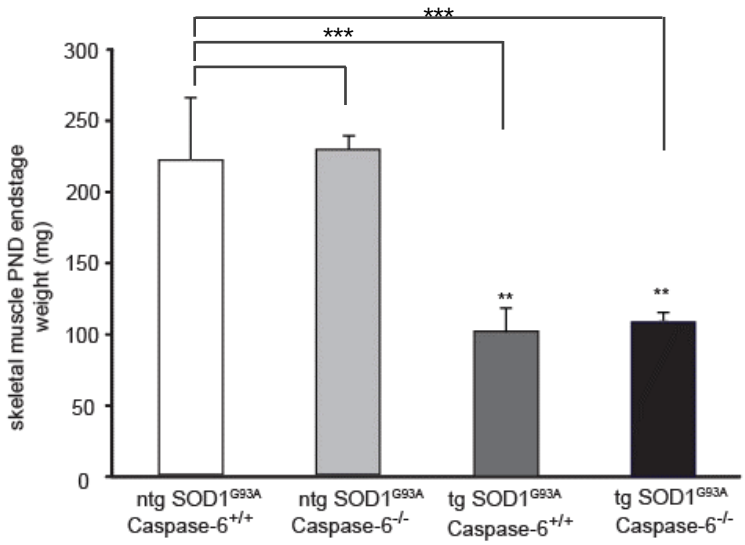

Figure 4.13: Characterization of gastrocnemius muscle at PND endstage in the SOD1^{G93A} Caspase-6 $^{-/-}$ colony shows a decrease in weight and morphology

A) Gastrocnemius muscles from ntg SOD1^{G93A}; c*aspase-6*$^{+/+}$, tg SOD1^{G93A}; *caspase-6*$^{+/+}$, ntg SOD1^{G93A}; c*aspase-6*$^{-/-}$, tg SOD1^{G93A};c*aspase-6*$^{-/-}$ were dissected and photographed to compare the degree of muscular atrophy. Images were taken with muscle samples in the order of: tg SOD1^{G93A}; *caspase-6*$^{+/+}$ (n=3), tg SOD1^{G93A}; c*aspase-6*$^{+/+}$ (n=3), ntg SOD1^{G93A};

caspase-6$^{+/+}$ (n=3), and tg SOD1^{G93A}; *caspase-6*$^{-/-}$ (n=3). B) Gastrocnemius muscles were weighed and averaged. Significance was detected between tg SOD1^{G93A}; *caspase-6* $^{-/-}$ and ntg SOD1^{G93A}; *caspase-6*$^{+/+}$ muscle. Transgenic SOD1^{G93A}; c*aspase-6*$^{-/-}$ muscle weight did not yield significance when compared to tg SOD1^{G93A}; c*aspase-6*$^{+/+}$ muscle. Data were analysed using one-way ANOVA. Data are mean ± SEM

4.3 Summary

Apoptosis has been implicated in ALS disease progression in humans and SOD1 mouse models (Portera-Cailiau *et al*. 1997; Sathasivam *et al*. 2001; Ghavami *et al*. 2014). Several groups have shown that deletion of *caspase-6 in vitro* may be beneficial in neurodegeneration (Nikolaev *et al*. 2009; Vohra *et al*. 2010), initiating an interest in caspase-6 as a therapeutic target for ALS. Uribe *et al* demonstrated through *in vitro* experiments that deletion of *caspase-6* in neurons promotes protection against excitotoxicity, nerve growth factor deprivation and myelin-induced axonal degeneration (Uribe *et al*. 2012). We wanted to determine if deletion of *caspase-6* would be beneficial *in vivo,* therefore we generated a cross-breeding program to include *caspase-6* deficiency in an ALS mouse model. Prior to the generation of the SOD1^{G93A}; c*aspase-6* colony, we showed that the phenotype, Rotarod performance, and body weight was not altered with the deletion of *caspase-6* compared to wildtype. We also investigated whether motor endplate morphology was altered in *caspase-6* deficient mice compared to ntg SOD1^{G93A} mice (Figure 4.2). Our findings showed no obvious signs of variation. To elucidate the role of caspase-6 in ALS, we generated a cross breeding to include: tg SOD1^{G93A}; c*aspase-6*$^{-/-}$, tg SOD1^{G93A}; c*aspase-6*$^{+/+}$, ntg SOD1^{G93A}; c*aspase-6*$^{-/-}$, tg SOD1^{G93A}; c*aspase-6*$^{-/-}$ (Figure 4.3).

To investigate the implications of a *caspase-6* deficiency *in vivo,* we monitored and recorded motor function performance and lifespan from pnd 63 to endstage. Our results showed that *caspase-6* deficiency in tg SOD1^{G93A}; c*aspase-6*$^{-/-}$ mice resulted in a decrease in survival compared to tg SOD1^{G93A}; c*aspase-6*$^{+/+}$ (Figure 4.11) and motor function performance (Figures 4.6-4.10). In skeletal muscle, we compared weight and morphology of gastrocnemius muscle in SOD1^{G93A} mice and showed that deletion of *caspase-6* does not affect muscular atrophy in this mouse model for ALS.

Our initial hypothesis was that deletion of *caspase-6* would protect neurons against cell death and therefore improve the phenotype in the SOD1^{G93A} ALS mouse model. However we found the opposite were true and that deletion of *caspase-6* enhanced disease progression and

decreased lifespan. This suggests that caspase-6 plays a crucial role in neuronal survival possibly via cell removal of damaged cells, for instance cells that have been damaged by ROS caused by SOD1 toxicity. It is possible that caspase-6 may be pivotal in the regulation of cell death decisions within damaged cells and may be necessary to prevent damage to neighbouring cells. It has been proposed that caspase-6 demonstrates an unrecognized extracellular role and is released from axonal terminals, regulates microglial TNF-α secretion, synaptic plasticity, and inflammatory pain and may have a beneficial role in neuropathy (Berta et al. 2014). This evidence supports our hypothesis that this executioner caspase is protective during ALS pathogenesis as the degenerative phenotype is worse when *caspase-6* is removed, however further work is required to fully characterise the role of caspase-6.

CHAPTER 5

Discussion

5.1 Caspase-6 and ALS

ALS is a neurodegenerative disease that is both progressive and incurable, with an incidence of 2-3 cases per 100,000 annually. The degeneration of motorneurons is key to the progression of the disease, resulting in muscle weakness and atrophy. For ALS, median survival time is typically 2-3 years post diagnosis. Significant data has been published since French neurologist Jean-Martin Charcot first described the progressive and fatal paralysis now known as ALS in 1869, yet the principle mediators of ALS remain elusive. Although the more recent development of the $SOD1^{G93A}$ mouse model of ALS has been beneficial to understanding the disease, in the past 3-4 years substantial advances have been made to identify other genes involved in ALS disease pathophysiology. This advancement has resulted in the development of additional mouse models including FUS and TARDBP (known as TDP-43) mice (reviwed in Leblond *et al*., 2014). Despite the recent genetic advances in addition to decades of research, no cure has been discovered for ALS. Causative factors which culminate in ALS have been identified including, glial cell pathology, glutamate excitotoxicity, growth factor deprivation, caspase mediated cell death, defects in axonal transport, mitochondrial dysfunction, oxidative damage and accumulation of intracellular aggregates (Pasinelli and Brown, 2006). Recent *in vivo* studies have shown that deletion of *caspase-6* prevents axonal degeneration (Uribe et al. 2012). We hypothesized that if we remove caspase-6 in the $SOD1^{G93A}$ mouse we may be able to prevent axonal degeneration and delay disease onset and progression. To assess this we generated a cross-bred colony to examine the effect of *caspase-6* deficiency on motor function and survival in the $SOD1^{G93A}$ ALS mouse model. However, surprisingly we found that elimination of caspase-6 significantly exacerbated the symptoms and decreased the lifespan of $SOD1^{G93A}$ mice. There are several reasons why this may be occurring. One explanation is that caspase-6 may be involved regulating cell removal of damaged cells, for instance cells that have been damaged by ROS caused by SOD1 toxicity. It is also possible that caspase-6 has a protective role that has not been characterized yet but which is evidenced by the degenerative phenotype which was increased when caspase-6 was removed.

5.2 The role of apoptosis in Amyotrophic Lateral Sclerosis

Apoptosis is central to the maintenance of cellular homeostasis, during embryonic development and for the removal of diseased or damaged cells in the body. *In vivo* studies on the effects of caspase deficiencies in mice have shown embryonic lethality for *caspase-9* deletion and also when *caspase-3* is removed but is strain dependent, whereas *caspase-6*

removal does not demonstrate an overtly altered phenotype (Kuida *et al*. 1996; Hakem *et al*. 1998). Understanding the apoptotic pathway is important for the study of diseases where excessive or insufficient cell death may play a part in disease pathogenesis. It has been suggested that caspase-6 may have an upstream role in the pathogenesis of neurodegenerative diseases (Graham *et al*. 2011) and may be a possible therapeutic target in neurodegenerative disease.

The primary pathogenic processes underlying MND are likely to be multifactorial, and the precise mechanisms underlying the cell death pathway are still unknown. Programmed cell death and caspase activation has been commonly studied as apoptotic dysfunction is a potential mediator for ALS disease progression. In the spinal cord of $SOD1^{G93A}$ mice, caspase-1 and caspase-3 expression and activation was shown to increase in symptomatic mice (Li *et al*. 2000). Caspase-9 is suggested to play a crucial role in the pathogenesis of ALS (Inoue et al., 2003) and activation has been detected in transgenic ALS mouse models (Guegan et al., 2001). Other evidence incudes a study completed by Tokuda *et al.*, that identified Caspase-3, -8 and -9 upregulation and activation in the spinal cord of transgenic SOD1 mice at 8 and 16 weeks (Tokuda *et al*. 2007). Further work *in vitro* has demonstrated that under unstressed basal culture conditions, mutant SOD1 containing cells appear to be ‘‘primed’’ for apoptosis as evidenced by increased amounts of phosphatidyl serine that are expressed on the cell surface and increased cleavage and activation of the initiator caspase-9 compared to control cells (Sathasivam, S. *et al*. 2005).

Several studies have shown neuronal caspase-6 activity is involved in axonal degeneration *in vivo* (Nickolaev *et al*. 2009; Simon *et al*. 2012; Uribe *et al*. 2012). We reason that caspase-6 may be involved in the phenomenon known as the “dying-back” hypothesis which shows a distal to proximal axonal degeneration in the $SOD1^{G93A}$ mouse model (Dadon-Nacum *et al*. 2011). This lead to the theory that motor unit loss and associated muscle function may precede motorneuron death (Fischer *et al*. 2004; Vinsant *et al*. 2013). In mouse models for ALS, muscle denervation has been shown to occur months before motorneuron death (Frey *et al*. 2000; Fischer *et al*. 2004; Gould *et al*. 2006; Pun *et al*. 2006). There are few studies of this issue in humans, but it appears that denervation also corresponds to early symptom onset in ALS patients (Ag-garwal and Nicholson, 2002; Fischer *et al*. 2004; Blijham *et al*. 2007). The specific molecular mechanisms mediating axon/synapse loss in ALS are unknown, but it has been suggested that mutant SOD1 may alter retrograde transport and synaptic stability by disrupting the cytoplasmic dynein motor in motorneurons (Ligon *et al*. 2005). Additional

evidence can be seen in a study that utilized the Loa (Legs at odd angle) mice that have a mutation in cytoplasmic dynein (Kieran *et al*. 2005) crossed with in the $SOD1^{G93A}$ mouse model, which showed that inhibition of retrograde transport may be protective, perhaps by inhibiting the transport of toxic negative signals (Ilieva *et al*. 2008). Similarly, one theory suggests an aggregation of insoluble complexes, possibly mutant SOD1, which causes an insufficient maintenance of the distal axon and results in axonal abnormalities that inhibit retrograde transport and allow for selective damage to motor neurons (Dadon-Nacum *et al*. 2011).

Caspase-6 cleavage of proteins in AD and HD promotes neurodegeneration by producing small toxic fragments of proteins (Galvan *et al*. 2006; Graham *et al*. 2006). It should be noted that, although compelling, evidence for AD and HD pathology provided by Galvan *et al*. and Graham et al. remains controversial due to conflicting data that was recently published. Harris *et al*. demonstrated through extensive neuronal and behavioral testing that impairment in transgenic mouse models of AD with mutations at the D664 site are independent of caspase cleavage of the amyloid precursor protein and inhibition of these mutations may have a lesser benefit than previously reported (Harris *et al*. 2010). In HD, it has been hypothesized that proteolysis of Htt at the caspase-6 cleavage site, amino acid Asp-586, plays a critical role in disease progression and pathogenesis (Hermel *et al*. 2004). Gafni *et al*. showed through in vivo studies utilizing caspase-$6^{-/-}$ mice that contradict this hypothesis but caspase-6 may have a role in clearance pathways for mHtt protein (Gafni *et al*. 2012). It is not likely activated caspase-6 triggers neurodegeneration by cleavage of one specific protein due to the fact that caspase-6 has a high number of protein substrates in neurons (Petzke *et al*. 2006). It has also been shown that caspase-6 has a unique substrate, lamin A/C, which is not cleaved by either caspase-3 or caspase-7 (Takahashi *et al*. 1996). Other substrates have been identified in degeneration including AT-rich binding protein-1 (SATB1) in apoptosis (Galande, S. *et al*. 2001), the neurodegenerative disease proteins Huntingtin (Graham *et al*. 2006) in HD, and amyloid precursor protein in AD (Pellegrini *et al*. 1999). It is possible that SOD1 could be a substrate unique to caspase-6 which may play a role in the degenerated phenotype in caspase-6 deficient $SOD1^{G93A}$ mice, but further work is necessary to provide evidence for this hypothesis.

It has been suggested that caspase-6 exhibits an atypical role from executioner protease (Graham *et al*. 2011), and demonstrates the ability to self-activate (Klaiman *et al*. 2008), therefore it is possible that caspase-6 may have a role in the regulation of toxic cells through

self-activated pathway that has not yet been identified. It has been proposed that caspase-6 has an extracellular role in signalling or eliciting an inflammatory response via TNF-α which may be protective, therefore it is possible that when caspase-6 is inhibited, protection against inflammation is decreased and the phenotype is exacerbated. Supporting this theory is a study completed by Berta *et al.* which showed that caspase-6 released from axonal terminals regulates microglial TNF-α secretion, synaptic plasticity, and inflammatory pain *in vivo* (Berta *et al*. 2014).

5.3 The role of caspase-6 in neurodegenerative disease

Increased apoptosis is associated with several neurodegenerative conditions like AD and HD (Okouchi *et al*. 2007). It has been hypothesized that caspase-6 has a role in disease pathology for ALS, and other neurodegenerative diseases. Active caspase-6 was discovered in post mortem brains of HD and AD subjects that did not have an apoptotic morphology, which suggests an alternative earlier function for caspase-6 other than an effector caspase (Albrecht *et al*. 2007, Graham *et al*. 2010) although this data is controversial. Studies have shown that active caspase-6 may contribute to the generation of AD pathology by evidence of increased production of Aβ in primary cultures of human neurons, as well as caspase-6 cleavage of tau and several synaptic proteins (LeBlanc *et al*. 1999, Albrecht *et al*, 2007). Through the use of a yeast artificial chromosome (YAC) model of HD, it was shown that expression of a mutation that eliminates cleavage at aa 586 of mutant Huntington (mhtt) by caspase-6 is sufficient to preserve striatal volume and cognitive and motor function (Graham *et al*. 2010). This evidence supports the theory that caspase-6 contributes negatively to neurodegeneration, but we have demonstrated that caspase-6 may provide a protective element in ALS.

Our data shows caspase-6 levels were elevated at endstage of the disease in $SOD1^{G93A}$ lumbar spinal cord and hypothesize that there is an increase in microglia at endstage of the disease. We were unable to locate pro or active caspase-6 in tg and ntg $SOD1^{G93A}$ skeletal muscle via immunohistochemical analysis (data not shown), but we found no evidence for alteration at the neuromuscular junction leading us to suggest that the beneficial role of caspase-6 occurs in the CNS. As such, our data suggests that the beneficial role of caspase-6 observed here may occur in other neurodegenerative diseases and caution should be exercised when investigating novel therapeutics targeting caspase-6.

5.4 Summary and Outlook

Riluzole is the only Food and Drug Administration (FDA)-approved treatment that is available to ALS patients and only extends the life of some ALS patients by 3-6 months while alleviating associated symptoms (Miller *et al*. 2007; Bellingham, 2011). Presently, there are no drugs on the market that reverse the disease. Successful inhibition of caspase-6 is an attainable goal since enzymes can be inhibited in several ways; they are viable targets for drug development. There are no known endogenous protein inhibitors of caspase-6 (Edigington *et al*. 2013). Phosphorylation is also an inhibitor of caspase-6 (Velazques-Delgado and Hardy, 2012). In addition, it has been reported that inhibitor of apoptosis protein (IAP) that inhibit active caspase-3, caspase-7, and caspase-9 do not inhibit caspase-6 (Deveraux and Roy *et al*. 1998). The use of zinc has been suggested as a potential inhibitor of selective caspase-6 due to its allosteric binding site that is unique to caspase-6, as the residues involved in zinc binding are not conserved across the caspase family (Velazques-Delgado and Hardy, 2012). It is important to note that no obvious developmental defects were initially discovered when the caspase deficient mouse was first developed (Zandy *et al*. 2005), but further studies have identified age-dependent and region-specific changes in the brains of caspase-6 deficient mice (Uribe et al. 2012). In order to most effectively target apoptosis in ALS, it is necessary to gain more information regarding the consequences of inhibition of caspase-6 as well as upstream activators of apoptosis in neurodegenerative diseases. Our data suggests that caspase-6 has a beneficial role in preventing disease progression in the $SOD1^{G93A}$ ALS mouse model and is therefore not a good target for novel therapeutics.

Based on our experiments, we conclude that genetic ablation of caspase-6 in the $SOD1^{G93A}$ mouse significantly affects motor function performance and survival, although molecular mechanisms are not fully understood. We cannot exclude the amelioration of additional parameters, for instance pre-symptomatic axonal abnormalities that inhibit retrograde transport and allow for selective damage to motor neurons. Future experiments to identify the role of caspase-6 may include a comparative behavioural study between caspase-3 and caspase-6 deficient mice crossed with other ALS mouse models for instance, TDP-43. A proteomic study would also be salient to determine if SOD1 is substrate of caspase-6. Other beneficial data regarding $SOD1^{G93A}$; c*aspase-6* cross-breed may include motorneuron counts compared to muscle denervation at different stages of ALS disease progression to determine the potential order and location of apoptotic events. A better understanding of the neuronal

death pathways may provide targets for the development of therapeutic interventions for ALS and other neurodegenerative diseases.

CHAPTER 6

References

Adrain,C., B.M. Murphy, S.J. Martin (2005). “Cytotoxic T Lymphocyte/Natural Killer Activation Cascade Initiated by the Molecular Ordering of the Caspase Developmental (CTL/NK) Protease Granzyme B.” J. Biol. Chem 280:4663-4673

Aggarwal, A., and G. Nicholson (2002). “Detection of preclinical motor neurone loss in SOD1 mutation carriers using motor unit number estimation.” J. Neurol. Neursurg. Psych. 73:199–201.

Albrecht, S., M. Bourdeau, D. Bennett, E. J. Mufson, M. Bhattacharjee and A. C. LeBlanc (2007). "Activation of caspase-6 in aging and mild cognitive impairment." Am J Pathol 170(4): 1200-1209.

Albrecht, S., N. Bogdanovic, B. Ghetti, B. Winblad, A.C. LeBlanc (2009) “Caspase-6 Activation in Familial Alzheimer Disease Brains Carrying Amyloid Precursor Protein, Presenilin I or Presenilin II Mutations.” J Neuropathol Exp Neurol 68(12): 1282–1293.

Al-Chalabi, A.,A. Jones, et al. (2012). "The genetics and neuropathology of amyotrophic lateral sclerosis." Acta Neuropathol.

Allsopp T.E., McLuckie J., Kerr L.E., Macleod M., Sharkey J., Kelly J.S. (2000). “Caspase-6 activity initiates caspase 3 activation in cerebellar granule cell apoptosis.” Cell Death Differ **7**: 984–993

Andersen, P. M. and A. Al-Chalabi (2011). "Clinical genetics of amyotrophic lateral sclerosis: what do we really know?" Nat Rev Neurol 7(11): 603-615.

Bellingham, M. C. (2011). "A review of the neural mechanisms of action and clinical efficiency of riluzole in treating amyotrophic lateral sclerosis: what have we learned in the last decade?" CNS Neurosci Ther 17(1): 4-31.

Berta, T., C. K. Park, Z. Z. Xu, R. G. Xie, T. Liu, N. Lu, Y. C. Liu and R. R. Ji (2014). "Extracellular caspase-6 drives murine inflammatory pain via microglial TNF-alpha secretion." J Clin Invest 124(3): 1173-1186.

Blijham, P. J., H. J. Schelhaas, H. J. Ter Laak, B. G. van Engelen and M. J. Zwarts (2007). "Early diagnosis of ALS: the search for signs of denervation in clinically normal muscles." J Neurol Sci 263(1-2): 154-157.

Block, M.L. and Hong, J.S. (2005). "Microglia and inflammation-mediated neurodegeneration: multiple triggers with a common mechanism." Prog Neurobiol. 76(2):77-98.

Boya P, Kroemer G. (2008) "Lysosomal membrane permeabilization in cell death." Oncogene. 27:6434–6451.

Brooks, S. P. and S. B. Dunnett (2009). "Tests to assess motor phenotype in mice: a user's guide." Nat Rev Neurosci 10(7): 519-529.

Brown, L. T., Jr. (1971). "Projections and termination of the corticospinal tract in rodents." Exp Brain Res 13(4): 432-450.

Byrne, S., P. Bede, et al. (2011). "Proposed criteria for familial amyotrophic lateral sclerosis." Amyotroph Lateral Scler 12(3): 157-159

Chen, S., S. Pavani, Z. Xiaojie, L. Weidong (2013). "Genetics of amyotrophic lateral sclerosis: An update." Molecular Neurodegeneration 8:28

Clement, A.M., M.D. Nguyen, E.A. Roberts, et al. (2003) Wild-type noneuronal cells extend survival of SOD1 mutant motor neurons in ALS mice. Science. 302:113–11

Cohen, G.M., (1997) "Caspases: The executioners of apoptosis." Biochem. J 326 (Pt1) 1–16.

Cory, S. and J. M. Adams (2002). "The Bcl2 family: regulators of the cellular life-ordeath switch." Nat Rev Cancer 2(9): 647-656.

Cowling, V. and Downward, J. (2002) “Caspase-6 is the direct activator of caspase-8 in the cytochrome c-induced apoptosis pathway: absolute requirement for removal of caspase-6 prodomain.” Cell Death Differ (10):1046-56.

Cozzolino, M. and M. T. Carri (2012). "Mitochondrial dysfunction in ALS." Prog Neurobiol 97(2): 54-66.

Dadon-Nachum, M., E. Melamed, D. Offen (2011). “The “Dying-Back” Phenomenon of Motor Neurons in ALS” (2010). J Mol Neurosci 43:470–477

De Vos K.J., Grierson A.J., Ackerley S., Miller C.C. (2008). “Role of axonal transport in neurodegenerative diseases.” Annu Rev Neurosci 31:151–173.

Deveraux Q.L., R. Takahashi, G.S. Salvesen, J.C. Reed (1997). “X-linked IAP is a direct inhibitor of cell-death proteases.” Nature 388: 300–304

Deveraux, Q.L., N. Roy, H.R. Stennicke, T. Van Arsdale1, Q. Zhou, S. M. Srinivasula, E.S. Alnemri, G.S. Salvesen, J.C. Reed (1998). “IAPs block apoptotic events induced by caspase-8 and cytochrome c by direct inhibition of distinct caspases.” EMBO Vol.17 No.8 pp.2215–2223

Doble, A. (1996) “The pharmacology and mechanism of action of Riluzole.” Neurology vol. 47 no. 6 Suppl 4 233S-241S

Doostzadeh-Cizeron J, S. Yin, D.W. Goodrich (2000). “Apoptosis induced by the nuclear death domain protein p84N5 is associated with caspase-6 and NF-κB activation.” J Biol Chem 275: 25336–25341

Edgington, L.E., et al. (2012). An Optimized Activity-Based Probe for the Study of Caspase-6 Activation.” Chemistry & Biology 19, 340–352

Ferrer, I. et al. (2000). “Differential c-Fos and caspase expression following kainic acid excitotoxicity.” Acta Neuropathol 99, 245-256.

Fischer, L. R., D. G. Culver, P. Tennant, A. A. Davis, M. Wang, A. Castellano-Sanchez, J. Khan, M. A. Polak and J. D. Glass (2004). "Amyotrophic lateral sclerosis is a distal axonopathy: evidence in mice and man." Experimental Neurology 185(2): 232-240.

Frey, D., C. Schneider, L. Xu, J. Borg, W. Spooren, and P. Caroni. (2000). "Early and selective loss of neuromuscular synapse subtypes with low sprouting competence in motoneuron diseases." J. Neurosci 20:2534–2542.

Fridovich I. (1995) "Superoxide radical and superoxide dismutases." Annu Rev Biochem 64:97–112

Friedlander, R. M. (2003). "Apoptosis and caspases in neurodegenerative diseases." N Engl J Med 348(14): 1365-1375.

Fuchs, Y. and H. Steller (2011). "Programmed cell death in animal development and disease." Cell 147(4): 742-758.

Gafni J, Papanikolaou T, Degiacomo F, Holcomb J, Chen S, Menalled L, Kudwa A, Fitzpatrick J, Miller S, Ramboz S, Tuunanen PI, Lehtimäki KK, Yang XW, Park L, Kwak S, Howland D, Park H, Ellerby LM. (2012) "Caspase-6 activity in a BACHD mouse modulates steady-state levels of mutant huntingtin protein but is not necessary for production of a 586 amino acid proteolytic fragment." J Neurosci. 32(22):7454-65

Galande, S., L.A. Dickinson, I.S. Mian, M. Sikorska, T. Kohwi-Shigematsu (2001). "SATB1 cleavage by caspase-6 distrupts PDZ domain-mediated dimerization, causing detachment from chromatin early in T-cell apoptosis." Mol. Cell Biol 21, 5591-5604.

Galvan, V., O. F. Gorostiza, S. Banwait, M. Ataie, A. V. Logvinova, S. Sitaraman, E. Carlson, S. A. Sagi, N. Chevallier, K. Jin, D. A. Greenberg and D. E. Bredesen (2006). "Reversal of Alzheimer's-like pathology and behavior in human APP transgenic mice by mutation of Asp664." Proc Natl Acad Sci U S A 103(18):7130-5

Gervais, F.G., D. Xu, G.S. Robertson, J.P. Vaillancourt, Y. Zhu, J. Huang, A. LeBlanc, D. Smith, M. Rigby, M. Shearman, M.S. et al. (1999). “Involvement of caspases in proteolytic cleavage of Alzheimer’s amyloid-beta precursor protein and amyloidogenic A beta peptide formation.” Cell 97,395-406

Ghavami, S., M. Hashemi, S.R Ande, B. Yeganeh, W. Xiao, M. Eshraghi, C.J Bus, K. Kadkhoda, E. Wiechec, A.J. Halayko, M. Los (2009). “Apoptosis and cancer: mutations within caspase genes. J. Med. Genet 46, 497–510.

Ghavami, S., S. Shojaei, B. Yeganeh, S. R. Ande, J. R. Jangamreddy, M. Mehrpour, J. Christoffersson, W. Chaabane, A. R. Moghadam, H. H. Kashani, M. Hashemi, A. A. Owji and M. J. Los (2014). "Autophagy and apoptosis dysfunction in neurodegenerative disorders." Prog Neurobiol 112: 24-49.

Gingras, M., V. Gagnon, et al. (2007). "Optimized protocols for isolation of primary motor neurons, astrocytes and microglia from embryonic mouse spinal cord." 27 Suppl 1: S128-136. J Neurosci Methods

Godefroy, N., B. Foveau, S. Albrecht, C. G. Goodyer and A. C. LeBlanc (2013). "Expression and activation of caspase-6 in human fetal and adult tissues." PLoS One 8(11): e79313.

Gordon, P. H. (2013). "Amyotrophic Lateral Sclerosis: An update for 2013 Clinical Features, Pathophysiology, Management and Therapeutic Trials." Aging Dis 4(5): 295-310.

Gould, T. W., R. R. Buss, S. Vinsant, D. Prevette, W. Sun, C. M. Knudson, C. E. Milligan and R. W. Oppenheim (2006). "Complete dissociation of motor neuron death from motor dysfunction by Bax deletion in a mouse model of ALS." J Neurosci 26(34): 8774-8786.

Graham, R. K., D. E. Ehrnhoefer and M. R. Hayden (2011). "Caspase-6 and neurodegeneration." Trends Neurosci 34(12): 646-656.

Graham, R. K., Y. Deng, J. Carroll, K. Vaid, C. Cowan, M. A. Pouladi, M. Metzler, N. Bissada, L. Wang, R. L. Faull, M. Gray, X. W. Yang, L. A. Raymond and M. R. Hayden (2010). "Cleavage at the 586 amino acid caspase-6 site in mutant huntingtin influences caspase-6 activation in vivo." J Neurosci 30(45): 15019-15029.

Graham, R.K. et al (2006). “Cleavage at the caspase-6 site is required for neuronal dysfunction and degeneration due to mutant huntingtin.” Cell 125(6):1179-91.

Green, E. L. (1976). "Biology of the Laboratory Mouse."

Gue´gan Christelle, Miquel Vila, N. and, Gorazd Rosoklija, Arthur P. Hays and a. S. Przedborsk (2001). "Recruitment of the mitochondrial-dependent apoptotic pathway in amyotrophic lateral sclerosis ".J Neurosci. 21(17):6569-76.

Guerrero, A.D., M. Chen, J. Wang (2008). “Delineation of the caspase-9 signaling cascade.” Apoptosis pp. 177–186

Guo, H., S. Albrecht, M. Bourdeau, T. Petzke, C. Bergeron and A. C. LeBlanc (2004). "Active Caspase-6 and Caspase-6-Cleaved Tau in Neuropil Threads, Neuritic Plaques, and Neurofibrillary Tangles of Alzheimer's Disease." The American Journal of Pathology 165(2): 523-531.

Gurney, M. E., H. Pu, et al. (1994). "Motor neuron degeneration in mice that express a human Cu,Zn superoxide dismutase mutation." Science 264(5166): 1772-1775.

Hakem R, Hakem A, Duncan GS, Henderson JT, Woo M, Soengas MS et al. (1998) “Differential requirement for caspase-9 in apoptotic pathways *in vivo*.” Cell 94: 339–352

Hall, E.D., J.A. Oostveen , M.E. Gurney (1998).“Relationship of microglia and astrocytic activation to disease onset and progression in a transgenic model of familial ALS.” Glia. (3): 249-56.

Hardiman, O., L. H. van den Berg and M. C. Kiernan (2011). "Clinical diagnosis and management of amyotrophic lateral sclerosis." Nat Rev Neurol 7(11): 639-649.

Henshall, D.C. et al. (2002). “Expression and differential processing of caspases 6 and 7 in relation to specific epileptiform EEG patterns following limbic seizures.” Neurobiol. Dis. 10, 71-87.

Hermel E, Gafni J, Propp SS, Leavitt BR, Wellington CL, Young JE, Hackam AS, Logvinova AV, Peel AL, Chen SF, Hook V, Singaraja R, Krajewski S, Goldsmith PC, Ellerby HM, Hayden MR, Bredesen DE, Ellerby LM. (2004). "Specific caspase interactions and amplification are involved in selective neuronal vulnerability in Huntington's disease." Cell Death Differ. (4):424-38.

Ilieva, H. S., K. Yamanaka, S. Malkmus, O. Kakinohana, T. Yaksh, M. Marsala and D. W. Cleveland (2008). "Mutant dynein (Loa) triggers proprioceptive axon loss that extends survival only in the SOD1 ALS model with highest motor neuron death." Proc Natl Acad Sci U S A 105(34): 12599-12604.

Inoue, S, G. Browne, G. Melino, G.M. Cohen (2009). "Ordering of caspases in cells undergoing apoptosis by the intrinsic pathway." Cell Death Differ 16: 1053–1061.

Kanaan, N.M., Pigino, G.F., Brady, S.T,. Lazarov, O., Binder, L.I., Morfini, G.A. (2013). "Axonal degeneration in Alzheimer's disease: when signaling abnormalities meet the axonal transport system." Exp Neurol. 246:44-53.

Kieran, D., B. Kalmar, et al. (2004). "Treatment with arimoclomol, a coinducer of heat shock proteins, delays disease progression in ALS mice." Nat Med 10(4): 402-405.

Kieran, D., M. Hafezparast, S. Bohnert, J. R. Dick, J. Martin, G. Schiavo, E. M. Fisher and L. Greensmith (2005). "A mutation in dynein rescues axonal transport defects and extends the life span of ALS mice." J Cell Biol 169(4): 561-567.

Kiernan, J. A. (2009). "Barr's The Human Nervous System, An Anatomical Viewpoint." Wolters Kluwer Health. Lippincott Williams and Wilkins. 9th Edition (9th Edition): 61-78.

Kiernan, M. C., S. Vucic, et al. (2011). "Amyotrophic lateral sclerosis." 9th Lancet 377(9769): 942-955.

Klaiman, G., N. Champagne and A. C. LeBlanc (2009). "Self-activation of Caspase-6 in vitro and in vivo: Caspase-6 activation does not induce cell death in HEK293T cells." Biochim Biophys Acta 1793(3): 592-601.

Knippenberg, S., N. Thau, et al. (2010). "Significance of behavioural tests in a transgenic mouse model of amyotrophic lateral sclerosis (ALS)." Behav Brain Res 213(1): 82-87.
Kuida K, Zheng TS, Na S, Kuan C, Yang D, Karasuyama H et al. (1996) Decreased apoptosis in the brain and premature lethality in CPP32-deficient mice. Nature **384**: 368–372.

Kroemer G, Martin SJ. (2005) "Caspase-independent cell death." Nature Med 11:725–730.

Kumar, D. R., F. Aslinia, S. H. Yale and J. J. Mazza (2011). "Jean-Martin Charcot: the father of neurology." Clin Med Res 9(1): 46-49.

LeBlanc, A. C. (2013). "Caspase-6 as a novel early target in the treatment of Alzheimer's disease." Eur J Neurosci 37(12): 2005-2018.

LeBlanc, A.C., H. Liu, C. Goodyer, C. Bergeron, J Hammond (1999). "Caspase-6 role in apoptosis of human neurons, amyloid oogenesis and Alzheimer's disease." J Biol Chem 274:23426–23436

LeBlanc, A.C., J Ramcharitar, V. Afonso, E. Hamel, D.A. Bennett, P. Pakavathkumar, S. Albrecht (2014). "Caspase-6 activity in the CA1 region of the hippocampus induces age-dependent memory impairment." Cell Death and Differentiation 1–11

Leblond, C. S., H. M. Kaneb, P. A. Dion and G. A. Rouleau (2014). "Dissection of genetic factors associated with amyotrophic lateral sclerosis." Exp Neurol DOI: 10.1016/j.expneurol.2014.04.013

Leitner, Melanie, S. M. a. C. L. (2009). Working with ALS Mice. The Jackson Laboratories.
Li, M. et al. (2000). "Functional Role of Caspase-1 and Caspase-3 in an ALS Transgenic Mouse Model." Science 288(5464): 335-339.

Ligon, L. A., B. H. LaMonte, K. E. Wallace, N. Weber, R. G. Kalb, and E. L. Holzbaur. (2005). “Mutant superoxide dismutase disrupts cytoplasmic dynein in motor neurons.” Neuroreport. 16:533–536.

Los, M., M. V. d. C., H. S. Louis C. Penningt, P. A. B. Michael Westendorp, P. H. K. Wulf Droge, Walter Fierst and B. K. Schulze-Osthoff (1995). "Requirement of an ICE/CED-3 protease for Fas/APO-1-mediated apoptosis." Nature. 375(6526):81-3.

Los, M., S. W. and a. K. Schulze-Osthoff (1999). "The role of caspases in development, immunity, and apoptotic signal transduction: lessons from knockout mice." Immunity 10(6):629-39.

Ludolph, A. C., C. Bendotti, et al. (2007). "Guidelines for the preclinical in vivo evaluation of pharmacological active drugs for ALS/MND: report on the 142nd ENMC international workshop." Amyotroph Lateral Scler 8(4): 217-223.

Ludolph, A. C., C. Bendotti, et al. (2010). "Guidelines for preclinical animal research in ALS/MND: A consensus meeting." Amyotroph Lateral Scler 11(1-2): 38-45.

Luo, G., J. Yi, C. Ma, Y. Xiao, F. Yi, T. Yu and J. Zhou (2013). "Defective mitochondrial dynamics is an early event in skeletal muscle of an amyotrophic lateral sclerosis mouse model." PLoS One 8(12): e82112.

Magrane J, Manfredi G. (2009) “Mitochondrial function, morphology, and axonal transport in amyotrophic lateral sclerosis.” Antioxid Redox Signal. 11(7):1615–1626.

Marino, G., M. Niso-Santano, E. H. Baehrecke and G. Kroemer (2014) "Self-consumption: the interplay of autophagy and apoptosis." Nat Rev Mol Cell Biol 15(2): 81-94.

Martinon, F. and Tschopp, J (2004) “Inflammatory Caspases: Linking an Intracellular Innate Immune System to Autoinflammatory Diseases.” Cell Press Volume 117, Issue 5, 28 May 2004, Pages 561–574

Miller R.G., T.L. Munsat, M. Swash, B.R. Brooks (1999) “Consensus guidelines for the design and implementation of clinical trials in ALS.” Journal of the Neurological Sciences 169 2–12

Miller, R. G., J. D. Mitchell, et al. (2007). "Riluzole for amyotrophic lateral sclerosis (ALS)/motor neuron disease (MND)." Cochrane Database Syst Rev (1): CD001447.

Milnerwood, A. J., C. M. Gladding, M. A. Pouladi, A. M. Kaufman, R. M. Hines, J. D. Boyd, R. W. Ko, O. C. Vasuta, R. K. Graham, M. R. Hayden, T. H. Murphy and L. A. Raymond (2010). "Early increase in extrasynaptic NMDA receptor signaling and expression contributes to phenotype onset in Huntington's disease mice." Neuron 65(2): 178-190.

Nguyen, T. V., V. Galvan, W. Huang, S. Banwait, H. Tang, J. Zhang and D. E. Bredesen (2008). "Signal transduction in Alzheimer disease: p21-activated kinase signaling requires C-terminal cleavage of APP at Asp664." J Neurochem 104(4): 1065-1080.

Nicholson D.W., N.A. Thornberry, (1997). “Caspases: killer proteases” Trends Biochem Sci. 299-306

Nikolaev, A., T. McLaughlin, D.D. O'Leary, M. Tessier-Lavigne (2009). “APP binds DR6 to trigger axon pruning and neuron death via distinct caspases.” Nature. 457(7232):981-9

Noorbakhsh, F., Ramachandran, R., Barsby, N., Ellestad K.K., LeBlanc, A.C., Dickie, P., Baker, G., Hollenberg, M.D., Cohen, E.A. Power, C. (2010) “MicroRNA profiling reveals new aspects of HIV neurodegeneration: caspase-6 regulates astrocyte survival.” FASEB J. 2010 24: 1799-1812.

Okouchi, O., O. Ekshyyan, M. Maracine, T.A. Aw (2007). “Neuronal apoptosis in neurodegeneration.” Antioxidants and Redox Signaling 9(8):1059-96.

Pandya, R. S., H. Zhu, W. Li, R. Bowser, R. M. Friedlander and X. Wang (2013). "Therapeutic neuroprotective agents for amyotrophic lateral sclerosis." Cell Mol Life Sci 70(24): 4729-4745.

Pansarasa, O., D. Rossi, A. Berardinelli and C. Cereda (2014). "Amyotrophic lateral sclerosis and skeletal muscle: an update." Mol Neurobiol 49(2): 984-990.

Pasinelli, P, D.R. Borchelt, M.K. Houseweart, D.W. Cleveland, R.H. Brown Jr (1998). "Caspase-1 is activated in neural cells and tissue with amyotrophic lateral sclerosis-associated mutations in copper-zinc superoxide dismutase." Proc. Natl. Acad. Sci. USA Vol. 95, pp. 15763–15768.

Pasinelli, P. and R. H. Brown (2006). "Molecular biology of amyotrophic lateral sclerosis: insights from genetics." Nat Rev Neurosci 7(9): 710-723.

Pasinelli, P., M. K. Houseweart, R. H. Brown, Jr. and D. W. Cleveland (2000). "Caspase-1 and -3 are sequentially activated in motor neuron death in Cu,Zn superoxide dismutase-mediated familial amyotrophic lateral sclerosis." Proc Natl Acad Sci U S A 97(25): 13901-13906.

Pellegrini, L., B.J. Passer, M. Tabaton, J.K. Ganjei, L. D'Adamio (1999). "Alternative, non-secretase processing of Alzheimer's beta-amyloid precursor protein during apoptosis by caspase-6 and -8." J. Biol. Chem 274, 21011-21016.

Petzke T.L., E. Rousselet, C. Goodyer, A.C. LeBlanc (2005) "Substrates of caspase-6 in human primary neurons: A proteomic study." Program No. 80.9.2005 AbstractViewer/ItineraryPlanner. Washington,DC: Society for Neuroscience. Online

Portera-Cailiau, C., D. Price, L.J. Martin (1997). "Excitotoxic neuronal cell death in the immature brain is an apoptosis-necrosis morphological continuum." J Comp Neurol 378: 70-78

Pun, S., A. F. Santos, S. Saxena, L. Xu and P. Caroni (2006). "Selective vulnerability and pruning of phasic motoneuron axons in motoneuron disease alleviated by CNTF." Nat Neurosci 9(3): 408-419.

Rademakers R, van Blitterswijk M. (2013) “Motor neuron disease in 2012: Novel causal genes and disease modifiers.” Nat Rev Neurol (2):63-4.

Raina AK, Hochman A, Zhu X, Rottkamp CA, Nunomura A, Siedlak SL, Boux H, Castellani RJ, Perry G, Smith MA. (2001) “Abortive apoptosis in Alzheimer's disease.” Acta Neuropathol. (4):305-10.

Ramcharitar J, Albrecht S, Afonso V.M., Kaushal V., Bennett D.A., Leblanc A.C. (2013) “Cerebrospinal fluid tau cleaved by caspase-6 reflects brain levels and cognition in aging and Alzheimer disease.” J Neuropathol Exp Neurol 72(9):824-32.

Rosen, D. R. (1993). "Mutations in Cu/Zn superoxide dismutase gene are associated with familial amyotrophic lateral sclerosis." Nature Clin Neurosci 364(6435): 362.

Rowland, L. P. and N. A. Shneider (2001). "Amyotrophic lateral sclerosis." N Engl JMed 344(22): 1688-1700.

Saccon, R. A., R. K. Bunton-Stasyshyn, E. M. Fisher and P. Fratta (2013). "Is SOD1 loss of function involved in amyotrophic lateral sclerosis?" Brain 136(Pt 8): 2342-2358.

Sathasivam, S. et al. (2001). “Apoptosis in amyotrophic lateral sclerosis: A review of the evidence.” Neuropathology and Applied Neurobiology 27, 257-274

Sathasivam, S., A.J. Grierson, P.J. Shaw (2005). “Characterisation of the caspase cascade in a cell culture model of SOD1-related FALS: expression, activation and therapeutic effects of inhibition.” Neuropath Appl Neurobiol (5):467-85.

Scott, S., J. E. Kranz, et al. (2008). "Design, power, and interpretation of studies in the standard murine model of ALS." Amyotroph Lateral Scler 9(1): 4-15

Shi P, Gal J, Kwinter DM, Liu X, Zhu H. (2009). “Mitochondrial dysfunction in amyotrophic lateral sclerosis.” Biochem Biophys Acta (1):45-51

Shi, Y. (2004) “Caspase activation, inhibition, and reactivation: A mechanistic view” Protein Sci. 13(8): 1979–1987.

Simon, D. J., R. M. Weimer, T. McLaughlin, D. Kallop, K. Stanger, J. Yang, D. D. O'Leary, R. N. Hannoush and M. Tessier-Lavigne (2012). "A caspase cascade regulating developmental axon degeneration." J Neurosci 32(49): 17540-17553.

Singh A.B, V. Kaushal, K. Judit, et al. (2002). “Cloning and expression of rat caspase-6 and its localization in renal ischemia/reperfusion injury.” Kidney International, Vol. 62 pp. 106–115

Slee, E. A., C. Adrain and S. J. Martin (2001). "Executioner caspase-3, -6, and -7 perform distinct, non-redundant roles during the demolition phase of apoptosis." J Biol Chem 276(10): 7320-7326.

Slee, E.A., M.T. Harte, R.M. Kluck, B.B. Wolf, C.A. Casiano, D.D. Newmeyer, H.G. Wang, J.C. Reed, D.W. Nicholson, E.S. Alnemri, D.R. Green, S.J. Martin (1999) “Ordering the cytochrome c initiated caspase cascade: hierarchical activation of caspases-2, -3, -6, -7, -8, and -10 in a caspase-9-dependent manner.” J Cell Biol 144(2):281-92.

Srinivasula, S.M., T. Fernandes-Alnemri, J. Zangrilli, N. Robertson, R.C. Armstrong, L. Wang, J.A. Trapani, K.J. Tomaselli, G. Litwack, E.S. Alnemri (1996). “The Ced-3/interleukin 1beta converting enzyme-like homolog Mch6 and the lamin-cleaving enzyme Mch2alpha are substrates for the apoptotic mediator CPP32” J. Biol. Chem 27099–27106.

Takahashi, A., E.S. Alnemri, Y.A. Lazenbnik et al. (1996). “Cleavage of lamin A by Mch2α, but not CPP32: Multiple interleukin 1β-converting enzyme-related proteases with distinct substrate recognition properties are active in apoptosis.” Proc. Natl. Acad. Sci. U.S.A. 93, 8395-8400.

Tan, W., P. Pasinelli and D. Trotti (2014). "Role of mitochondria in mutant SOD1 linked amyotrophic lateral sclerosis." Biochim Biophys Acta 1842(8): 1295-1301.

Thornberry, N. A., T. A. Rano, et al. (1997). "A combinatorial approach defines specificities of members of the caspase family and granzyme B. Functional relationships established for key mediators of apoptosis." J Biol Chem 272(29): 17907-17911.

Tokuda, E., Ono, S., Ishige, K., Watanabe, S., Okawa, E., Ito, Y., and Suzuki, T. (2007). Dysequilibrium between caspases and their inhibitors in a mouse model for amyotrophic lateral sclerosis. Brain Res 1148: 234-242.

Uribe, V., K.Y. Wong et al. (2012). "Rescue from excitotoxicity and axonal degeneration accompanied by age-dependent behavioral and neuroanatomical alterations in caspase-6-deficient mice." Hum Mol Genet 21(9): 1954–1967**.**

Vehviläinen, P., J. Koistinaho, G. Goldsteins (2014). "Mechanisms of mutant SOD1 induced mitochondrial toxicity in amyotrophic lateral sclerosis." Frontiers in Cellular Neuroscience V8:126

Velázquez-Delgado, E.M, J.A. Hardy (2012). "Zinc-mediated Allosteric Inhibition of Caspase-6." J Biol Chem. 287(43): 36000–36011.

Vinsant, S., C. Mansfield, R. Jimenez-Moreno, V. Del Gaizo Moore, M. Yoshikawa, T. G. Hampton, D. Prevette, J. Caress, R. W. Oppenheim and C. Milligan (2013). "Characterization of early pathogenesis in the SOD1(G93A) mouse model of ALS: part I, background and methods." Brain Behav 3(4): 335-350.

Vinsant, S., C. Mansfield, R. Jimenez-Moreno, V. Del Gaizo Moore, M. Yoshikawa, T. G. Hampton, D. Prevette, J. Caress, R. W. Oppenheim and C. Milligan (2013). "Characterization of early pathogenesis in the SOD1(G93A) mouse model of ALS: part II, results and discussion." Brain Behav 3(4): 431-457.

Vohra, B. P., Y. Sasaki, B. R. Miller, J. Chang, A. DiAntonio and J. Milbrandt (2010). "Amyloid precursor protein cleavage-dependent and -independent axonal degeneration programs share a common nicotinamide mononucleotide adenylyltransferase 1-sensitive pathway." J Neurosci 30(41): 13729-13738.

Vucic, S. and M. C. Kiernan (2009). "Pathophysiology of neurodegeneration in familial amyotrophic lateral sclerosis." Curr Mol Med 9(3): 255-272

Vukosavic, S., Caiping Chen, Leonidas Stefanis, Michel Dubois-Dauphin, Vernice Jackson-Lewis, a. S. Przedborski, Christelle Gue´ gan and N. Romero (2000). "Delaying caspase activation by bcl-2: a clue to disease retardation in a transgenic mouse model of amyotrophic lateral sclerosis ".J Neurosci. 20(24):9119-25.

Waldron-Roby, E., T. Ratovitski, X. Wang, M. Jiang, E. Watkin, N. Arbez, R. K. Graham, M. R. Hayden, Z. Hou, S. Mori, D. Swing, M. Pletnikov, W. Duan, L. Tessarollo and C. A. Ross (2012). "Transgenic mouse model expressing the caspase 6 fragment of mutant huntingtin." J Neurosci 32(1): 183-193.

Wang X.J., Q. Cao , X. Liu ,K.T. Wang, W Mi, Y. Zhang, L.F. Li, A.C. LeBlanc, X.D. Su . (2010). "Crystal structures of human caspase 6 reveal a new mechanism for intramolecular cleavage self-activation." EMBO Rep 11: 841–847.

Watanabe, C., Shu, G.L., Zheng, T.S., Flavell, R.A., Clark, E.A. (2008) "Caspase-6 Regulates B Cell Activation and Differentiation into Plasma Cells." The Journal of Immunology. 181: 6810–6819.

Weydt, P., S. Y. Hong, et al. (2003). "Assessing disease onset and progression in the SOD1 mouse model of ALS." Neuroreport 14(7): 1051-1054

Wong, M. and L. J. Martin (2010). "Skeletal muscle-restricted expression of human SOD1 causes motor neuron degeneration in transgenic mice." Hum Mol Genet 19(11): 2284-2302.

Yeretssian, G., R. G. Correa, et al. (2011). "Non-apoptotic role of BID in inflammation and innate immunity." Nature 474(7349): 96-99

Youle, R. J. and A. Strasser (2008). "The BCL-2 protein family: opposing activities that mediate cell death." Nat Rev Mol Cell Biol 9(1): 47-59

Zandy, A. J., S. Lakhani, T. Zheng, R. A. Flavell and S. Bassnett (2005). "Role of the executioner caspases during lens development." J Biol Chem 280(34): 30263-30272.